

# Coordinated Pandemic Control with Large Language Model Agents as Policymaking Assistants

Ziyi Shi<sup>1,†</sup>, Xusen Guo<sup>2,†</sup>, Hongliang Lu<sup>1,\*</sup>, Mingxing Peng<sup>2</sup>, Haotian Wang<sup>2</sup>, Zheng Zhu<sup>3</sup>,  
Zhenning Li<sup>4</sup>, Yuxuan Liang<sup>2</sup>, Xinhua Zheng<sup>2</sup>, and Hai Yang<sup>1,\*</sup>

<sup>1</sup>The Hong Kong University of Science and Technology, Hong Kong

<sup>2</sup>The Hong Kong University of Science and Technology (Guangzhou), China

<sup>3</sup>Zhejiang University, China

<sup>4</sup>University of Macau, Macau

\*corresponding authors: Hongliang Lu and Hai Yang

†These authors contributed equally to this work

## ABSTRACT

Effective pandemic control requires timely and coordinated policymaking across administrative regions that are intrinsically interdependent. However, human-driven responses are often fragmented and reactive, with policies formulated in isolation and adjusted only after outbreaks escalate, undermining proactive intervention and global pandemic mitigation. To address this challenge, here we propose a large language model (LLM) multi-agent policymaking framework that supports coordinated and proactive pandemic control across regions. Within our framework, each administrative region is assigned an LLM agent as an AI policymaking assistant. The agent reasons over region-specific epidemiological dynamics while communicating with other agents to account for cross-regional interdependencies. By integrating real-world data, a pandemic evolution simulator, and structured inter-agent communication, our framework enables agents to jointly explore counterfactual intervention scenarios and synthesize coordinated policy decisions through a closed-loop simulation process. We validate the proposed framework using state-level COVID-19 data from the United States between April and December 2020, together with real-world mobility records and observed policy interventions. Compared with real-world pandemic outcomes, our approach reduces cumulative infections and deaths by up to 63.7% and 40.1%, respectively, at the individual state level, and by 39.0% and 27.0%, respectively, when aggregated across states. These results demonstrate that LLM multi-agent systems can enable more effective pandemic control with coordinated policymaking. More broadly, this study presents a generalizable framework for operationalizing LLM agents in large-scale public policy settings, offering a promising decision-support paradigm for future pandemics and other complex societal challenges characterized by strong regional interdependence.

**Keywords:** Pandemic Control, Large Language Models, Multi-Agent System, Coordinated Policymaking

## Introduction

Pandemic control compels policymakers to make effective policies to safeguard public health. However, effective coordination across regions is intrinsically challenging, as many jurisdictions tend to prioritize short-term containment actions over coordinated, long-term planning<sup>1,2</sup>. Such fragmented and myopic responses increase the difficulty of global pandemic control and, in some cases, may even exacerbate disease spread<sup>3</sup>. A key reason is regional heterogeneity. Pandemic situations vary widely across regions due to differences in population density, mobility patterns, healthcare capacity, socioeconomic structure, and data availability<sup>4,5</sup>. Policymakers need to handle large volumes of heterogeneous information, often under severe time pressure, making it difficult to design both region-specific and globally coordinated interventions. Moreover, effective pandemic control necessitates proactive intervention under deep uncertainty. Transmission dynamics are multifactorial and evolve rapidly over time, meaning that delays in policy response can lead to irreversible public health consequences<sup>6,7</sup>. Yet institutional constraints such as jurisdictional silos, delayed surveillance, and limited forecasting capacity often prevent governments from anticipating pandemic trends and acting preemptively<sup>8</sup>. Even well-resourced governments have struggled to assess intervention trade-offs in advance and to deploy timely preventive measures<sup>9</sup>. Taken together, policymaking for pandemic control faces three fundamental challenges: 1) enabling effective coordination across regions, 2) accounting for region-specific and data-intensive heterogeneity, and 3) supporting proactive policy interventions under uncertainty.

The COVID-19 pandemic exemplified these challenges. During the global fight against COVID-19, the international response revealed substantial fragmentation across all levels of governance, from global coordination to local implementation<sup>8</sup>. Many regions pursued policies independently; however, these siloed policies were often conflicting, leading to detrimental

consequences for both public health and economic stability<sup>2</sup>. This phenomenon is particularly pronounced in highly connected regions<sup>10</sup>. When neighboring regions adopted fragmented interventions, such as asynchronous lockdowns, uneven travel restrictions, or divergent reopening timelines, population mobility allowed the virus to continue circulating across administrative boundaries<sup>11-14</sup>. As a result, stringent control measures implemented by individual regions were frequently undermined by inflows of infections from less-restricted neighbors, rendering localized efforts partially ineffective. Modeling studies of the United States have demonstrated that such uncoordinated interventions led to significant efficiency losses and worsened overall outcomes<sup>2</sup>. Similar patterns were also observed in Europe<sup>10,15</sup>. As concluded by the Lancet Commission, “*widespread, global failures at multiple levels in the COVID-19 response led to millions of preventable deaths*”<sup>16</sup>. A critical lesson is highlighted: it is difficult for purely human-driven policymaking to achieve effective coordination and real-time response; what often follows are miscommunication, policy misalignment, and suboptimal public health outcomes<sup>3,4</sup>.

In response to these challenges, policymakers have resorted to established response paradigms and local heuristics. Intervention packages are typically designed based on past influenza models, community norms, and classical epidemiological strategies, such as the influenza control framework proposed by Ferguson et al.<sup>17</sup>. However, real-world implementation remains piecemeal and reactive, largely due to fragmented governance structures, delayed situational awareness, and limited capacity to synthesize heterogeneous data into timely, coordinated policy decisions. At both national and regional levels, policy actions were frequently triggered by case surges or political pressure rather than informed by forward-looking analysis<sup>18,19</sup>. Converging evidence suggests that proactive strategies would have substantially outperformed reactive ones. For example, Sacco et al. showed that jurisdictions adopting preemptive interventions exhibited far greater resilience than those that delayed action until outbreaks intensified<sup>9</sup>. Yet effective decision-support tools and institutional agility remain limited, leaving pandemic policymaking heavily dependent on static “plans on paper” and expert judgment. Even where complex epidemiological models were available, their influence on decision-making was often constrained. In a few cases, such as Austria’s national modeling consortium, ensembles of epidemiological forecasts were used to inform the timing of policy interventions<sup>19</sup>. More commonly, however, officials defaulted to simple rules of thumb, resulting in a patchwork of measures shaped by local political considerations rather than systematic optimization. Therefore, an effective paradigm is urgently needed to transform policymaking from a siloed, reactive process into a more coordinated and proactive one<sup>6,7</sup>.

Recent advances in large language models (LLMs) have demonstrated their outstanding ability to handle heterogeneous information, perform natural language reasoning, and adapt to complex and evolving contexts<sup>20</sup>. Compared with conventional policy support methods based on fixed rules or pre-established optimization objectives, LLMs offer flexible, context-aware reasoning capabilities, making them promising tools for interpreting ever-changing pandemic situations. Existing studies have explored LLM applications in disease forecasting<sup>21,22</sup>, pandemic modeling and simulation<sup>23,24</sup>, and public health information analysis<sup>25,26</sup>. However, these works primarily treat LLMs as predictive models or heterogeneous information processors, lacking mechanisms for interaction with dynamic environments or decision adaptation through feedback. Consequently, they fall short of addressing the sequential, interactive, and coordination-intensive demands of real-world pandemic control. Against this backdrop, the recent emergence of LLM agents opens a new window. LLM agents operationalize language models as autonomous decision-making entities that maintain internal state and interact with environments or other agents<sup>27,28</sup>. This agent-based paradigm enables LLMs to support sequential decision-making, adapt to evolving system dynamics, and reason about coordination among multiple stakeholders. Such capabilities align naturally with coordinated pandemic control, where policies must be continuously made under uncertainty and coordinated across regions and administrative levels. Given the prowess of LLM agents, a compelling question arises: if we had LLM agents as our policymaking assistants during past pandemics, could more effective pandemic control have been achieved?

In this study, we develop an LLM multi-agent policymaking framework for coordinated pandemic control, in which each LLM agent serves as a regional AI assistant to support proactive and coordinated policymaking across administrative units. As illustrated in Fig. 1, our framework follows a three-step closed-loop decision process. First, for each region, the LLM agent calibrates a pandemic transmission model using observed epidemiological and mobility data, and uses it to simulate short-term pandemic evolution. This step captures how inter-regional mobility shapes the pandemic situation, as reflected in some key indicators like active case counts and mortality. Second, these pandemic indicators and mobility flow data are fed into the LLM multi-agent policymaking system. Through inter-agent communication and collective reasoning, these agents exchange information and jointly determine policy actions designed to control disease spread by adjusting inter-regional mobility. Finally, the policies are applied to update inter-regional mobility flows, which are fed back into the pandemic transmission model to simulate the pandemic evolution under the new policy settings. The updated pandemic situations subsequently serve as inputs to the next decision cycle, enabling iterative and anticipatory policy refinement. We validate the proposed framework using real-world COVID-19 data from the United States between April and December 2020, together with high-resolution mobility records and real-world policies. Compared to real-world pandemic situations, our LLM-agent system, 1) at the individual-state level, reduces cumulative infections and deaths by up to 63.7% and 40.1%, respectively; and 2) at the aggregate level across states, reduces cumulative infections and deaths by 39.0% and 27.0%, respectively. Looking ahead, this study showcases

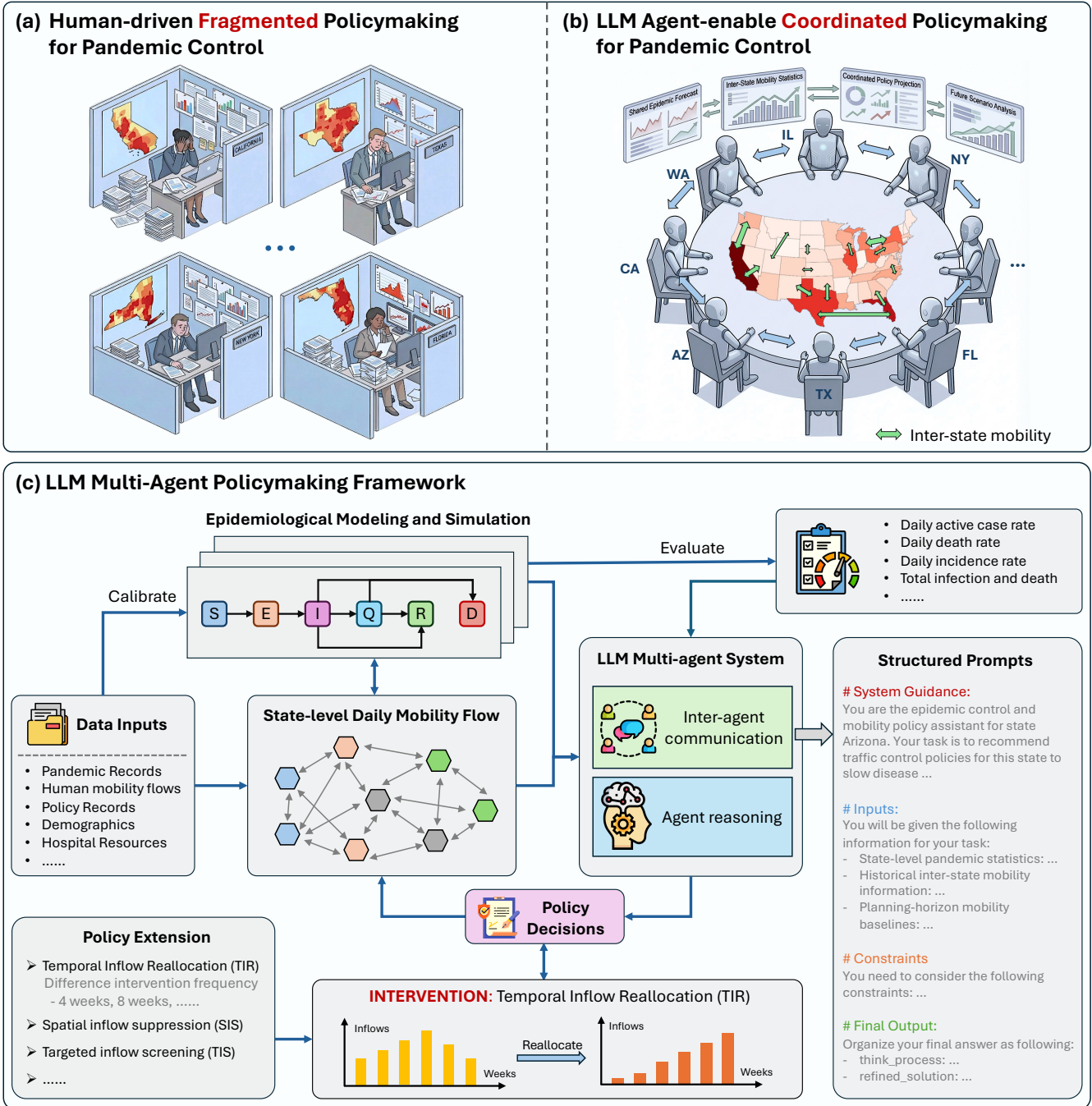


**Figure 1.** Comparison between traditional pandemic policymaking and our proposed LLM-agent-enabled coordinated policymaking. **a**, Traditional pandemic policymaking under fragmented coordination. Regional authorities operate largely in isolation, relying on delayed or incomplete information and independent analyses. Limited cross-region communication and asynchronous interventions lead to misaligned policies and inefficient pandemic control. **b**, LLM multi-agent system for coordinated pandemic policymaking. Each administrative region is represented by an LLM agent that exchanges information with others, enabling collaborative reasoning and coordinated policy decisions across regions while accounting for inter-state mobility. **c**, Architecture of the proposed LLM-agent system for pandemic policymaking. Each regional agent integrates epidemiological modeling, real-world data inputs (case records, mobility flows, demographics, and healthcare resources), and structured prompts to reason about policy actions. Inter-regional mobility is modeled through state-level mobility flows, inducing cross-region transmission dynamics. Agents communicate, evaluate outcomes, and generate coordinated policy decisions, which are instantiated as intervention strategies (e.g., temporal inflow reallocation, spatial inflow suppression, and targeted inbound screening) and fed back into the pandemic simulation loop.

a generalizable framework for operationalizing LLM agents into large-scale public policy systems, suggesting a promising decision-support paradigm for future pandemics and other complex societal crises that require cross-regional coordination.

## Results

### LLM Multi-Agent Policymaking Framework

To facilitate coordinated pandemic control among multiple states, we develop a multi-agent policymaking framework. Below, we illustrate how the framework operates.

**Formulation:** In our framework, each state is assigned an LLM agent as the policymaking assistant, which leverages real-time pandemic information from its own state as well as other states to dynamically manage local inbound mobility. Central to our policymaking is the Temporal Inflow Reallocation (TIR) protocol, under which the total inbound volume from each origin state is held constant over a prescribed planning horizon (e.g., eight weeks). Accordingly, the study period is divided into multiple reallocation cycles. In each cycle, the agents proactively redistribute weekly quotas to modulate the influx rate for their origin states. To illustrate, if State A's total inbound flow from State B is 80,000 over 8 weeks, TIR does not alter this 80,000-person aggregate; instead, it would reallocate the distribution from a uniform 10,000 per week to a non-linear schedule (e.g., 5,000 in week 1 and 15,000 in week 4) based on real-time pandemic situations. This design ensures that our results remain grounded in realistic mobility constraints, while enabling the exploration of potentially more effective pandemic control policies.

**Data:** We leverage real-world COVID-19 data from the United States spanning April to December 2020. To consider multi-source and heterogeneous pandemic information, we incorporate and align three categories of data: 1) state-level daily pandemic records across the United States; 2) state-to-state daily human mobility flows; and 3) state-level policy records.

**Simulation:** We conduct simulation experiments based on real-world pandemic and mobility data spanning from April 12 to December 31, 2020. Once interstate flows are regulated by LLM-agent-generated policies, the SEIQRD model-based epidemiological simulator evolves the pandemic dynamics accordingly<sup>29,30</sup>, as reflected in variations in state-level changes in infection and mortality.

To provide a detailed policy analysis, a 5-state experiment is first conducted among Arizona (AZ), Mississippi (MS), New Mexico (NM), Texas (TX), and Virginia (VA). We then verify our framework on 20 states to examine its scalability. A detailed formulation is provided in the Methods section.

**Prompt:** Statistics observed during the simulation are collected at each policymaking cycle and standardized into structured textual inputs for prompt construction. Each prompt comprises three components: 1) system guidance, which defines the objective for mitigating pandemic spread and the control strategy (e.g., TIR, see Appendix for prompt example); 2) state-level pandemic statistics, which capture the spatio-temporal epidemiological trajectories within the local state and its neighboring states (e.g., daily infection counts and mortality rate); and 3) mobility information, which integrates historical inter-state mobility patterns and anticipated inbound mobility flow from other states over the planning horizon.

Ultimately, the framework outputs a set of reallocation proportions, which specify how the total inflow is partitioned over the planning horizon.

**Evaluation:** Cumulative metrics and temporal indicators, obtained from the simulation, are used for evaluation. The cumulative metrics, including total infections and mortality, serve as an aggregate measure of long-term policy efficacy. Regarding temporal indicators, we monitor the daily incidence rate (IR), death rate (DR), and active case rate (ACR) for each state. In doing so, we can evaluate both localized performance at the state level while quantifying the emergent systemic impact at the aggregate level.

**Validation:** We consider and compare four distinct policymaking paradigms in our validation: 1) LLM-agent-based policymaking, which performs coordinated policymaking based on system dynamics; 2) ground-truth policymaking, reflecting real-world, human-led pandemic control measures; 3) expert-guided policymaking, in which heuristic travel control strategies are designed based on changes in pandemic statistics; and 4) random policymaking, which adjusts mobility in the absence of explicit optimization objectives.

**Extension:** To test the extensibility of our framework, we account for a diverse set of policy designs. In particular, we evaluate policy outcomes under varying policymaking frequencies (i.e., reallocation cycle lengths), including bi-monthly (8-week TIR) and monthly (4-week TIR) planning horizons, as well as different intervention strategies such as direct mobility suppression (i.e., spatial inflow suppression, SIS) and targeted inbound screening (TIS).

### 5-state Results of Policy Evaluation and Interpretation

In this section, we evaluate the proposed LLM multi-agent policymaking framework on a 5-state setting, comparing its performance against the ground-truth, expert-guided, and random policymaking paradigms, with the planning horizon set to 6 weeks by default. We then analyze the interpretability of policy outcomes from both qualitative and quantitative perspectives.

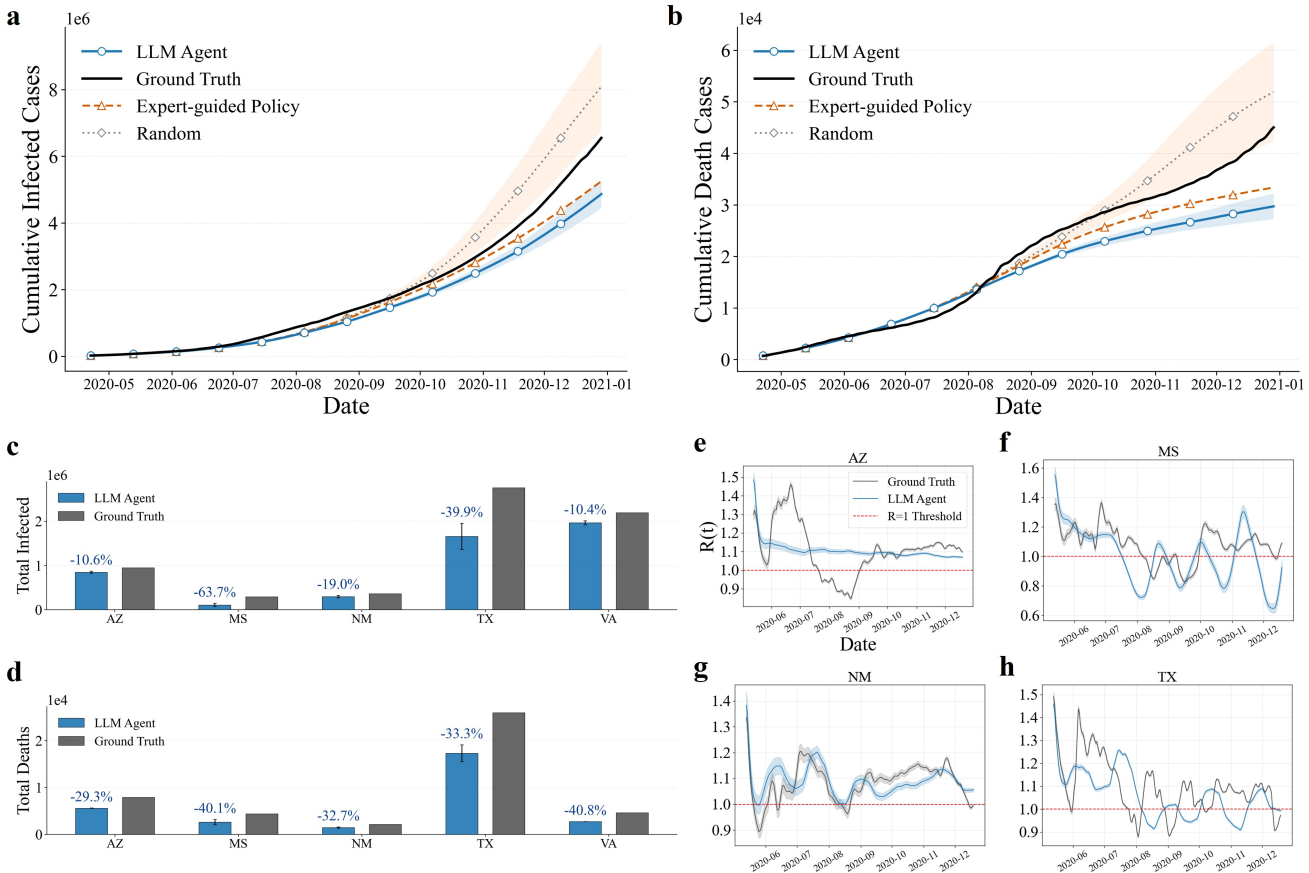


**Figure 2. Effectiveness of the LLM multi-agent policymaking framework in mitigating pandemic spread.** The cumulative confirmed infections (a) and cumulative deaths (b) vary across the time (from May 2020 to December 2020). Results are compared across different intervention strategies, including the LLM agent-based policymaking, expert-experience-based policymaking, random policymaking, and the observed ground-truth policymaking. c,d, The overall reduction in cumulative infections and deaths achieved by the LLM agent-based policy differ across five states, where numerical annotations on each bar denote the percentage reduction in cumulative infections and mortality relative to the ground truth. Furthermore, e-h, LLM agent-based policy stabilizes the temporal dynamics of effective reproduction number  $R_t$  and reduces its mean value.

Fig. 2a-d show the results of the proposed framework in pandemic control at aggregate- and state-level. First, at the aggregate level, the policy generated by LLM agents reduces the total cumulative infected and death cases by 25.7% and 34.0% compared with the ground truth. The random policy performs worse than the ground-truth policy due to its lack of a consistent objective. Although the expert-guided policy controls the spread of the pandemic, the LLM agent policy further improves overall performance. These results underscore both the importance of cross-state coordination and the challenges of achieving it when individual states pursue self-interested policies. Second, at the state level, the LLM agent policy exhibits positive but heterogeneous levels of effectiveness across states. In states with less restrictive ground-truth control policies, such as MS and TX, performance improvements are more pronounced (from 33.3% to 63.7%). For states where ground-truth measures are strict, such as AZ and VA, the reduction in infection counts remains modest (approximately 10%), whereas the reduction in mortality is substantial (29.3% and 40.8%, respectively). Moreover, Fig. 2e-2h present the variation of effective reproduction number  $R_t$  across states, characterizing the pandemic transmissibility (See "Method" Section for the calculation of  $R_t$ ). The LLM agent policy mitigates transmissibility by lowering and stabilizing  $R_t$ . However,  $R_t$  remains above the threshold of one, indicating that an infected individual generates more than one case on average. So, transmission is slowed but not fully suppressed.

To illustrate how LLM agents operate in policymaking, we select Mississippi (MS) as an example and compare the LLM agent policy with the observed real-world one. Fig. 3a shows the comparison results in IR. The implementation of the LLM agent policy is marked by orange five-pointed stars, which divide the experimental period into six successive reallocation cycles. Under the LLM agent policy, IR is maintained below 40, whereas under the ground-truth policymaking, IR rises to

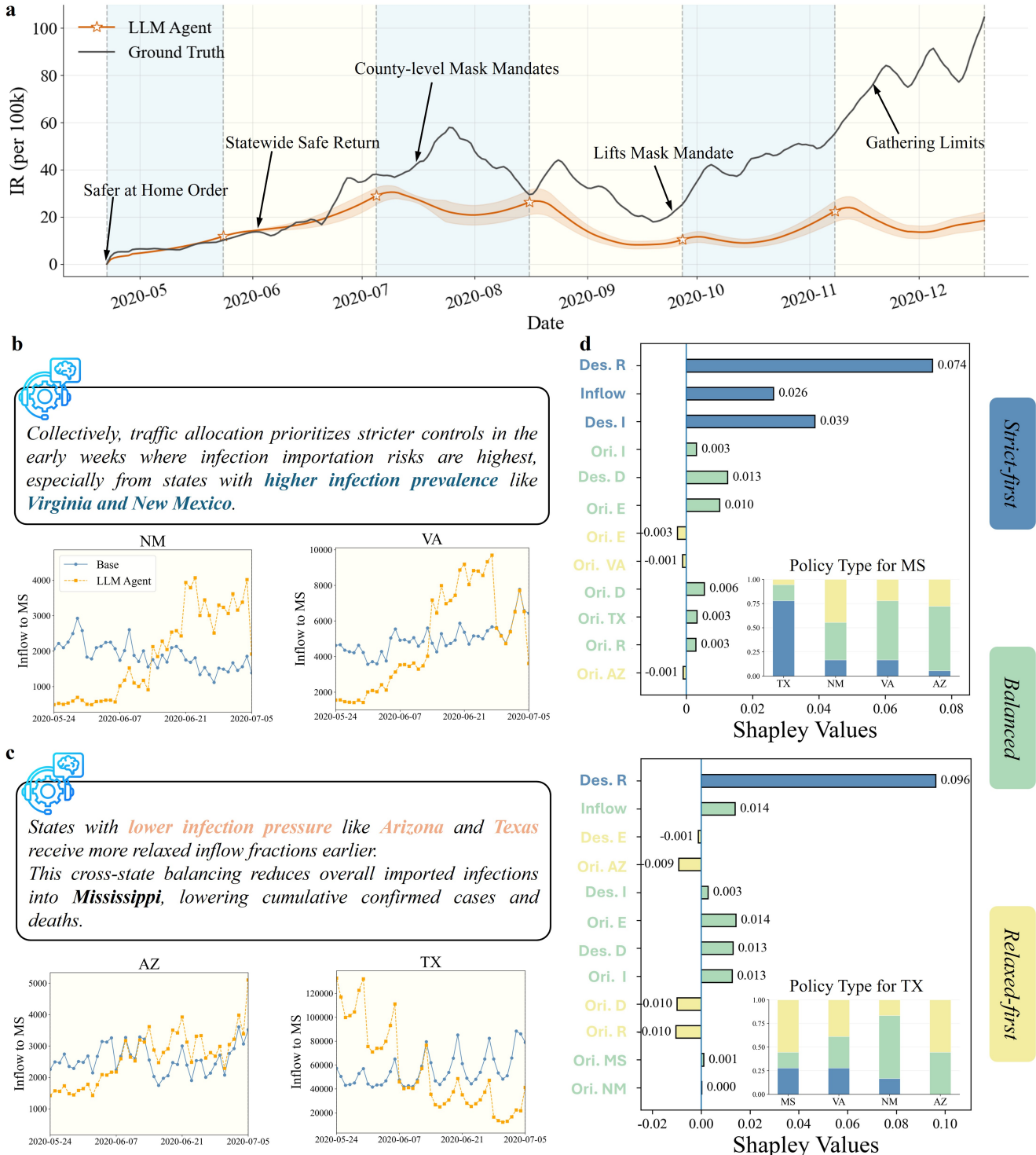


**Figure 3. State-level intervention illustration and interpretation.** **a**, The real-world policy is compared with the mobility reallocation policy generated by the LLM agent in MS (Mississippi), together with the corresponding daily incidence rate. Each reallocation cycle is highlighted in the background using alternating light blue and yellow shading. **b,c**, The specific mobility adjustments during the second reallocation cycle and the reasoning process of LLM agents are illustrated. Moreover, **d**, LLM agent policy are classified into three types (strict-first, balanced, and relaxed-first). Policy-type distributions for Mississippi and Texas are presented, along with each feature’s marginal contribution (i.e., the Shapley Values) on strict-first policy.

nearly 60 by the end of July 2020 and continues to increase over 80 after November 2020. This divergence emerges after June 2020, following the issuance of the “Statewide Safe Return” policy in reality. Thereafter, despite the implementation of mask mandates and limits on gatherings, pandemic transmission accelerated and became out of control. To detail LLM agent policy during the same period, we visualize the state-to-state inflow to MS before and after the adjustment at the second reallocation cycle in Fig. 3b and 3c, alongside the LLM reasoning process for qualitative explanations. The reasoning result shows that LLM agents can identify high-risk origin states (i.e., NM and VA) and impose stricter early-stage interventions, resulting in inbound flow quotas below the uniform level. This strategy limits the early imported infections from high-risk origins, thereby reducing the initial incidence rate and preventing subsequent exponential amplification of transmission. For states with lower infection pressure (AZ and TX), they have more relaxed inflow fractions in the early weeks. Under a fixed quota, this approach constrains subsequent mobility and mitigates pandemic propagation driven by later infection surges.

Next, we provide a quantitative interpretation of LLM agent policymaking. Based on the adjusted inflow distributions, state-level policies at each reallocation cycle are classified into three types: strict-first, relaxed-first, and balanced, corresponding to different pandemic phases and risk levels across states (see the Methods section for detailed classification criteria). Their distribution and feature attribution for states MS and TX are illustrated in Fig. 3d. Policymaking in MS prioritizes a strict-first intervention on TS, because TS exhibits the fastest growth in infections, while applying a balanced control strategy to the other three states. As for Policymaking in TX, the relaxed-first policy is frequently applied to the origin states MS and AZ. This policy decision indicates that MS and AZ pose a non-negligible but manageable importation risk to TX, for which gradual restrictions are effective to curb transmission.

To further quantify the impact of state-level features on the choice of policy types, we use the Shapley value to estimate each feature’s average marginal contribution to policymaking across all feature combinations. We compile epidemiological statistics—including recovered, exposed, infected, and deceased counts—for both origin and destination states, together with inflow volumes and a one-hot representation of the origin state. The Shapley values of these features for “strict-first” policy are illustrated in Fig. 3d, and key findings are summarized. First, for MS and TX, the recovery count in the destination state contributes largely to the strict-first policy (Shapley values 0.074 and 0.096, respectively), followed by inflow volume (0.026 and 0.014, respectively). This result suggests that the agent imposes early stringent interventions when the local state has experienced extensive past transmission and faces elevated inflow pressure. Second, infection counts in both the origin and destination states are positively associated with the adoption of the strict-first policy. In contrast, higher exposure levels (at the origin for MS and destination for TX) reduce the likelihood of adopting a strict-first policy. These conditions, which signal potential infection growth in subsequent weeks, call for a gradual tightening of interventions. Moreover, in TX, origin-level recoveries and deaths exhibit negative Shapley values for the adoption of the strict-first policy, whereas such effects are not observed in MS. This asymmetry reflects TX’s role as a high-mobility hub, where rapid population movements render current infection levels (i.e., infected and exposed cases) more informative for early intervention than historical pandemic levels (recoveries and deaths).

## 5-state Results of Policy Extension

Beyond TIR, we extend the proposed policymaking framework to additional intervention strategies for comparison. Specifically, we consider two alternatives: Spatial Inflow Suppression (SIS) and Targeted Inbound Screening (TIS). For SIS, each state identifies a specific high-risk origin state to reduce its inbound traffic flow by half over a two-week window, with policy decisions updated biweekly throughout the study period. While this strategy provides immediate localized mitigation for the destination state, it also induces a spatial spillover effect, where suppressed traveler flows are redistributed to alternative, non-restricted states. Under TIS, each state implements screening for travelers from a specific origin state over the subsequent two-week period, with policy decisions updated on the same biweekly schedule. This screening process identifies asymptomatic or presymptomatic individuals (E and I compartments) and transfers them into the confirmed (Q) compartment, thereby neutralizing their potential for onward transmission. In both SIS and TIS, each decision round targets only one origin state to avoid excessive simultaneous restrictions.

Most states experience reductions in total infections and deaths under different intervention strategies, as shown in Fig. 4a and 4b. Taking TX, the most severely affected state, as an example, total deaths are reduced by 33%, 41%, and 16% under TIR, SIS, and TIS, respectively. Meanwhile, the three intervention strategies exhibit distinct effect patterns across states. 1) For SIS, although infections are reduced by more than 50% in MS, NM, and TX, pandemic spread is even exacerbated in AZ and VA, with more than 10% infection. This effect is induced by the spatially redistributed interstate flows: mobility suppressed from high-risk origins is diverted to alternative, non-restricted states, unintentionally increasing their exposure and amplifying local transmission. 2) TIS exhibits weaker but more stable effects than SIS and fails to reduce mortality in MS. 3) Under TIR, infection and death counts decrease across all five states, achieving the most stable performance among the intervention strategies.

Fig. 4c and 4d show system-level trade-offs between effectiveness (i.e., reduction in total infection or deaths) and equity

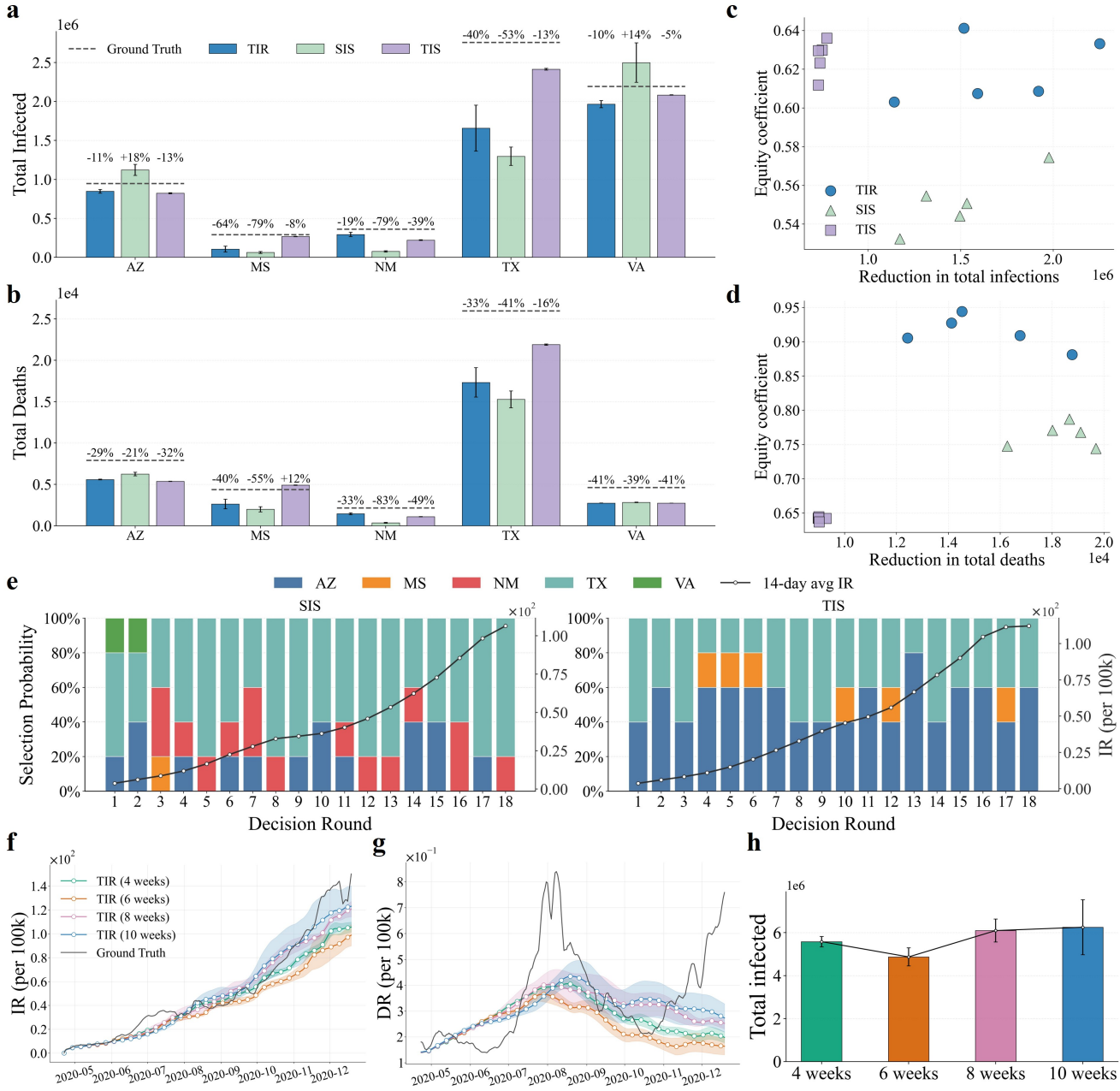


**Figure 4. Performance comparison across multi-dimensional policies.** First, **a,b**, the state-level performance of different intervention strategies (TIR, SIS, and TIS) in terms of total infections and deaths is illustrated. The real-world conditions are indicated by black dashed lines, with the corresponding increase or reduction percentages under different intervention strategies annotated above. Then, **c,d**, the system-level indicators, equity coefficient and the total reductions in infections and deaths, are compared across strategies. Each strategy is evaluated over five runs, with each point representing a single run. **e**, The selection probabilities of different states under SIS and TIS across the study period are presented. Moreover, **f-h**, TIR under planning horizons of 4, 6, 8, and 10 weeks is compared, evaluated by incidence rate (IR), death rate (DR), and total infections.

(i.e., dispersion of improvements among states), where each point corresponds to a single run of the strategy. A higher equity coefficient indicates a more evenly distributed improvement (see Methods for detailed calculation of equity coefficient). The main findings are summarized as follows: First, for both infection and death outcomes, TIR largely dominates the Pareto frontier, indicating its overall superior capability in balancing equity and efficiency in pandemic control. Second, with respect to infection control, TIS exhibits relatively high equity but limited effectiveness, whereas SIS achieves lower equity. Third,

SIS substantially reduces total deaths, albeit with lower equity compared to TIR. It is mainly because SIS induces inter-agent competition through spatial flow redistribution, whereas TIR mitigates such competition.

To further examine inter-agent competition, the detailed policies under SIS and TIS are illustrated in Fig. 4e. Specifically, the bar charts report, for each decision round, the proportion of times each state is selected by other destination states as the intervention state under SIS or TIS. Under TIS, selection probabilities remain stable throughout the study period, with AZ and TX being the primary targets for screening. By contrast, under SIS, when a particular high-risk state is identified by all other states, coordination is effectively enforced, thereby eliminating flow spillover effects. However, such coordination is not always achieved, resulting in diverted flows that surge into other states (e.g., in rounds 4 and 6, not all states suppress flows from TX). As a result, SIS and TIS exhibit comparable IR, as the spillover-induced amplification under SIS offsets its localized suppression benefits.

Finally, we examine how the policymaking frequency of LLM agents influences the effectiveness of pandemic control. Different planning-horizon lengths (4, 6, 8, and 10 weeks) are compared under TIR, with the corresponding IR, DR, and total infections shown in Fig. 4f-4h. Overall, results across these strategies follow the ground-truth trend while attenuating transmission intensity and mortality to varying extents. Notably, total infections under the 6-week TIR setting are reduced by more than 8% relative to the 4-week and 8-week TIR settings. This finding suggests that planning horizons that are either too long or too short lead to inferior performance. The detailed state-level comparison results are presented in the Supplementary Figs 1-15.

## 20-state Results of Scalability

To further evaluate the scalability of the proposed LLM multi-agent policymaking framework, we extend the analysis to a large scale. After excluding states with incomplete statistical records, a total of U.S. 20 states are included in the experiment: Alabama (AL), Arizona (AZ), Arkansas (AR), Idaho (ID), Indiana (IN), Iowa (IA), Kentucky (KY), Michigan (MI), Minnesota (MN), Mississippi (MS), Nebraska (NE), New Mexico (NM), Ohio (OH), Oklahoma (OK), South Carolina (SC), Tennessee (TN), Texas (TX), Utah (UT), Virginia (VA), and Wisconsin (WI). By comparing state-level transmissibility with cumulative infections and deaths, we examine the performance of the proposed framework in large-scale pandemic control.

At the state level, infection and mortality rate under LLM agent policy are lower than those observed under ground-truth policymaking. The IR, DR, and ACR with different policy designs (4-week TIR, 8-week TIR, SIS, and TIS) across states are illustrated in Fig. 5a. LLM agent policies lead to reductions in the ACR in almost all states, indicating suppression of active cases and an alleviation of healthcare system burdens. A similar downward pattern is observed for IR and DR, indicating reductions in transmissibility and mortality. By comparison, 8-week TIR delivers more stable and effective outcomes than 4-week TIR, especially in AL, AZ, AR, and IN. As noted earlier, SIS exhibits greater variability in its state-level effects. In some states, such as ID and NE, SIS achieves stronger outcomes than 8-week TIR, whereas in others (e.g., AR and OH) this strategy results in the weakest improvement among strategies. TIS exhibits relatively stable effects across states; however, because this strategy does not alter mobility volumes, its impact remains modest in some states like MS and TX.

At the aggregate level, the LLM multi-agent policymaking framework mitigates the pandemic burden by reducing total infection and death counts. By the end of 2020, cumulative infections and deaths across the 20 states can be reduced by more than  $2.6 \times 10^6$  and  $2.5 \times 10^4$ , respectively. Fig. 5b illustrates the temporal evolution of aggregate infections and deaths under different policy designs, with distinct colors representing alternative intervention trajectories. All four tested policymaking strategies outperform the ground-truth policy, with reductions becoming pronounced after September 2020. By comparison, 8-week TIR achieves the strongest improvement, followed by TIS. Notably, even the least effective intervention yields substantial system-level benefits, establishing a conservative lower bound on the effectiveness of coordinated policymaking at scale. To further demonstrate the control effects, we forecast cumulative infections and deaths over the subsequent 180 days under different policymaking. By that time, cumulative infections are reduced by approximately 47–53% relative to the ground-truth policy, while cumulative deaths decline by 58–62%. The detailed state-level results for total infection and deaths are listed in Supplementary Figs 29–48. These results underscore the sustained and long-term effectiveness of LLM-agent–enabled policymaking in mitigating pandemic outcomes.

## Discussion

Our work introduces an LLM multi-agent framework for coordinated pandemic policymaking, in which LLM agents serve as regional policy assistants that collaborate across administrative boundaries. In contrast to traditional approaches that rely on static rules or siloed policymaking<sup>31</sup>, the proposed framework enables coordinated policymaking by allowing agents to share regional pandemic situations and jointly make policies that regulate cross-region mobility over time. Empirical validation using COVID-19 data shows that this coordination-centric paradigm improves pandemic control compared with ground-truth, human-driven responses. Moreover, our framework is scalable and generalizable: it can be deployed at the national scale by instantiating each administrative unit as an autonomous agent, and beyond SEIQRD, it can accommodate diverse policy

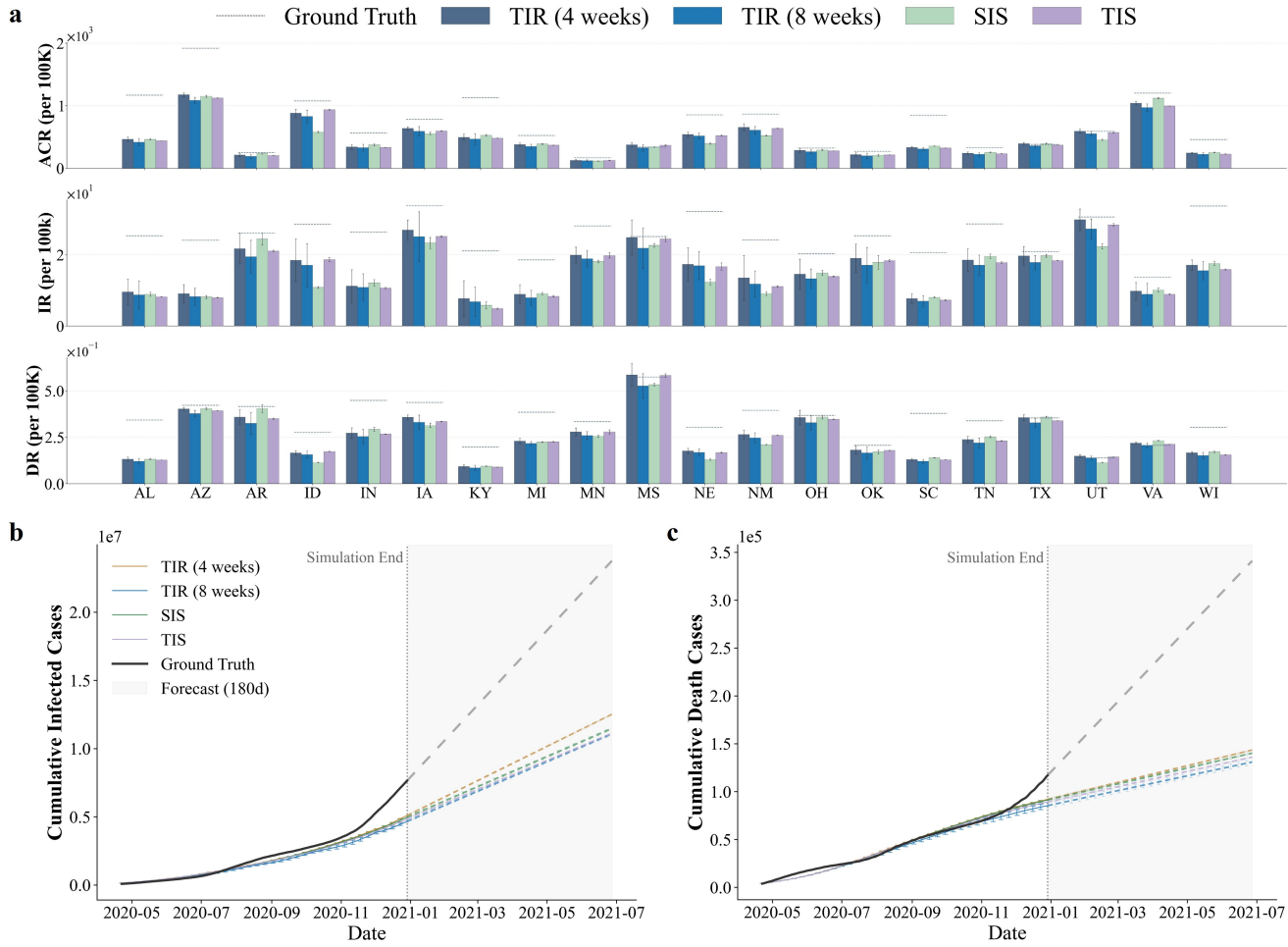


**Figure 5. Pandemic control performance in 20-state experiments.** **a**, State-level comparisons of the average daily active case rate (ACR), daily incidence rate (IR), and daily death rate (DR) across 20 states demonstrate the generalizability of the proposed framework. **b**, Total cumulative infected cases under the LLM agent-based policy are compared with the ground-truth outcomes over the study period. In addition, we project the evolution of cumulative infections over the subsequent 180 days under this intervention pattern to demonstrate the long-term performance.

interventions by incorporating different domain-specific simulators, without altering the underlying coordination and reasoning mechanisms. Together, these properties demonstrate the potential of LLM multi-agent systems for assisting real-world pandemic policymaking, particularly in mitigating the fragmentation and reactivity that characterize many conventional approaches.

Considering the diversity of LLMs, we evaluate the proposed framework using multiple LLM backbones while keeping the agent architecture and policy settings fixed. As shown in extended Fig. 6 in Appendix B, the framework exhibits consistent improvement across the tested models relative to ground-truth policymaking, although the magnitude and stability of these improvements vary across models. More capable models yield more coherent and balanced coordination effects across states, whereas less capable models exhibit greater variability in policy quality and regional outcomes. Therefore, LLM reasoning capacity remains essential for effective coordinated policymaking. In addition to LLM itself, system-level designs play a critical role in overall performance. The coordination protocol, such as the number of inter-agent communication rounds, directly affects the degree of strategic alignment across regions. Likewise, planning horizons determine the balance between anticipatory coordination and uncertainty accumulation: too short horizons limit forward-looking reasoning, while overly long horizons introduce additional noise. Therefore, effective coordinated policymaking emerges not from any single component alone, but from the interaction between LLM reasoning capability, coordination design, and planning horizon.

Despite these encouraging results, it is important to clarify the scope and limitations of the proposed framework. In practice, LLM agents operate within the bounds of their prompt design and learned representations<sup>32,33</sup>. When domain knowledge is incomplete, contextual signals are poorly specified, or coordination protocols are suboptimal, agent reasoning

may fail to capture critical system dynamics, leading to less effective policy recommendations. Beyond agent reasoning, real-world policy effectiveness may be further constrained by political, administrative, and logistical factors, as well as imperfect individual compliance, where travel and mobility decisions do not fully align with prescribed interventions. These execution and compliance frictions introduce discrepancies between simulated policies and their realized outcomes. Moreover, the policy interventions examined in this study operate primarily at a macro level and focus on regulating inter-regional mobility, representing only one dimension of real-world pandemic control. Real-world interventions often involve a broader and more heterogeneous set of measures, such as vaccination campaigns, mask mandates, testing strategies, and their combined deployment. Extending the framework to incorporate diverse interventions, and to reason over multimodal information, remains an important direction for future research.

Beyond pandemic control, the proposed framework may also inform a broader class of coordination problems involving interconnected regions or sectors that share resources, such as regional power grid load balancing<sup>34</sup>, traffic routing in urban networks<sup>35</sup>, or coordination of humanitarian aid flows<sup>36</sup>. In these domains, localized decision-making and inter-regional spillovers similarly give rise to system-level externalities that benefit from coordinated reasoning. By embedding domain-specific simulation models into each agent's reasoning process and aligning decisions through structured communication, LLM agents could support coordinated decision-making in a principled manner. Nevertheless, each new application would require careful modeling of domain dynamics and thoughtful prompt design. In this sense, our study does not claim direct applicability across domains, but rather illustrates a general paradigm: LLM agents can act as synthetic policy advisors that enable systematic reasoning over interconnected decisions. As LLM technology continues to evolve, more capable multi-agent architectures<sup>27</sup> may further enhance decision support in complex policy settings by complementing expert judgment and traditional optimization tools.

## Methods

### Raw Data Description

Multiple categories of data are applied within the LLM multi-agent policymaking framework, including spatial, epidemiological time-series, state-to-state human mobility flow, and public health policy data. All spatial data are provided at the state level, and all time-varying data are provided at daily resolution.

**Epidemiological time-series data.** State-level epidemiological time series were collected from April 12, 2020 to December 31, 2020. Each daily record is indexed by the state name and includes the latitude and longitude of the state's geographic centroid for visualization purposes. The dataset reports Confirmed cases and Deaths, which may include both confirmed and probable counts when available. Recovered cases are compiled from the COVID Tracking Project and may underestimate the true<sup>37</sup>. Active cases are calculated as confirmed cases minus recovered cases minus deaths.

**Human mobility flow data.** Human mobility flows were obtained as daily origin-destination (OD) records covering January 1, 2019, to April 15, 2021. Each record describes movements from an origin state to a destination state on a given date. For both origin and destination states, the latitude and longitude of the geographic centroid are provided. Two flow measures are included: the detected number of visitors traveling from origin to destination, and a corresponding population-flow estimate inferred from the detected flow. The latter is used as the daily state-to-state flow in this study.

**Public health policy data.** Public health policy data were compiled for each U.S. state from March 2020 to 2021 and stored as CSV files with daily updates. For each state and date, the dataset records policy categories and corresponding implementation details, including reopening status, mask mandates, health/medical measures, and social distancing, etc. Specifically, mobility-related policies are extracted with the assistance of an LLM and used as the ground-truth policy set (see the Supplementary Notes 1.4 and Tables 4-10 for the detailed prompts and corresponding results, respectively).

### Framework Design

We propose a decentralized, LLM multi-agent policymaking framework in which each administrative region is represented by an autonomous policy agent. The framework is designed to support coordinated sequential decision-making under heterogeneous regional conditions and explicit inter-regional coupling induced by population mobility (Fig. 1c).

**LLM agents as policy decision units.** Large language models can be viewed as parametric models that learn a conditional distribution over sequences,  $p_\theta(y | x)$ , where  $x$  denotes a contextual input expressed in natural language and  $y$  denotes the generated response. Through large-scale pretraining on diverse corpora, LLMs acquire latent representations that implicitly encode semantic regularities and causal patterns, enabling contextual reasoning over heterogeneous and partially structured information. In this sense, an LLM can be regarded as a flexible reasoning operator,  $y = f_\theta(x)$ , capable of synthesizing evidence, inferring relationships, and evaluating trade-offs without explicitly defined decision rules. An *agent* augments such a reasoning model with interaction and persistence. Formally, an agent can be defined as a tuple  $A = (O, f_\theta, P, T)$ , where  $O$  denotes the observation space,  $f_\theta$  is the LLM-based reasoning function,  $P$  is the policy action space, and  $T$  is a transition operator that maps actions to environment state changes. At each decision epoch  $t$ , the agent receives an observation  $o_t \in O$ , produces an action  $u_t = f_\theta(o_t)$ , and influences system evolution through  $T$ . This abstraction enables sequential decision-making with feedback, transforming LLMs from static predictors into goal-directed decision units.

**Agent-based policymaking architecture.** Let  $R = \{1, \dots, N\}$  denote the set of states. Each region  $i \in R$  is associated with an LLM-based policy agent  $A_i$ . At each decision epoch  $t$ , agent  $A_i$  observes a structured state representation

$$O_i(t) = (\mathbf{x}_i(t), \{\mathbf{x}_j(t)\}_{j \in N_i}, \mathbf{m}_{\rightarrow i}(t), \theta_i), \quad (1)$$

where  $\mathbf{x}_i(t)$  summarizes the local pandemic state of region  $i$ ,  $N_i$  denotes neighboring or epidemiologically coupled regions,  $\mathbf{m}_{\rightarrow i}(t)$  represents projected inbound mobility flows from other regions, and  $\theta_i$  encodes region-specific attributes such as population structure and healthcare capacity. These heterogeneous inputs are standardized and embedded into structured prompts that serve as the perception interface of each agent. Each agent reasons over its observation using an LLM to generate a policy proposal. Formally, the agent implements a mapping  $\pi_i : O_i(t) \rightarrow P_i(t)$ , where  $P_i(t)$  denotes the space of admissible policy actions for region  $i$ . In this work, actions primarily operate on inter-regional mobility as a controllable policy lever, although the framework is not limited to a single intervention modality.

**Multi-agent coordination and communication.** A key feature of the framework is explicit coordination among regional agents. Agents do not act in isolation; instead, they exchange summarized policy-relevant signals, including projected pandemic trends, risk assessments, and proposed interventions. This inter-agent communication induces a coupled decision process in

which each agent conditions its policy on the anticipated actions of others. We model coordination as an iterative message-passing process. At decision epoch  $t$ , each agent  $A_i$  broadcasts a message  $M_i(t) = \phi(O_i(t), P_i(t))$  to other agents, where  $\phi(\cdot)$  extracts salient information such as planned mobility adjustments or inferred transmission risk. Received messages  $\{M_j(t)\}_{j \neq i}$  are incorporated into the subsequent prompt context of agent  $i$ , allowing the LLM to reason about cross-regional spillovers and align decisions with system-level objectives. This communication mechanism enables decentralized yet coordinated policymaking: agents retain autonomy over regional decisions while implicitly negotiating policies through shared information and iterative reasoning.

**Policy parameterization and feasibility constraints.** To ensure realism and comparability with observed policies, agent actions are parameterized under explicit feasibility constraints. For the primary intervention studied—*Temporal Inflow Reallocation (TIR)*—each agent outputs a normalized allocation vector

$$p_i = (p_{i,1}, \dots, p_{i,H}), \quad \sum_{h=1}^H p_{i,h} = 1, \quad p_{i,h} > 0, \quad (2)$$

which specifies how the total inbound mobility volume over a planning horizon of  $H$  weeks is redistributed across time. Importantly, the aggregate inflow remains fixed, preserving economic and social plausibility while allowing agents to modulate *when* mobility occurs. The same agent architecture supports alternative intervention classes, such as *Spatial Inflow Suppression* or *Targeted Inbound Screening*, by modifying the action space  $P_i(t)$  while keeping the perception, reasoning, and coordination modules unchanged. This modularity enables systematic comparison across policy mechanisms within a unified framework.

**Closed-loop interaction with the simulation environment.** The proposed framework operates through an explicit closed-loop interaction between policy agents and a mechanistic pandemic simulation environment. At each decision epoch  $t$ , the simulator first evolves the pandemic dynamics forward using a calibrated pandemic transmission model,

$$\mathbf{X}(t+1) = \mathbf{T}(\mathbf{X}(t), \mathbf{M}(t)), \quad (3)$$

where  $\mathbf{T}$  denotes the transition operator induced by the mechanistic pandemic simulator;  $\mathbf{X}(t) = \{\mathbf{x}_i(t)\}_{i \in \mathcal{R}}$  denotes the collection of region-level SEIQRD states and  $\mathbf{M}(t) = \{\mathbf{m}_{\rightarrow i}(t)\}_{i \in \mathcal{R}}$  collects region-level inbound mobility flows. From the simulated SEIQRD trajectories, evaluation metrics such as active cases, incidence rate, and mortality are derived and provided to the agents as part of their observations. Conditioned on these evaluated pandemic indicators and the current mobility flows, LLM agents engage in multi-agent communication and reasoning to determine coordinated policy actions. For region  $i$ , the agent outputs a parameterized intervention  $p_i(t) \in P_i(t)$  that reallocates inbound mobility over the planning horizon. Let  $M_i$  denote the total inbound mobility volume of region  $i$ , which is preserved under a total volume constraint. The realized mobility after policy enactment is given by

$$m_{i,h}(t) = p_{i,h}(t) \cdot M_i, \quad \sum_{h=1}^H m_{i,h}(t) = M_i. \quad (4)$$

Once enacted, the updated mobility configuration  $\mathbf{M}(t+1)$  is fed back into the pandemic simulator, which re-evaluates disease transmission under the new policy setting. The resulting pandemic states  $\mathbf{X}(t+1)$  form the input to the next decision epoch, completing a closed observation–decision–transition loop. This iterative interaction enables agents to anticipate downstream consequences of policy choices, continuously adapt to evolving pandemic conditions, and refine coordinated interventions over time.

Overall, the proposed framework integrates structured data inputs, LLM agent reasoning, inter-agent communication, and constrained policy execution into a unified multi-agent decision system. This design allows coordinated, forward-looking policymaking to emerge endogenously from decentralized agent interactions, providing a flexible foundation for AI-assisted pandemic control.

## Epidemiological Modeling and Simulation

State-level pandemic dynamics are simulated using a discrete-time SEIQRD model with daily updates. For each state  $i$ , the population is partitioned into six compartments: susceptible  $S_i$ , exposed  $E_i$ , infected  $I_i$ , quarantined  $Q_i$ , recovered  $R_i$ , and deceased  $D_i$ . The model captures: 1) latent infection prior to infectiousness ( $E$ ), 2) isolation of detected infected individuals ( $Q$ ), and 3) mortality ( $D$ )<sup>30,38</sup>.

First,  $t$  denotes the day index, and  $\Delta t = 1\text{day}$ . The within-state force of infection is  $\lambda_{i,t} = \beta_i^I \frac{I_{i,t}}{N_{i,t}} + \beta_i^Q \frac{Q_{i,t}}{N_{i,t}}$ , where  $N_{i,t} = S_{i,t} + E_{i,t} + I_{i,t} + Q_{i,t} + R_{i,t}$  is the living population, and the  $\beta_i^I$  and  $\beta_i^Q$  is the transmission rate for infectious and quarantined individuals, respectively. Quarantined individuals are assumed to have lower onward transmission, i.e.,  $\beta_i^Q < \beta_i^I$ .

Next, to incorporate inter-state mobility,  $m_{j \rightarrow i,t}$  denotes the inbound flow from origin state  $j$  to destination state  $i$ <sup>29</sup>. Inter-state mobility affects the epidemic dynamics by redistributing individuals across compartments. The resulting daily compartment updates are:

$$S_{i,t+1} = S_{i,t} - (\lambda_{i,t} S_{i,t}) + \sum_{j \neq i} m_{j \rightarrow i,t} \frac{S_{j,t}}{N_{j,t}} - \sum_{j \neq i} m_{i \rightarrow j,t} \frac{S_{i,t}}{N_{i,t}}, \quad (5)$$

$$E_{i,t+1} = E_{i,t} + (\lambda_{i,t} S_{i,t}) - \sigma_i E_{i,t} + \sum_{j \neq i} m_{j \rightarrow i,t} \frac{E_{j,t}}{N_{j,t}} - \sum_{j \neq i} m_{i \rightarrow j,t} \frac{E_{i,t}}{N_{i,t}}, \quad (6)$$

$$I_{i,t+1} = I_{i,t} + \sigma_i E_{i,t} - (\delta_{i,t} + \gamma_{i,t} + \mu_{i,t}) I_{i,t} + \sum_{j \neq i} m_{j \rightarrow i,t} \frac{I_{j,t}}{N_{j,t}} - \sum_{j \neq i} m_{i \rightarrow j,t} \frac{I_{i,t}}{N_{i,t}}, \quad (7)$$

$$Q_{i,t+1} = Q_{i,t} + \delta_{i,t} I_{i,t} - (\gamma_{i,t} + \mu_{i,t}) Q_{i,t}, \quad (8)$$

$$R_{i,t+1} = R_{i,t} + \gamma_{i,t} I_{i,t} + \gamma_{i,t} Q_{i,t} + \sum_{j \neq i} m_{j \rightarrow i,t} \frac{R_{j,t}}{N_{j,t}} - \sum_{j \neq i} m_{i \rightarrow j,t} \frac{R_{i,t}}{N_{i,t}}, \quad (9)$$

$$D_{i,t+1} = D_{i,t} + \mu_{i,t} I_{i,t} + \mu_{i,t} Q_{i,t}. \quad (10)$$

Here,  $\sigma_i$  denotes the progression rate from the exposed to the infectious compartment,  $\delta_{i,t}$  represents the detection rate,  $\gamma_{i,t}$  is the recovery rate for infectious and quarantined individuals, and  $\mu_{i,t}$  denotes the mortality rate. Quarantined individuals are assumed not to be allowed to move across states. All parameters are calibrated using the ground-truth simulation (see Supplementary Note 1.5 for the detailed calibration strategy).

Policy interventions affect the pandemic dynamics by modulating 1) the inter-state mobility matrix  $m_{j \rightarrow i,t}$ , and 2) the effective detection rate  $\delta_{i,t}$  through targeted screening, thereby altering the transition from  $E$  and  $I$  to  $Q$ .

## Evaluation Metrics in Pandemic Control

**Cumulative metrics.** Total infections are measured using the cumulative quarantined count at the end of the simulation, reflecting the same case-recording practice adopted in official statistics to ensure fair comparison. Total deaths are defined as the cumulative number of deaths at the end of the simulation.

**Temporal indicators.** Daily incidence rate (IR), death rate (DR), and active case rate (ACR) are used to evaluate the performance of intervention in pandemic control<sup>39</sup>. IR measures the number of newly confirmed infections per day, capturing the short-term transmission intensity of the pandemic<sup>40</sup>.

$$\text{IR}_{i,t} = \frac{Q_{i,t+1} - Q_{i,t}}{N_i}. \quad (11)$$

ACR quantifies the number of currently active confirmed infections, defined as the population remaining in quarantined compartments. ACR reflects the ongoing disease burden on the healthcare system and is closely associated with hospital occupancy and resource utilization<sup>41</sup>.

$$\text{ACR}_{i,t} = \frac{Q_{i,t}}{N_i}. \quad (12)$$

DR measures daily new deaths per capita and serves as a key indicator of severe outcomes

$$\text{DR}_{i,t} = \frac{D_{i,t+1} - D_{i,t}}{N_i}, \quad (13)$$

The effectiveness of each policy is also evaluated using the average IR, ACR, and DR across all time periods for a overall assessment.

## Estimation of the Effective Reproduction Number $R_t$

The effective (time-varying) reproduction number  $R_t$  is estimated from the daily observed incidence series using a renewal-process formulation with Bayesian updating, following the widely used framework for real-time transmissibility inference<sup>42,43</sup>.  $Q'_t = Q_t - Q_{t-1}$  denotes the number of newly infected (incident) cases on day  $t$ . Incident infections on day  $t$  arise from past infections weighted by a discretized serial interval distribution.

**Discrete serial interval.** The serial interval is modeled as a Gamma distribution with mean  $\mu_{\text{SI}} = 5$  days and standard deviation  $\sigma_{\text{SI}} = 2$  days, reflecting the typical delay between symptom onset in an exposed case and symptom onset in infected cases<sup>44</sup>. The corresponding Gamma shape and scale parameters are  $k = \left(\frac{\mu_{\text{SI}}}{\sigma_{\text{SI}}}\right)^2$ ,  $\theta = \frac{\sigma_{\text{SI}}^2}{\mu_{\text{SI}}}$ . This distribution is discretized into daily probabilities over lags  $s = 1, \dots, S$  with  $S = 20$  days:

$$w_s = F_{\Gamma}(s; k, \theta) - F_{\Gamma}(s-1; k, \theta), \quad s = 1, \dots, S, \quad (14)$$

where  $F_{\Gamma}(\cdot; k, \theta)$  is the Gamma cumulative distribution function. The weights are normalized such that  $\sum_{s=1}^S w_s = 1$ .

**Renewal equation and infectiousness.** Define the total infectiousness (renewal intensity) on day  $u$  as  $\Lambda_u = \sum_{s=1}^S Q'_{u-s} w_s$ , with the convention  $Q'_{u-s} = 0$  when  $u - s < 0$ . Under the renewal model, conditional on  $R_u$ , the incidence satisfies

$$Q'_u | R_u \sim \text{Poisson}(R_u \Lambda_u). \quad (15)$$

**Sliding-window Bayesian inference.** To stabilize estimation,  $R_t$  is assumed to be constant within a sliding window of length  $W = 21$  days. For each evaluation time  $t \geq W$ ,  $Q_{\Sigma}^{(t)} = \sum_{u=t-W}^{t-1} Q'_u$ , and  $\Lambda_{\Sigma}^{(t)} = \sum_{u=t-W}^{t-1} \Lambda_u$ . A Gamma prior is placed on  $R_t$ ,  $R_t \sim \text{Gamma}(a, b)$ , where  $a = 1$  and  $b = 1$  denote the prior shape and rate parameters, respectively. Combining the Poisson likelihood with the Gamma prior yields a conjugate Gamma posterior<sup>45</sup>:

$$R_t | \{Q'_u\}_{u=t-W}^{t-1} \sim \text{Gamma}\left(a + Q_{\Sigma}^{(t)}, b + \max(\Lambda_{\Sigma}^{(t)}, \varepsilon)\right), \quad (16)$$

where  $\varepsilon$  is a small positive constant to avoid numerical instability.

**Point and interval estimates.** The posterior mean of  $R_t$  is  $\hat{R}_t = \mathbb{E}[R_t | \cdot] = \frac{a + Q_{\Sigma}^{(t)}}{b + \max(\Lambda_{\Sigma}^{(t)}, \varepsilon)}$ . A 95% credible interval  $[\hat{R}_t^{\text{low}}, \hat{R}_t^{\text{high}}]$  is kept, using the 2.5% and 97.5% posterior quantiles of the Gamma distribution in Eq. (16). The above procedure produces a time series of  $\hat{R}_t$  and its uncertainty bounds.

## Policy Type Classification

To characterize the qualitative patterns of adaptive policy responses, policy outputs are categorized into three representative types based on their temporal allocation under TIR<sup>46</sup>. Taking 6-week TIR for illustration, each policy response specifies weekly reallocation levels for each state over a six-week planning horizon.

First,  $\mathbf{p}_i = [p_{i,1}, \dots, p_{i,6}]$  denotes the six-week policy sequence for state  $i$ , where  $p_{i,h}$  indicates the proportion of inbound mobility allocated to week  $h$  within the planning horizon and  $\sum_{h \in \{1, \dots, 6\}} p_{i,h} = 1$ . The six-length proportions are aggregated into three consecutive periods, corresponding to the early, middle, and late phases of the planning horizon.  $[\bar{p}_i^1, \bar{p}_i^2, \bar{p}_i^3]$  represent weeks 1–2, 3–4, and 5–6, respectively. Here, the subscript  $t$  is omitted for clarity.

Next, each policy instance is classified into one of three types:

- **Strict-first:** policies allowing relatively low inbound flow in the early period but higher inflow in the late period, defined by  $\bar{p}_i^1 \leq 0.3$  and  $\bar{p}_i^3 \geq 0.4$ ;
- **Relaxed-first:** policies characterized by relaxed early interventions followed by restriction in later stages, defined by  $\bar{p}_i^1 \geq 0.4$  and  $\bar{p}_i^3 \leq 0.3$ ;
- **Balanced:** all remaining policies that do not exhibit a pronounced shift toward either early strictness or late strictness.

## Feature Attribution on Policy Type

To interpret the determinants underlying the emergence of *strict-first* policy patterns, a feature attribution analysis is conducted using Shapley values. The propensity of adopting a strict-first policy is modeled as a supervised learning task, in which a tree-based ensemble model maps contextual features to the corresponding policy classification outcome<sup>47</sup>.

Feature contributions are quantified using Shapley additive explanations, which attribute the prediction of a model to individual input features based on cooperative game theory<sup>48</sup>.  $f(\mathbf{x})$  denotes the trained prediction function and  $\mathbf{F} = \{1, \dots, M\}$  the set of input features. The Shapley value for feature  $j$  is defined as

$$\phi_j = \sum_{S \subseteq \mathbf{F} \setminus \{j\}} \frac{|S|!(M-|S|-1)!}{M!} [f(\mathbf{x}_{S \cup \{j\}}) - f(\mathbf{x}_S)], \quad (17)$$

where  $S$  denotes a subset of features excluding  $j$ , and  $\mathbf{x}_S$  represents the input vector in which only features in  $S$  are present. This formulation measures the expected marginal contribution of feature  $j$  across all possible feature coalitions.

## Equity Coefficient Calculation

To quantify the equity of policy-induced benefits across states, an *equity coefficient* is defined based on the Gini index, which measures the dispersion of improvements among states<sup>49</sup>. The coefficient is computed separately for total infections and total deaths.

**Improvement of state.**  $G_i^{\text{inf}}$  and  $G_i^{\text{dea}}$  is the cumulative total infections and deaths observed in the ground-truth scenario ( $i \in \{1, \dots, N\}$  index states), while  $A_i^{\text{inf}}$  and  $A_i^{\text{dea}}$  is the corresponding cumulative outcomes under the agent-based policy at the end of the simulation. The relative improvement in total infections and deaths for state  $i$  is

$$\Delta_i^{\text{inf}} = \frac{G_i^{\text{inf}} - A_i^{\text{inf}}}{\max(|G_i^{\text{inf}}|, \epsilon)}, \quad \Delta_i^{\text{dea}} = \frac{G_i^{\text{dea}} - A_i^{\text{dea}}}{\max(|G_i^{\text{dea}}|, \epsilon)}, \quad (18)$$

where  $\epsilon$  is a small positive constant to avoid numerical instability. To ensure that the equity measure reflects, only the distribution of benefits, we focus on non-negative improvements:

$$\Delta_i^{\text{inf},+} = \max(\Delta_i^{\text{tot}}, 0), \quad \Delta_i^{\text{dea},+} = \max(\Delta_i^{\text{dea}}, 0). \quad (19)$$

**Gini-based equity coefficient.** Given a non-negative improvement vector  $\mathbf{x} = (x_1, \dots, x_N)$ , the Gini coefficient is defined as

$$G(\mathbf{x}) = \frac{1}{N \sum_{r=1}^N x_r} \sum_{r=1}^N (2r - N - 1) x_r, \quad (20)$$

where  $x_r$  denotes the  $r$ -th smallest element of  $\mathbf{x}$ . A smaller Gini coefficient indicates a more equal distribution of improvements across states<sup>50</sup>.

The equity coefficient is defined as  $E(\mathbf{x}) = 1 - G(\mathbf{x})$ , such that larger values indicate greater equity, with  $E = 1$  corresponding to perfectly equal benefit allocation. Applying this definition to infection and death reductions yields

$$E^{\text{inf}} = 1 - G(\{\Delta_i^{\text{inf},+}\}_{i=1}^N), \quad E^{\text{dea}} = 1 - G(\{\Delta_i^{\text{dea},+}\}_{i=1}^N). \quad (21)$$

## Forecasting Subsequent 180-Day Cumulative Infections and Deaths

To facilitate a consistent comparison of long-term outcomes across policies, cumulative infections and deaths are extrapolated up to 180 days beyond the simulation horizon using a local trend-based approach<sup>51,52</sup>.  $C_t$  denotes the cumulative number of infections or deaths at day  $t$ . The local daily growth rate is estimated as the average increment over the most recent 14 days,

$$\bar{c}_t = \frac{1}{14} \sum_{i=1}^{14} (C_{t-i+1} - C_{t-i}). \quad (22)$$

Cumulative outcomes are extrapolated recursively for  $h = 1, \dots, 180$  days according to

$$C_{t+h} = C_{t+h-1} + \bar{c}_t, h \in \{1, \dots, 180\}. \quad (23)$$

## Competing interests

The authors declare no competing interests.

## References

1. Asthana, S. *et al.* Decision-making under epistemic, strategic and institutional uncertainty during covid-19: findings from a six-country empirical study. *BMJ Glob. Heal.* **10** (2025).
2. Holtz, D. *et al.* Interdependence and the cost of uncoordinated responses to covid-19. *Proc. Natl. Acad. Sci.* **117**, 19837–19843 (2020).
3. Graff Zivin, J. & Sanders, N. The spread of covid-19 shows the importance of policy coordination. *Proc. Natl. Acad. Sci.* **117**, 32842–32844 (2020).
4. Flaxman, S. *et al.* Estimating the effects of non-pharmaceutical interventions on covid-19 in europe. *Nature* **584**, 257–261 (2020).
5. Chang, S. L., Harding, N., Zachreson, C., Cliff, O. M. & Prokopenko, M. Modelling transmission and control of the covid-19 pandemic in australia. *Nat. communications* **11**, 5710 (2020).
6. Kissler, S. M., Tedijanto, C., Goldstein, E., Grad, Y. H. & Lipsitch, M. Projecting the transmission dynamics of sars-cov-2 through the postpandemic period. *Science* **368**, 860–868 (2020).
7. Prem, K. *et al.* The effect of control strategies to reduce social mixing on outcomes of the covid-19 epidemic in wuhan, china: a modelling study. *The lancet public health* **5**, e261–e270 (2020).
8. Domenici, I. & Villarreal, P. A. The fragmented nature of pandemic decision-making: A comparative and multilevel legal analysis. *Eur. J. Heal. Law* **29**, 1–5 (2022).
9. Sacco, P. L., Valle, F. & De Domenico, M. Proactive vs. reactive country responses to the covid-19 pandemic shock. *PLOS Glob. Public Heal.* **3**, e0001345 (2023).
10. Pacces, A. M. & Weimer, M. From diversity to coordination: A european approach to covid-19. *Eur. journal risk regulation* **11**, 283–296 (2020).
11. Althouse, B. M. *et al.* The unintended consequences of inconsistent closure policies and mobility restrictions during epidemics. *BMC Glob. Public Heal.* **1**, 28 (2023).
12. Lu, Y. & Giuliano, G. Understanding mobility change in response to covid-19: A los angeles case study. *Travel. Behav. Soc.* **31**, 189–201 (2023).
13. van der Zanden, B., Kauhl, B., Hackert, V. & Hoebe, C. J. Four million covid-19 cases in four european cross-border regions reveal minimal cross-border transmission effect on domestic burden: space-time cluster analysis. *BMC Infect. Dis.* **25**, 1528 (2025).
14. Perofsky, A. C. *et al.* Impacts of human mobility on the citywide transmission dynamics of 18 respiratory viruses in pre-and post-covid-19 pandemic years. *Nat. communications* **15**, 4164 (2024).
15. Ruktanonchai, N. W. *et al.* Assessing the impact of coordinated covid-19 exit strategies across europe. *Science* **369**, 1465–1470 (2020).
16. Sachs, J. D. *et al.* The lancet commission on lessons for the future from the covid-19 pandemic. *The Lancet* **400**, 1224–1280 (2022).
17. Ferguson, N. M. *et al.* Strategies for mitigating an influenza pandemic. *Nature* **442**, 448–452 (2006).
18. McKee, M., Rosenbacke, R. & Stuckler, D. The power of artificial intelligence for managing pandemics: A primer for public health professionals. *The Int. journal health planning management* **40**, 257–270 (2025).
19. Bicher, M. *et al.* Supporting covid-19 policy-making with a predictive epidemiological multi-model warning system. *Commun. medicine* **2**, 157 (2022).
20. Zhao, W. X. *et al.* A survey of large language models. *arXiv preprint arXiv:2303.18223* **1** (2023).
21. Saeed, F., Aldosari, M., Arpinar, I. B. & Miller, J. A. Llm4cast: repurposed llm for viral disease forecasting. In *2024 IEEE International Conference on Big Data (BigData)*, 1428–1433 (IEEE, 2024).
22. Du, H. *et al.* Advancing real-time infectious disease forecasting using large language models. *Nat. Comput. Sci.* 1–14 (2025).
23. Kwok, K. O. *et al.* Utilizing large language models in infectious disease transmission modelling for public health preparedness. *Comput. Struct. Biotechnol. J.* **23**, 3254–3257 (2024).
24. Williams, R., Hosseinichimeh, N., Majumdar, A. & Ghaffarzadegan, N. Epidemic modeling with generative agents. *arXiv preprint arXiv:2307.04986* (2023).

25. Zhou, Z., Yang, T. & Hu, K. Traditional chinese medicine epidemic prevention and treatment question-answering model based on llms. In *2023 IEEE International Conference on Bioinformatics and Biomedicine (BIBM)*, 4755–4760 (IEEE, 2023).
26. Consoli, S. *et al.* Epidemic information extraction for event-based surveillance using large language models. In *International Congress on Information and Communication Technology*, 241–252 (Springer Nature Singapore Singapore, 2024).
27. Guo, T. *et al.* Large language model based multi-agents: A survey of progress and challenges. *arXiv preprint arXiv:2402.01680* (2024).
28. Chopra, A., Kumar, S., Giray-Kuru, N., Raskar, R. & Quera-Bofarull, A. On the limits of agency in agent-based models. *arXiv preprint arXiv:2409.10568* (2024).
29. Wang, J., Wang, X. & Wu, J. Inferring metapopulation propagation network for intra-city epidemic control and prevention. In *Proceedings of the 24th ACM SIGKDD international conference on knowledge discovery & data mining*, 830–838 (2018).
30. Balcan, D. *et al.* Multiscale mobility networks and the spatial spreading of infectious diseases. *Proc. national academy sciences* **106**, 21484–21489 (2009).
31. Berger, L. *et al.* Rational policymaking during a pandemic. *Proc. Natl. Acad. Sci.* **118**, e2012704118 (2021).
32. Zhao, A. *et al.* Expel: Llm agents are experiential learners. In *Proceedings of the AAAI Conference on Artificial Intelligence*, vol. 38, 19632–19642 (2024).
33. Sahoo, P. *et al.* A systematic survey of prompt engineering in large language models: Techniques and applications. *arXiv preprint arXiv:2402.07927* (2024).
34. Rahman, A., Liu, X. & Kong, F. A survey on geographic load balancing based data center power management in the smart grid environment. *IEEE Commun. Surv. & Tutorials* **16**, 214–233 (2013).
35. Garroso, M. T., Kalac, M. & Lorenzen, T. Geo-routing in urban vehicular ad-hoc networks: A literature review. In *2017 International Conference on Computing, Networking and Communications (ICNC)*, 865–871 (IEEE, 2017).
36. Akhtar, P., Marr, N. & Garnevska, E. Coordination in humanitarian relief chains: chain coordinators. *J. humanitarian logistics supply chain management* **2**, 85–103 (2012).
37. Dong, E., Du, H. & Gardner, L. An interactive web-based dashboard to track covid-19 in real time. *The Lancet infectious diseases* **20**, 533–534 (2020).
38. Tan, Y., Zhang, Y., Cheng, X. & Zhou, X.-H. Statistical inference using gleam model with spatial heterogeneity and correlation between regions. *Sci. Reports* **12**, 16630 (2022).
39. Cabezudo-García, P. *et al.* Incidence and case fatality rate of covid-19 in patients with active epilepsy. *Neurology* **95**, e1417–e1425 (2020).
40. Xiong, C., Hu, S., Yang, M., Luo, W. & Zhang, L. Mobile device data reveal the dynamics in a positive relationship between human mobility and covid-19 infections. *Proc. Natl. Acad. Sci.* **117**, 27087–27089 (2020).
41. Li, Z. *et al.* Active case finding with case management: the key to tackling the covid-19 pandemic. *The lancet* **396**, 63–70 (2020).
42. Cori, A., Ferguson, N. M., Fraser, C. & Cauchemez, S. A new framework and software to estimate time-varying reproduction numbers during epidemics. *Am. journal epidemiology* **178**, 1505–1512 (2013).
43. Thompson, R. N. *et al.* Improved inference of time-varying reproduction numbers during infectious disease outbreaks. *Epidemics* **29**, 100356 (2019).
44. Yin, M.-Z., Zhu, Q.-W. & Lü, X. Parameter estimation of the incubation period of covid-19 based on the doubly interval-censored data model. *Nonlinear Dyn.* **106**, 1347–1358 (2021).
45. Ghahramani, Z. Probabilistic machine learning and artificial intelligence. *Nature* **521**, 452–459 (2015).
46. Nouvellet, P. *et al.* Reduction in mobility and covid-19 transmission. *Nat. communications* **12**, 1090 (2021).
47. Chan, J. C.-W. & Paelinckx, D. Evaluation of random forest and adaboost tree-based ensemble classification and spectral band selection for ecotope mapping using airborne hyperspectral imagery. *Remote. Sens. Environ.* **112**, 2999–3011 (2008).
48. Zhao, Y., Wang, P., Zhao, Y., Du, H. & Yang, H. F. Safetraffic copilot: adapting large language models for trustworthy traffic safety assessments and decision interventions. *Nat. Commun.* **16**, 8846 (2025).

49. Scheffer, M., Van Bavel, B., van de Leemput, I. A. & van Nes, E. H. Inequality in nature and society. *Proc. Natl. Acad. Sci.* **114**, 13154–13157 (2017).
50. Blesch, K., Hauser, O. P. & Jachimowicz, J. M. Measuring inequality beyond the gini coefficient may clarify conflicting findings. *Nat. human behaviour* **6**, 1525–1536 (2022).
51. Xia, Y. *et al.* Future reductions of china's transport emissions impacted by changing driving behaviour. *Nat. Sustain.* **6**, 1228–1236 (2023).
52. Althoff, T. *et al.* Countrywide natural experiment links built environment to physical activity. *Nature* **645**, 407–413 (2025).

## A Structured Prompts

Here, an example prompt for 6-week TIR is provided.

### # System Guidance:

You are the epidemic control & mobility policy assistant for state *Arizona*. Your task is to recommend traffic control policies for this state to slow disease spread. For each origin state, determine the inbound traffic allocation into *Arizona* for the next 6 weeks. Total inbound Flow over 6 weeks must stay constant (equal to the ground truth); you may adjust weekly proportions.

### # Inputs:

You will be given the following information for your task:

- **State-level pandemic statistics:** The current population composition of the state *Arizona* and its neighboring states, including Susceptible (S), Exposed (E), Infected (I), Confirmed (Q), Recovered (R), Deaths (D)
- **Historical inter-state mobility information:** Past 21-day average daily inbound flow (from other state to *Arizona*)
- **Planning-horizon mobility baselines:** average daily inbound flow for the upcoming 42 days

### # Constraints:

You need to consider the following constraints:

- output *six* fractions for each origin state  $i$ ,  $[p_{i,1}, p_{i,2}, p_{i,3}, p_{i,4}, p_{i,5}, p_{i,6}]$  with  $\sum_{m \in \{1, \dots, 6\}} p_{i,m} = 1$ , and  $p_{i,m} > 0$  ;
- Week  $m$  inbound flow from origin state  $i$  = Total Flow \*  $p_{i,m}$
- Low  $p_{i,m}$  means strict mobility control; high  $p_{i,m}$  means relaxed control

### # Final Output:

Organize your final answer as following:

- **think\_process:** up to 200 words summary of reasoning process.
- **refined\_solution:** {"state\_i":  $[p_{i,1}, p_{i,2}, p_{i,3}, p_{i,4}, p_{i,5}, p_{i,6}]$ , ...}

## B Performance Comparison across LLM Models

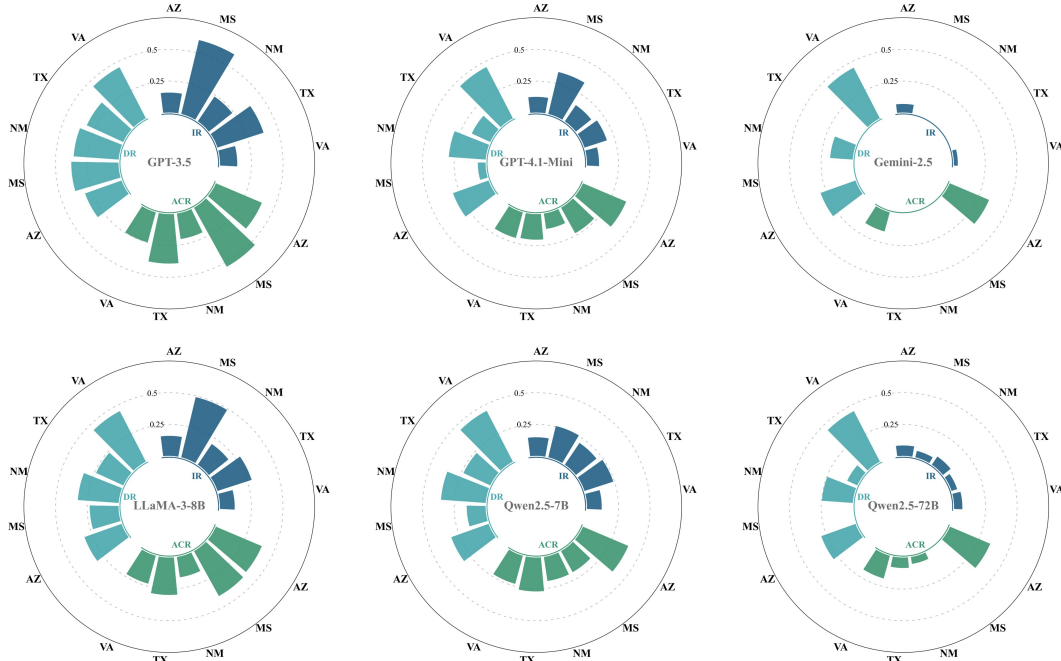


**Figure 6. Performance Comparison across LLM Models.** The proposed framework is tested with different LLM models, including GPT-3.5, GPT-4.1-Mini, Gemini-2.5, LLaMA-3-8B, Qwen2.5-7B, and Qwen2.5-72B. The improvement of DR, IR, and ACR, compared to the ground-truth policymaking in different states, is illustrated. GPT-3.5, GPT-4.1-Mini, LLaMA-3-8B, and Qwen-2.5-7B exhibit stable performance in pandemic control across states.

# Coordinated Pandemic Control with Large Language Model Agents as Policymaking Assistants

Ziyi Shi<sup>1,†</sup>, Xusen Guo<sup>2,†</sup>, Hongliang Lu<sup>1,\*</sup>, Mingxing Peng<sup>2</sup>, Haotian Wang<sup>2</sup>, Zheng Zhu<sup>3</sup>,  
Zhenning Li<sup>4</sup>, Yuxuan Liang<sup>2</sup>, Xinhua Zheng<sup>2</sup>, and Hai Yang<sup>1,\*</sup>

<sup>1</sup>The Hong Kong University of Science and Technology, Hong Kong

<sup>2</sup>The Hong Kong University of Science and Technology (Guangzhou), China

<sup>3</sup>Zhejiang University, China

<sup>4</sup>University of Macau, Macau

\*corresponding authors: Hongliang Lu and Hai Yang

†These authors contributed equally to this work

## Contents

<b>1</b>	<b>Supplementary Notes</b>	<b>2</b>
1.1	Prompt for intervention of TIR	2
1.2	Prompt for intervention of SIS	3
1.3	Prompt for intervention of TIS	4
1.4	LLM-assisted extraction of ground-truth mobility policies	5
1.5	Pandemic simulation calibration	6
<b>2</b>	<b>Supplementary Figures</b>	<b>8</b>
<b>3</b>	<b>Supplementary Tables</b>	<b>52</b>

# 1. Supplementary Notes

## 1.1 Prompt for intervention of TIR

Here, a structured prompt for TIR (Temporal Inflow Reallocation) strategy is provided. This prompt guides the LLM agent to adjust the weekly fraction inflow for the subsequent  $M$  weeks.

Beyond the control action itself, the agent is required to output an explicit *decision rationale* at each decision round to support interpretability and auditing (Jiang et al. 2025; Guo et al. 2025). Specifically, for every policy decision, the agent returns (i) the selected intervention (e.g., target origin state and inflow adjustment), and (ii) a structured explanation describing *why* this action is chosen given the current system state.

### # System Guidance:

You are the epidemic control & mobility policy assistant for *state name*. Your task is to recommend traffic control policies for this state to slow disease spread. For each origin state, determine the inbound traffic allocation into *state name* for the next  $M$  weeks. Total inbound Flow over  $M$  weeks must stay constant (equal to the ground truth); you may adjust weekly proportions.

### # Inputs:

You will be given the following information for your task:

- **State-level pandemic statistics:** The current population composition of the state *state name* and its neighboring states, including Susceptible (S), Exposed (E), Infected (I), Confirmed (Q), Recovered (R), Deaths (D)
- **Historical inter-state mobility information:** Past 21-day average daily inbound flow (from other state to *state name*)
- **Planning-horizon mobility baselines:** average daily inbound flow for the upcoming  $M$  weeks

### # Constraints:

You need to consider the following constraints:

- output *six* fractions for each origin state  $i$ ,  $[p_{i,1}, p_{i,2}, p_{i,3}, p_{i,4}, \dots, p_{i,M}]$  with  $\sum_m p_{i,m} = 1$ , and  $p_{i,m} > 0$  ;
- Week  $m$  inbound flow from origin state  $i$  = Total Flow \*  $p_{i,m}$
- Low  $p_{i,m}$  means strict mobility control; high  $p_{i,m}$  means relaxed control

### # Intervention Reasoning:

Include concise but explicit reasoning covering,

- Risk assessment of each origin state using SEIQRD indicators.
- Quantitative import logic with explaining expected imported infections.
- Choose one pattern: balanced / strict-first / relaxed-first/ or others to describe the traffic allocation, and explain why (Justify the pattern using infection pressure trends.)

### # Final Output:

Organize your final answer as following:

- **think\_process:** up to 200 words summary of reasoning process.
- **refined\_solution:**  $\{ \text{"state\_i": } [p_{i,1}, p_{i,2}, p_{i,3}, p_{i,4}, \dots, p_{i,M}], \dots \}$

## 1.2 Prompt for intervention of SIS

A structured prompt is used for the SIS (Spatial Inflow Suppression) strategy, directing the agent to reduce inbound flow (by  $\alpha\%$ ) from at most one selected origin state for the next  $M$  weeks (Oh et al. 2021).

### # System Guidance:

You are the epidemic control & mobility policy assistant for *state name*. Your task is to recommend traffic control policies for this state to slow disease spread. For next  $M$  weeks, you may choose at most one origin state to apply a temporary inbound travel restriction. If an origin state is selected, its inbound flow into *state name* in the next  $M$  weeks is reduced by  $\alpha\%$ . The reduced portion of this flow is not eliminated, but may be reallocated to other destination states according to the baseline mobility structure of the origin state. If no origin state is selected, all origin states keep their baseline inbound flow in the next  $M$  weeks.

### # Inputs:

You will be given the following information for your task:

- **State-level pandemic statistics:** The current population composition of the state *state name* and its neighboring states, including Susceptible (S), Exposed (E), Infected (I), Confirmed (Q), Recovered (R), Deaths (D)
- **Historical inter-state mobility information:** Past 21-day average daily inbound flow (from other state to *state name*)
- **Planning-horizon mobility baselines:** average daily inbound flow for the upcoming  $M$  weeks

### # Constraints:

You need to consider the following constraints:

- At most one origin state is selected for restriction.
- Week  $m$  inbound flow from the restricted origin state = Initial Flow \*  $\alpha$ .

### # Intervention Reasoning:

Include concise but explicit reasoning covering,

- Risk assessment of each origin state using SEIQRD indicators.
- Quantitative import logic with explaining expected imported infections.
- Justification of the selection.

### # Final Output:

Organize your final answer as following:

- **think\_process:** up to 200 words summary of reasoning process.
- **refined\_solution:** {"restricted state": "state\_i"}

### 1.3 Prompt for intervention of TIS

A structured prompt is used for the TIS (Targeted Inbound Screening) strategy, directing the agent to screen ( $\beta\%$ ) inbound flow from at most one selected origin state for the next  $M$  weeks (Figueroa et al. 2021).

#### # System Guidance:

You are the epidemic control & mobility policy assistant for *state name*. Your task is to recommend traffic control policies for this state to slow disease spread. For next  $M$  weeks, you may choose at most one origin state to apply a Targeted Inbound Screening policy. If an origin state is selected, for travelers who still enter *state name* in next  $M$  weeks, a rigorous  $\beta\%$  screening mandate is enforced. This screening identifies and moves individuals from the Exposed (E) and Infected (I) compartments directly into the Confirmed (Q) compartment upon arrival. This significantly reduces the "hidden" infectious population entering your community. If no origin state is selected, all inbound flows remain at baseline, and no enhanced screening occurs at the border.

#### # Inputs:

You will be given the following information for your task:

- **State-level pandemic statistics:** The current population composition of the state *state name* and its neighboring states, including Susceptible (S), Exposed (E), Infected (I), Confirmed (Q), Recovered (R), Deaths (D)
- **Historical inter-state mobility information:** Past 21-day average daily inbound flow (from other state to *state name*)
- **Planning-horizon mobility baselines:** average daily inbound flow for the upcoming  $M$  weeks

#### # Constraints:

You need to consider the following constraints:

- At most one origin state is selected for restriction.
- In week  $m$ , a fraction  $\beta\%$  of the inbound flow from the restricted origin state is screened. Upon arrival, screened individuals in the Exposed (E) or Infected (I) compartments are immediately transferred to the Confirmed (Q) compartment.

#### # Intervention Reasoning:

Include concise but explicit reasoning covering,

- Risk assessment of each origin state using SEIQRD indicators.
- Quantitative import logic with explaining expected imported infections.
- Justification of the selection.

#### # Final Output:

Organize your final answer as following:

- **think\_process:** up to 200 words summary of reasoning process.
- **refined\_solution:** {"restricted state": "state\_i"}

## 1.4 LLM-assisted extraction of ground-truth mobility policies

Mobility-related COVID-19 interventions were extracted from state policy logs stored as CSV files using a dialogue-box (prompted) LLM workflow. For each state, the CSV content was provided to the LLM together with a fixed prompt specifying (i) the inclusion criterion for “mobility-related” measures and (ii) a standardized output schema. The model was instructed to return a table with five fields (Date, Policy, Description, Primary mobility impact, Source), and missing fields were left blank.

An LLM was used in place of fully manual coding to improve scalability and procedural consistency across states. Policy narratives vary substantially in phrasing and granularity; prompt-based extraction enables semantically equivalent measures to be normalized into a uniform schema using the same inclusion rules, reducing inter-coder variability and manual workload while maintaining traceability through retained source links.

### # System Guidance:

You are the mobility-policy extraction assistant. Your task is to scan multiple state `policy.csv` files (e.g., `*_policies_2020_EN.csv`) and extract all policies that are *mobility-related*, i.e., any policy that directly affects human movement/travel (e.g., stay-at-home/curfew, travel restrictions, closures/re-openings that change trips, gathering limits, entry quarantine/testing, transit rules). For each extracted policy, generate one record and consolidate all records into a single table with columns: *Date*, *Policy*, *Description*, *Primary mobility impact*, *Source*.

### # Inputs:

You will be given the following information for your task:

- **State policy CSV files:** one or more `policy.csv` files, each containing dated policy entries and (optionally) descriptions, mobility impact notes, and source URLs.

### # Constraints:

You need to consider the following constraints:

- **Inclusion rule:** Only include policies that directly influence mobility/flows/travel/commuting/access to venues.
- **No fabrication:** Do not invent dates, policy content, mobility impacts, or URLs.
- **Missing fields:** If a required field is absent in the CSV, leave that cell blank.
- **Multiple sources:** If multiple URLs exist for one policy, keep all and separate them with semicolons.
- **Ordering:** Sort the final consolidated table by **Date (ascending)**.

### # Final Output:

Organize your final answer as following:

- **refined\_solution:** a single consolidated table with columns { "Date", "Policy", "Description", "Primary mobility impact", "Source" }, sorted by Date ascending, output in the requested format (CSV).

## 1.5 Pandemic simulation calibration

**Overview.** A two-stage calibration strategy is adopted to identify epidemiological parameters for the multi-state SEIRD simulation. The key rationale is to decouple (i) within-state disease dynamics, which can be reliably inferred from state-level epidemic time series, from (ii) mobility-induced spatial coupling, which modifies the effective force of infection and therefore requires a system-level re-calibration. This staged procedure improves numerical stability, mitigates parameter non-identifiability, and provides informative initialization for large-scale optimization.

**Stage 1: within-state SEIQRD fitting (mobility-agnostic baseline).** In Stage 1, each state is calibrated independently under a mobility-agnostic SEIQRD model to obtain baseline parameter estimates (Alleman et al. 2021).  $\theta = \{\beta, \delta, \gamma, \mu, \dots\}$  denote the set of epidemiological and surveillance-related parameters, where  $\beta$  is the transmission rate and  $\delta$  is the case detection (or confirmation) rate; the remaining parameters describe progression, recovery, and mortality processes. For each state  $i$ , baseline estimates  $\theta_i^{(0)}$  are obtained by minimizing the discrepancy between simulated trajectories and observed epidemic time series (e.g., cases and deaths) within the state. This step yields state-specific parameters reflecting local transmission intensity and reporting characteristics under a closed-population approximation.

**Stage 2: mobility-aware re-calibration (system-level refinement).** In Stage 2, the simulator incorporates inter-state daily mobility flows that couple states through travel-mediated mixing. Starting from the Stage 1 estimates  $\theta_s^{(0)}$  as initialization, the parameters are re-optimized to obtain refined estimates  $\theta_s^{(1)}$  that best reproduce the observed epidemic dynamics under mobility coupling. This mobility-aware calibration is formulated as a optimization problem: each trial samples a candidate parameter set, runs the coupled multi-state simulator, and evaluates an objective function (loss) computed from the mismatch between simulated and observed time series across states.

**Parameter search with Optuna.** The parameter search in Stage 2 is implemented using Optuna with a Tree-structured Parzen Estimator (TPE) sampler and Hyperband pruning to reduce computational cost by early-terminating unpromising trials (Akiba et al. 2019; Ozaki et al. 2020). A large startup phase is adopted to ensure sufficient exploration prior to exploitation ( $n_{\text{startup}} = 200$ ). The optimization budget is set to up to 10,000 trials with single-worker execution ( $n_{\text{jobs}} = 1$ ), and an early-stopping callback halts the optimization if no improvement is observed over a predefined patience window (e.g., 2000 trials).

**Loss function desin** The calibration objective is defined over a set of states. For each state  $i \in \mathcal{R}$ , the simulator produces predicted time series for (i) cumulative confirmed (quarantined) cases  $Q_{i,t}^{\text{pred}}$ , (ii) cumulative deaths  $D_{i,t}^{\text{pred}}$ , and (iii) cumulative recoveries  $R_{i,t}^{\text{pred}}$ , which are compared against the corresponding ground-truth observations  $Q_{i,t}^{\text{gt}}$ ,  $D_{i,t}^{\text{gt}}$ , and  $R_{i,t}^{\text{gt}}$  at time index  $t \in \mathcal{T}$ .

For each state  $i$ , the pointwise squared errors are

$$e_{i,t}^Q = \left( Q_{i,t}^{\text{pred}} - Q_{i,t}^{\text{gt}} \right)^2, \quad (1)$$

$$e_{i,t}^D = \left( D_{i,t}^{\text{pred}} - D_{i,t}^{\text{gt}} \right)^2, \quad (2)$$

$$e_{i,t}^R = \left( R_{i,t}^{\text{pred}} - R_{i,t}^{\text{gt}} \right)^2. \quad (3)$$

To balance signals across states with different epidemic magnitudes, each error term is normalized by the maximum observed value of the corresponding series within that state (Wang, Wang, and Wu 2018):

$$\bar{Q}_i = \max_{t \in \mathcal{T}_i} Q_{i,t}^{\text{gt}}, \quad \bar{D}_i = \max_{t \in \mathcal{T}_i} D_{i,t}^{\text{gt}}, \quad \bar{R}_i = \max_{t \in \mathcal{T}_i} R_{i,t}^{\text{gt}}. \quad (4)$$

A small constant  $\varepsilon$  is included for numerical stability. The state-level loss is then defined as

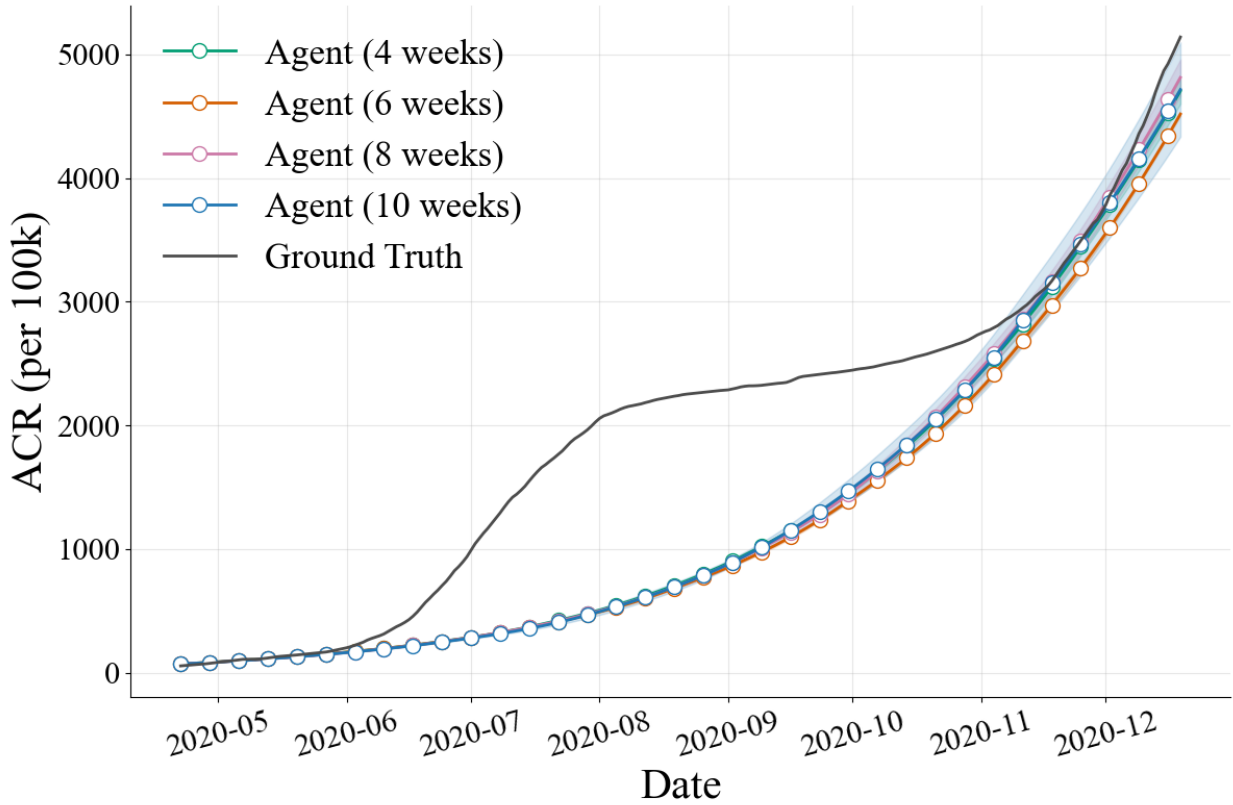
$$\mathcal{L}_i = \frac{1}{|\mathcal{T}_i|} \sum_{t \in \mathcal{T}_i} \left( \frac{e_{i,t}^Q}{\bar{Q}_i + \varepsilon} + \frac{e_{i,t}^D}{\bar{D}_i + \varepsilon} + \frac{e_{i,t}^R}{\bar{R}_i + \varepsilon} \right). \quad (5)$$

Finally, the total loss is computed as the average of state-level losses across all states:

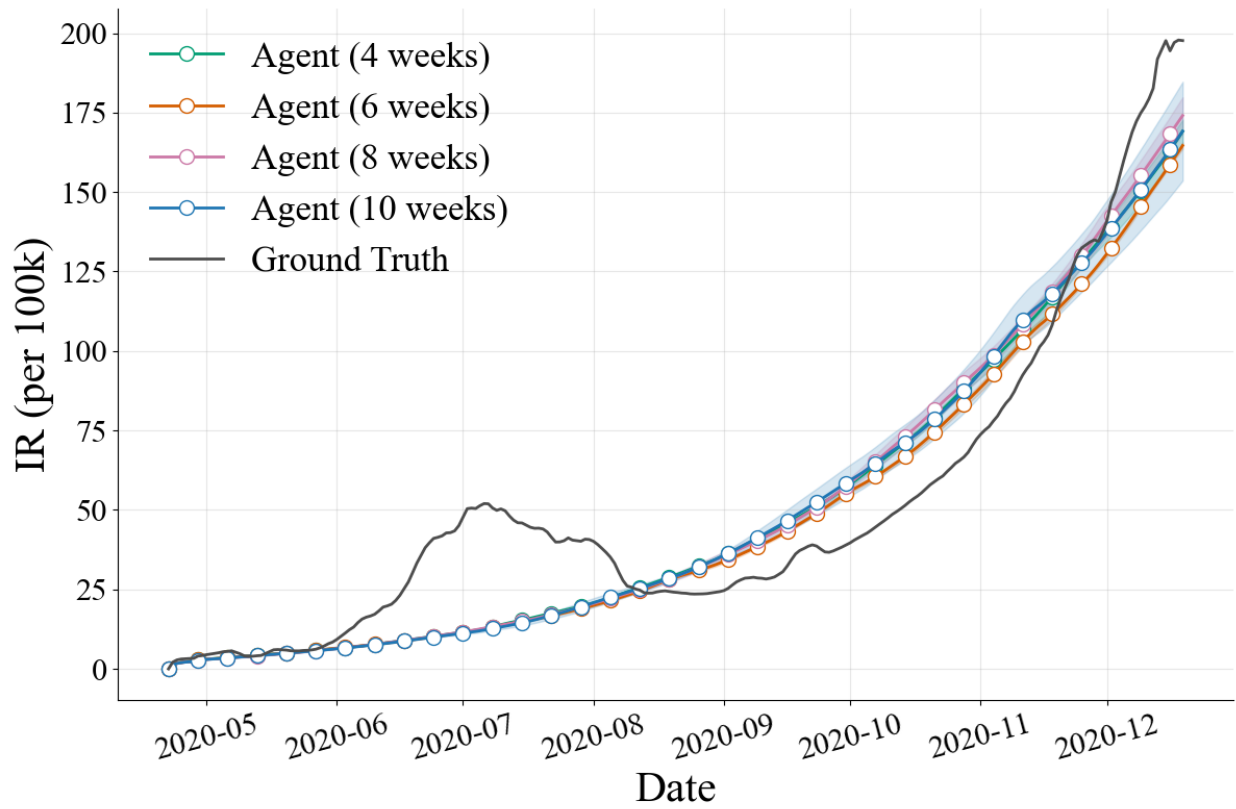
$$\mathcal{L} = \frac{1}{|\mathcal{R}|} \sum_{i \in \mathcal{R}} \mathcal{L}_i. \quad (6)$$

**Outcome** The two-stage procedure provides (i) interpretable state-level baseline parameters  $\theta_s^{(0)}$  and (ii) mobility-consistent refined parameters  $\theta_s^{(1)}$ , enabling subsequent intervention experiments to be evaluated.

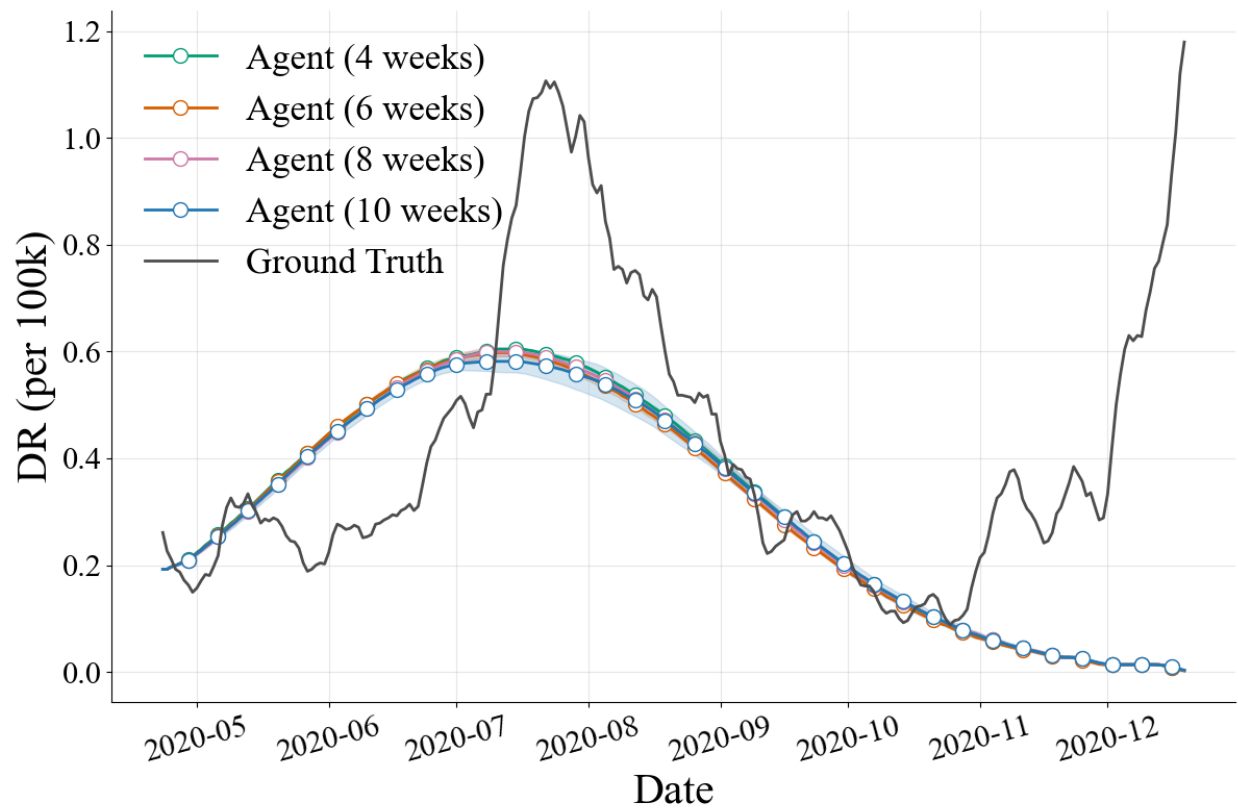
## 2. Supplementary Figures



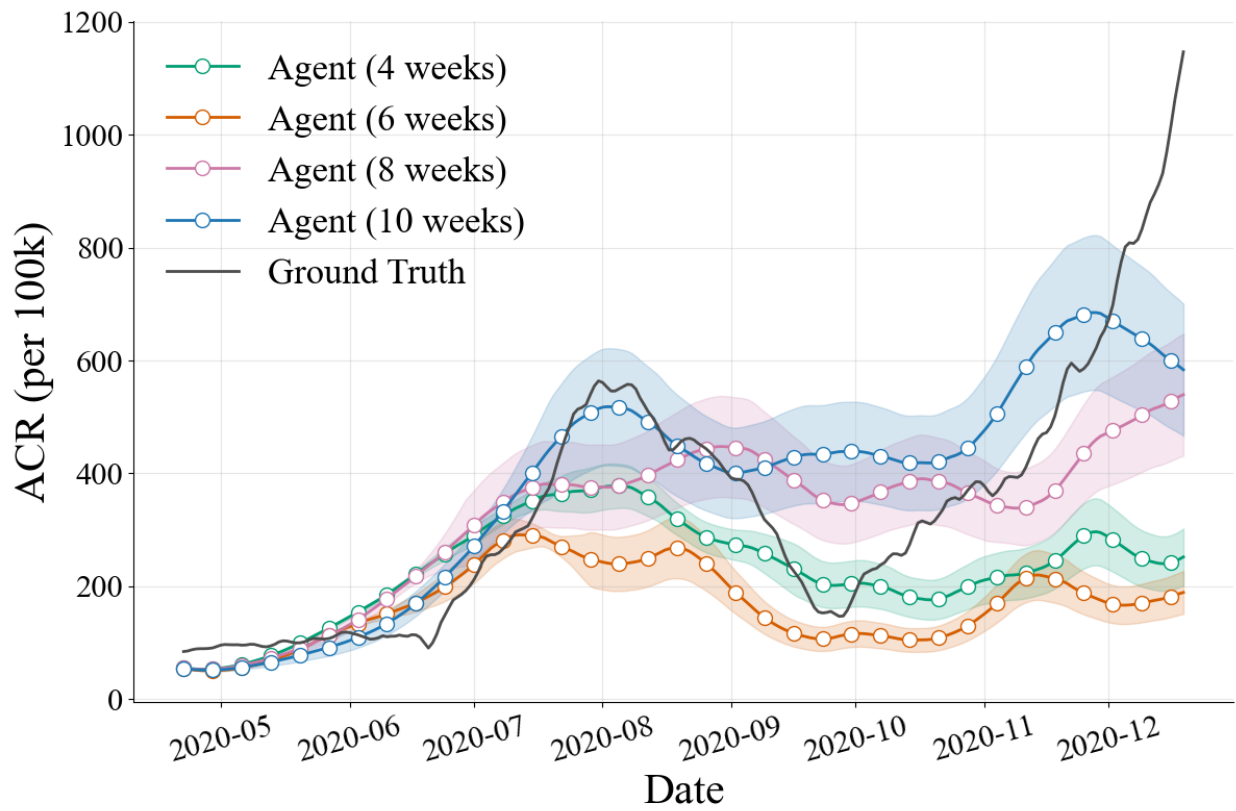
**Supplementary Figure 1.** Daily Active Case Rate in Arizona with different policy frequency. TIR with 4-, 6-, 8-, and 10-week reallocation cycles are evaluated. These interventions reduce ACR, with 6-week TIR achieving the best performance.



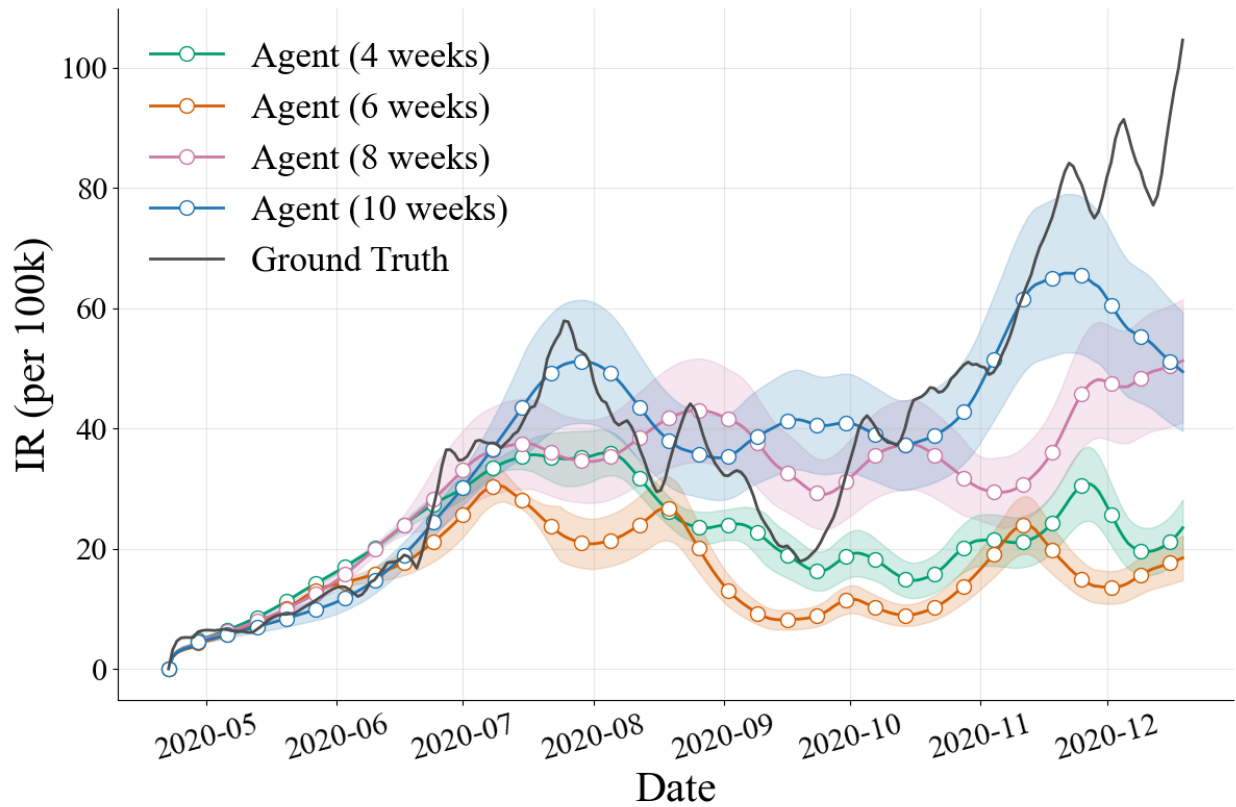
**Supplementary Figure 2.** Daily Incidence Rate in Arizona with different policy frequency. TIR with 4-, 6-, 8-, and 10-week reallocation cycles are evaluated. These interventions reduce IR, with 6-week TIR achieving the best performance.



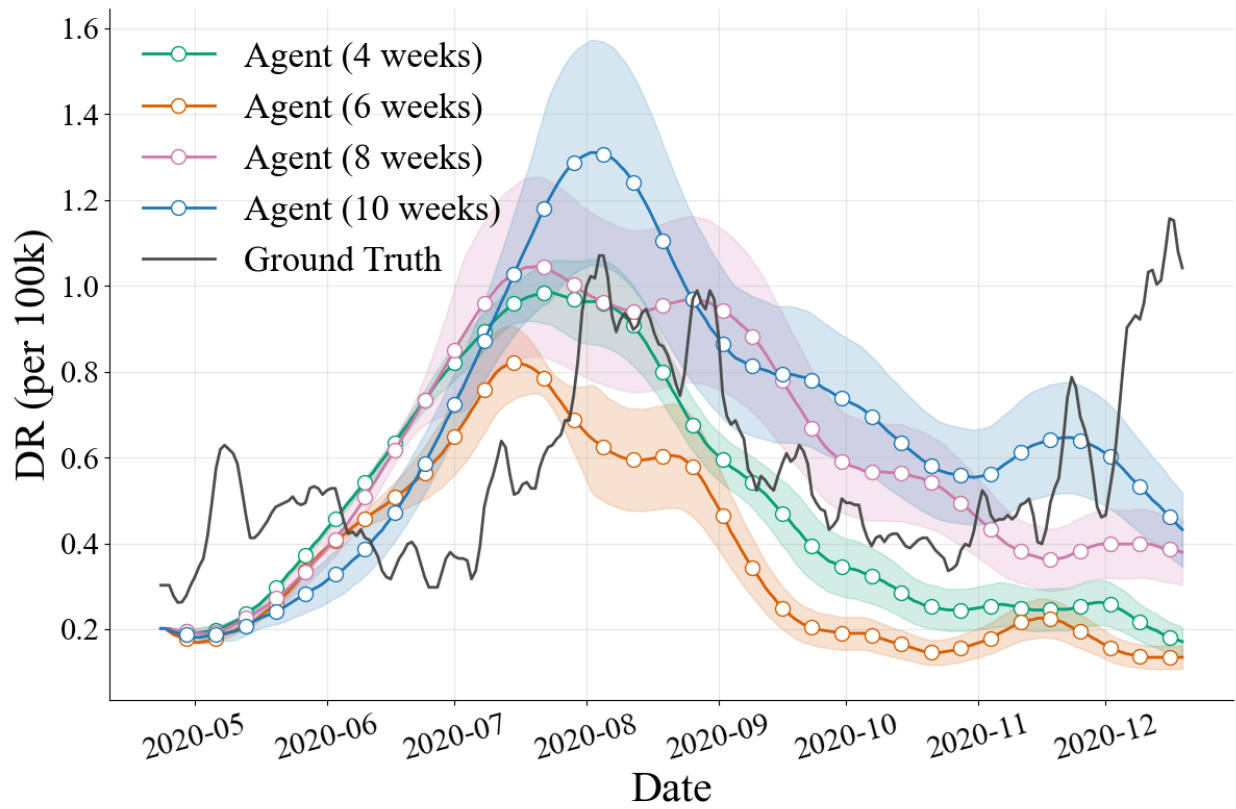
**Supplementary Figure 3.** Daily Death Rate in Arizona with different policy frequency. TIR with 4-, 6-, 8-, and 10-week reallocation cycles are evaluated. These interventions reduce IR, with 8-week TIR achieving the best performance.



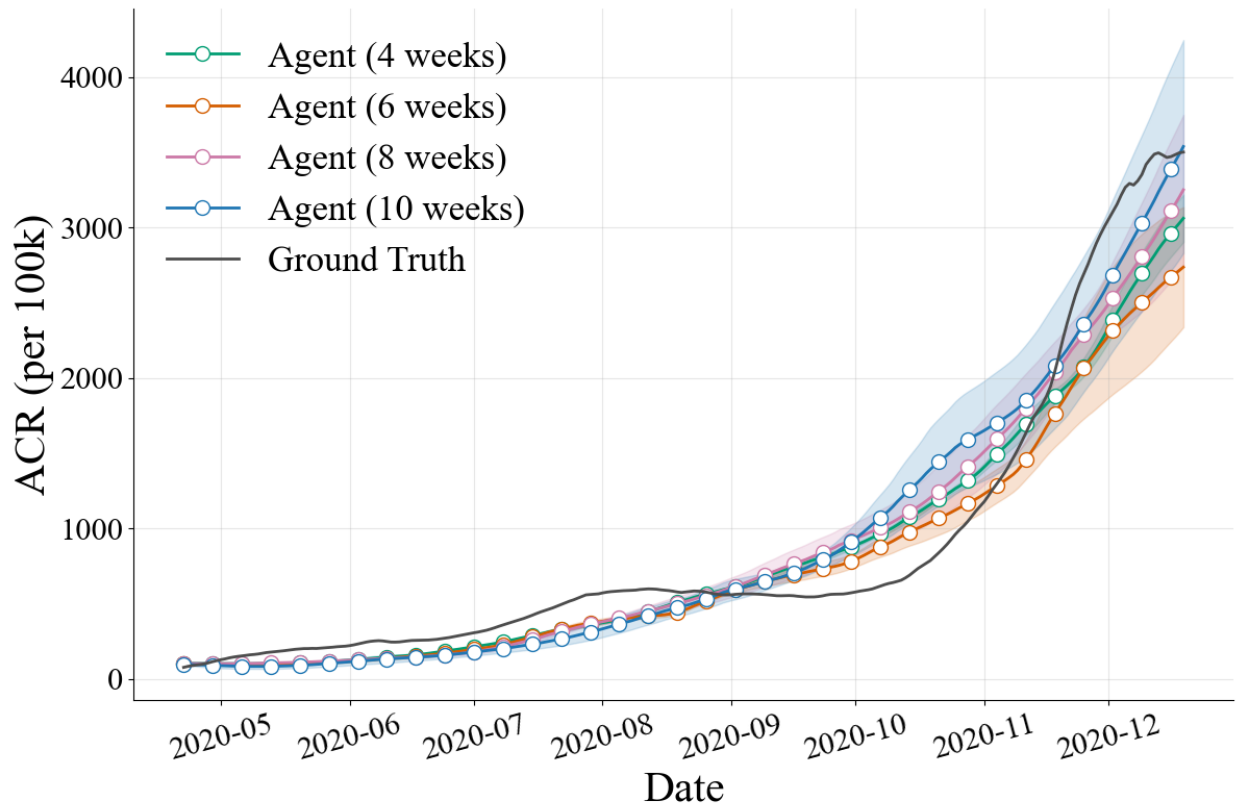
**Supplementary Figure 4.** Daily Active Case Rate in Mississippi with different policy frequency. TIR with 4-, 6-, 8-, and 10-week reallocation cycles are evaluated. 6-week TIR achieves the best performance while 10-week TIR has weak impact in the reduction of ACR.



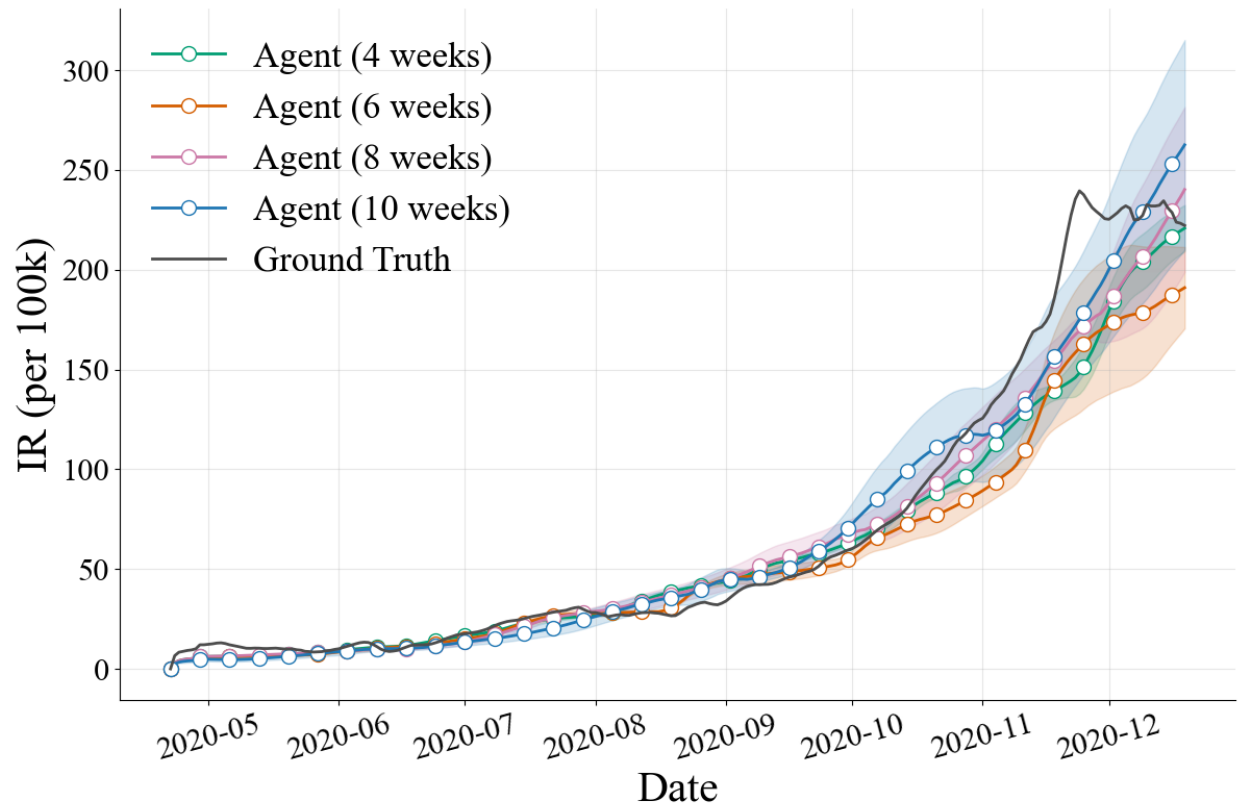
**Supplementary Figure 5.** Daily Incidence Rate in Mississippi with different policy frequency. TIR with 4-, 6-, 8-, and 10-week reallocation cycles are evaluated. 6-week TIR achieves the best performance while 10-week TIR has weak impact in the reduction of IR.



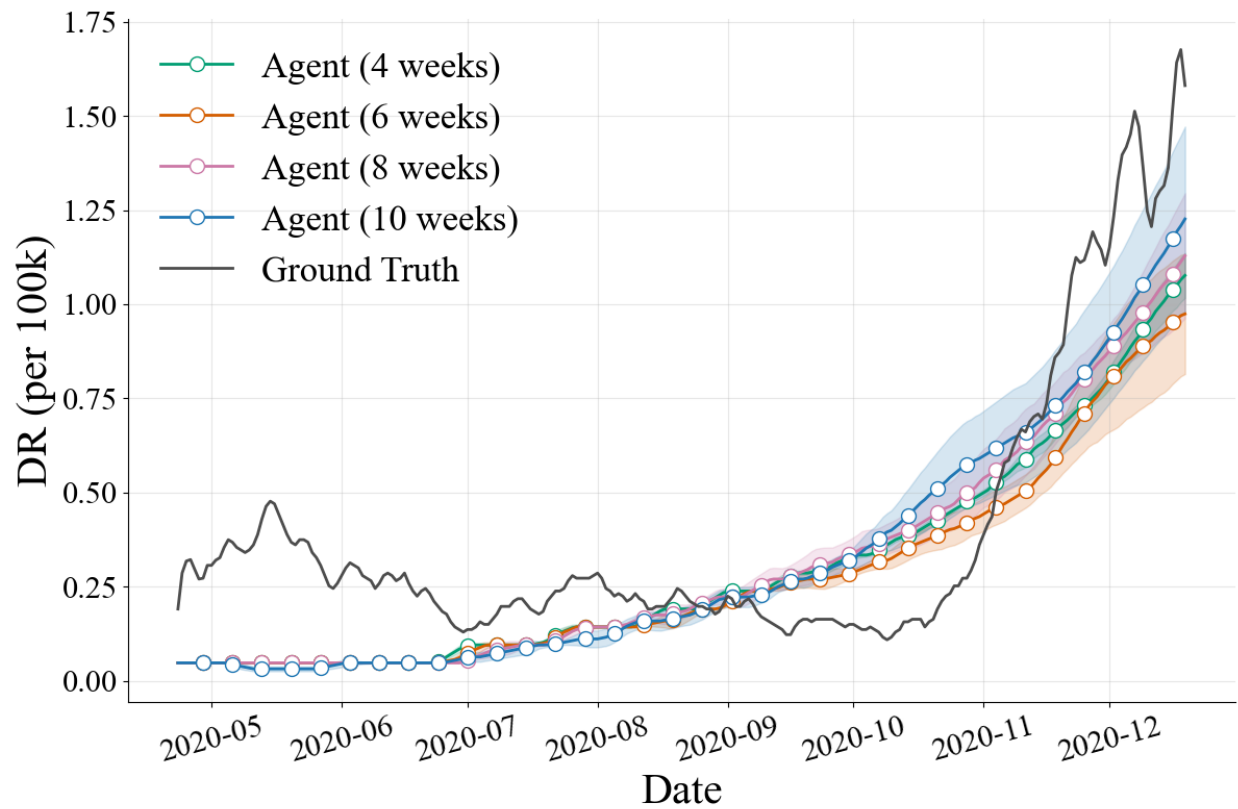
**Supplementary Figure 6.** Daily Death Rate in Mississippi with different policy frequency. TIR with 4-, 6-, 8-, and 10-week reallocation cycles are evaluated. 6-week TIR achieves the best performance while 10-week and 8-week TIR have weak impact in the reduction of DR.



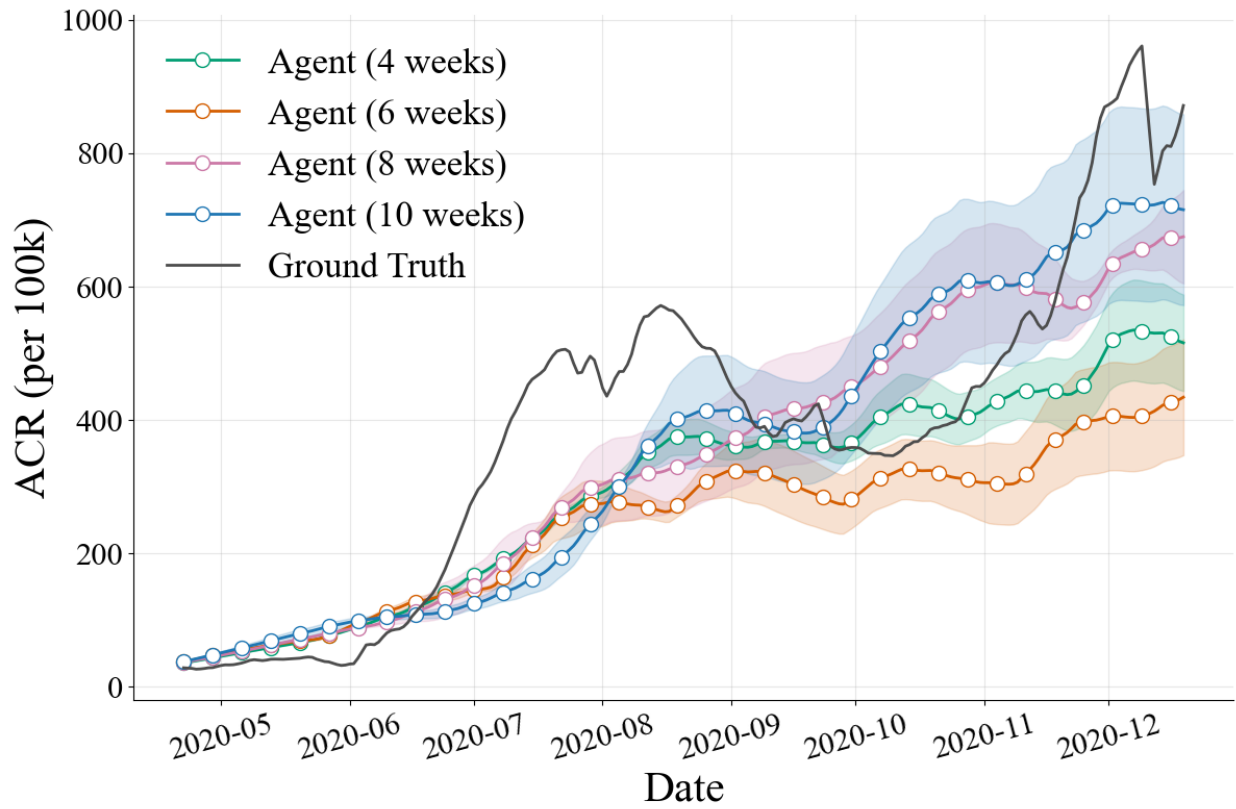
**Supplementary Figure 7.** Daily Active Case Rate in New Mexico with different policy frequency. TIR with 4-, 6-, 8-, and 10-week reallocation cycles are evaluated. Most of these interventions reduce IR. 6-week TIR achieves the best performance while 10-week TIR has weak impact in the reduction of ACR.



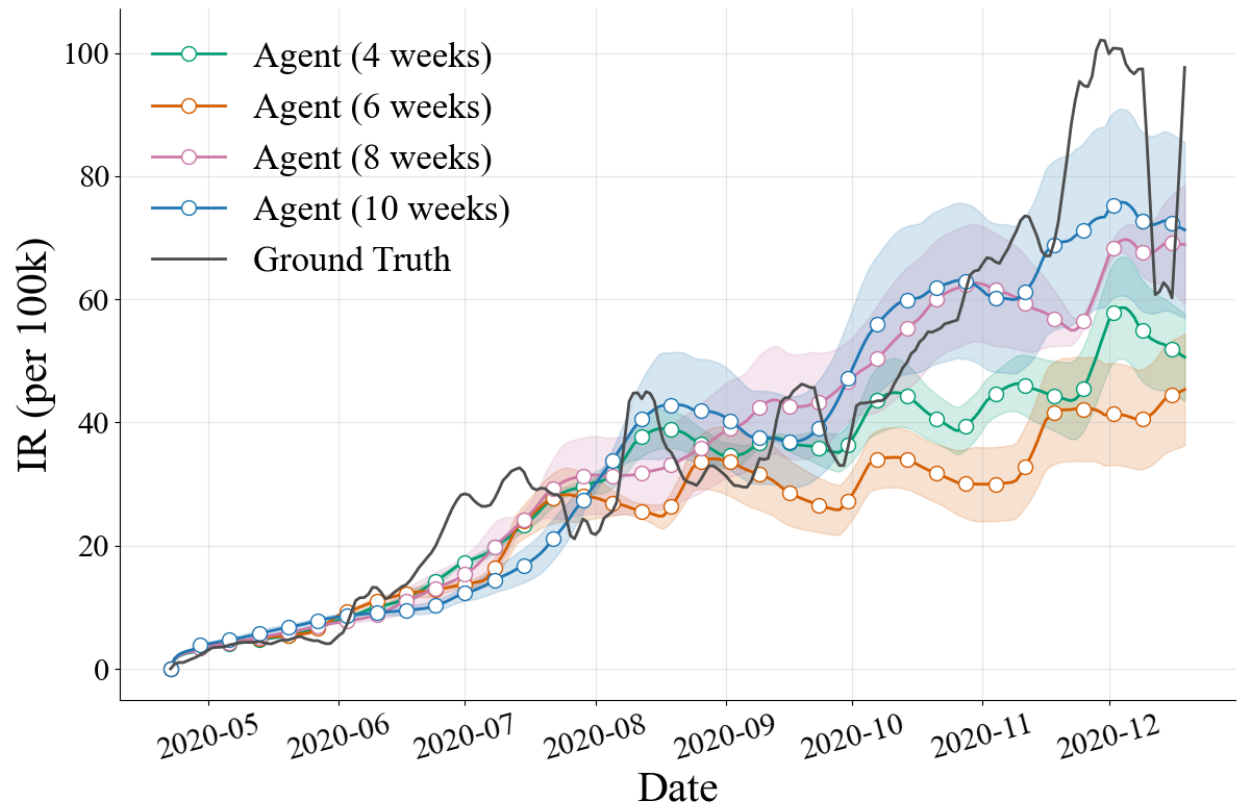
**Supplementary Figure 8.** Daily Incidence Rate in New Mexico with different policy frequency. TIR with 4-, 6-, 8-, and 10-week reallocation cycles are evaluated. 6-week TIR achieves the best performance while 10-week and 8-week TIR have weak impact in the reduction of IR.



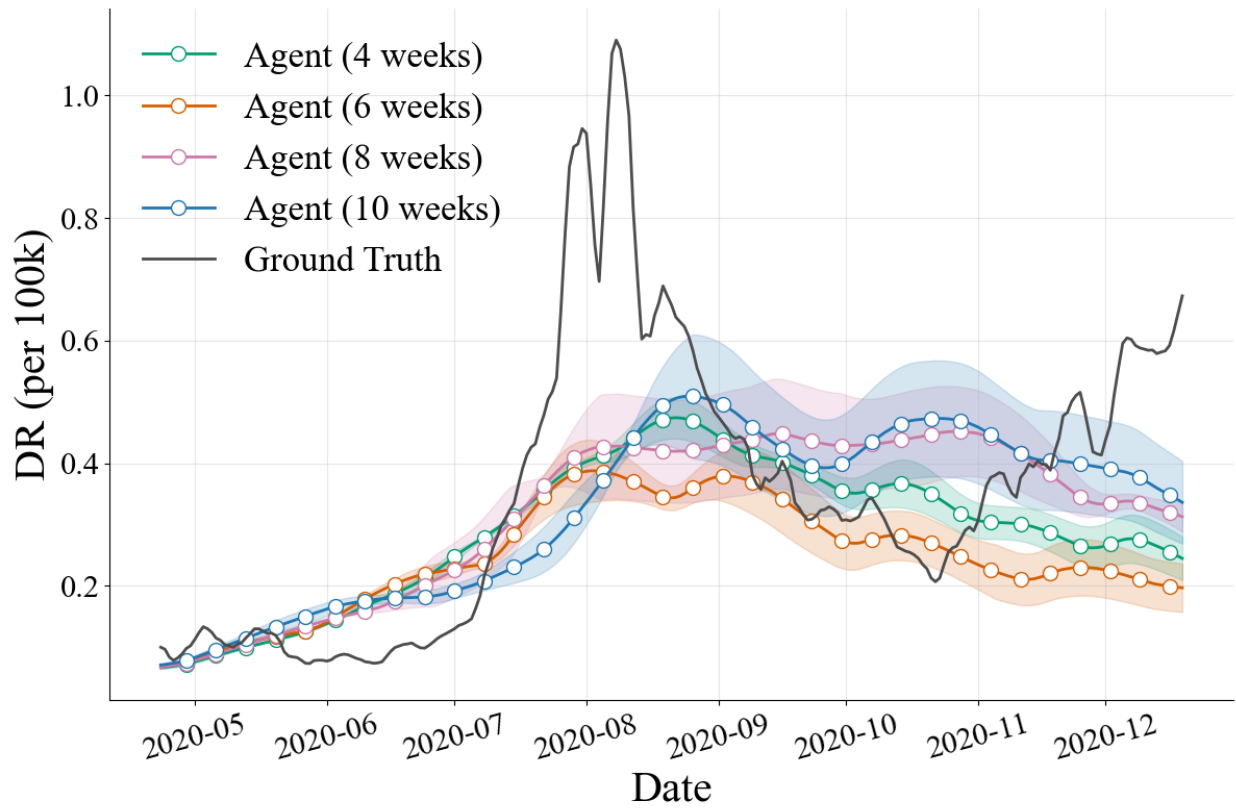
**Supplementary Figure 9.** Daily Death Rate in New Mexico with different policy frequency. TIR with 4-, 6-, 8-, and 10-week reallocation cycles are evaluated. All of these interventions reduce DR. 6-week TIR achieves the best performance while 10-week TIR has weak impact in the reduction of DR.



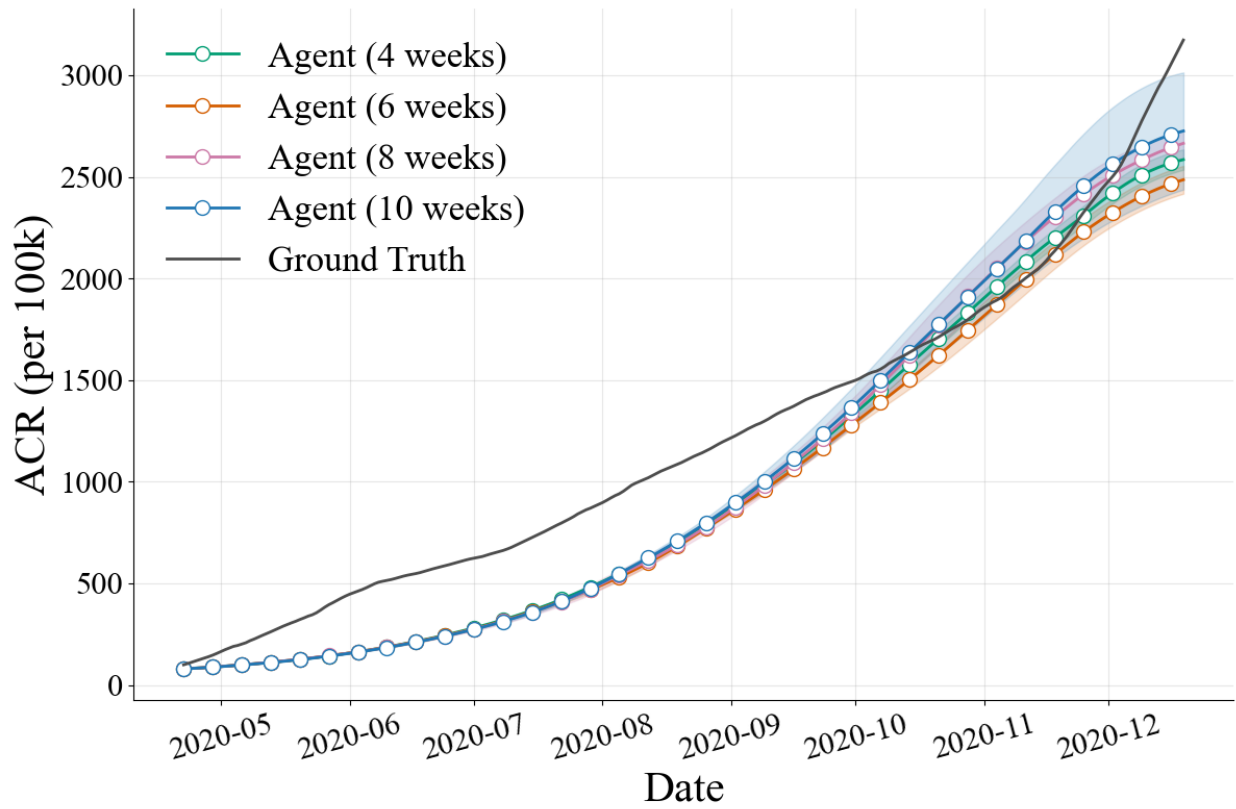
**Supplementary Figure 10.** Daily Active Case Rate in Texas with different policy frequency. TIR with 4-, 6-, 8-, and 10-week reallocation cycles are evaluated. All interventions reduce ACR by the end of 2020; however, during September–October 2020, ACR under the 8- and 10-week TIR exceeds the ground-truth level. The 6-week TIR achieves the best performance.



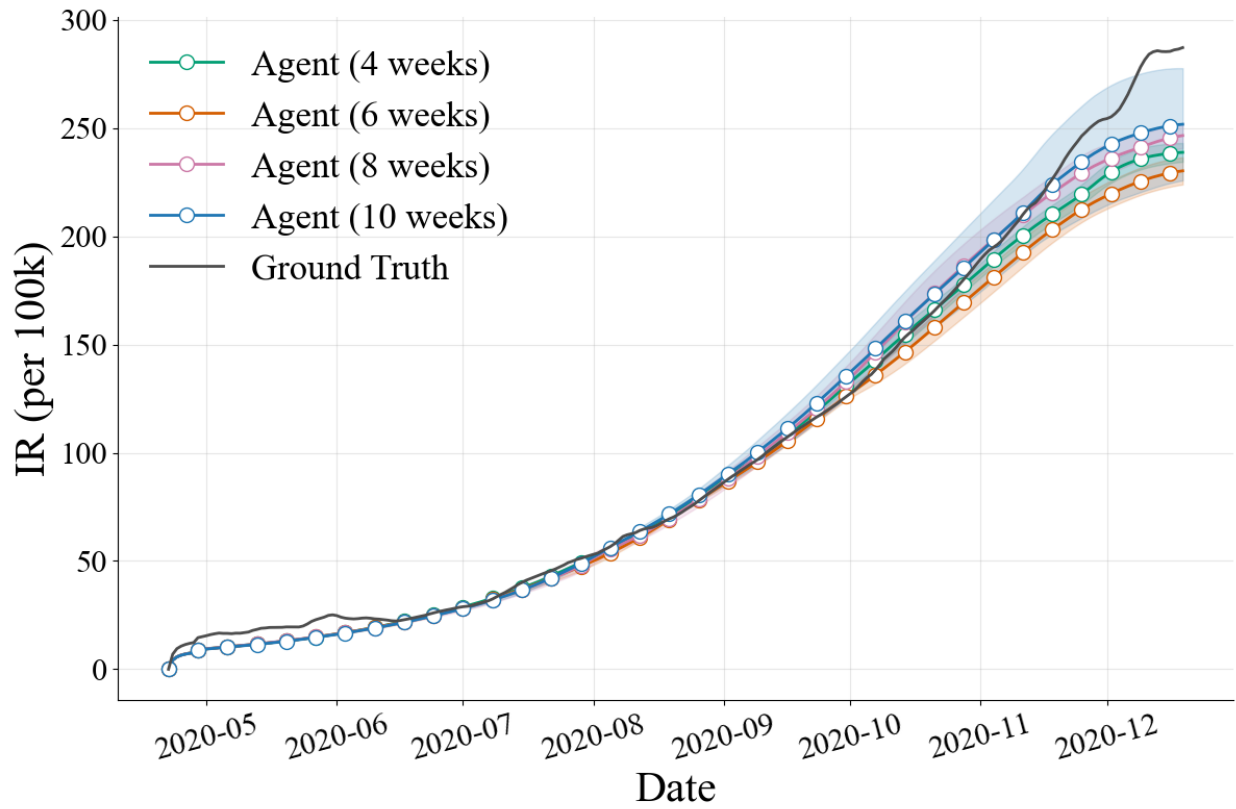
**Supplementary Figure 11.** Daily Incidence Rate in Texas with different policy frequency. TIR with 4-, 6-, 8-, and 10-week reallocation cycles are evaluated. All interventions reduce IR by the end of 2020; however, during October 2020, IR under the 8- and 10-week TIR exceeds the ground-truth level. Overall, 6-week TIR achieves the best performance.



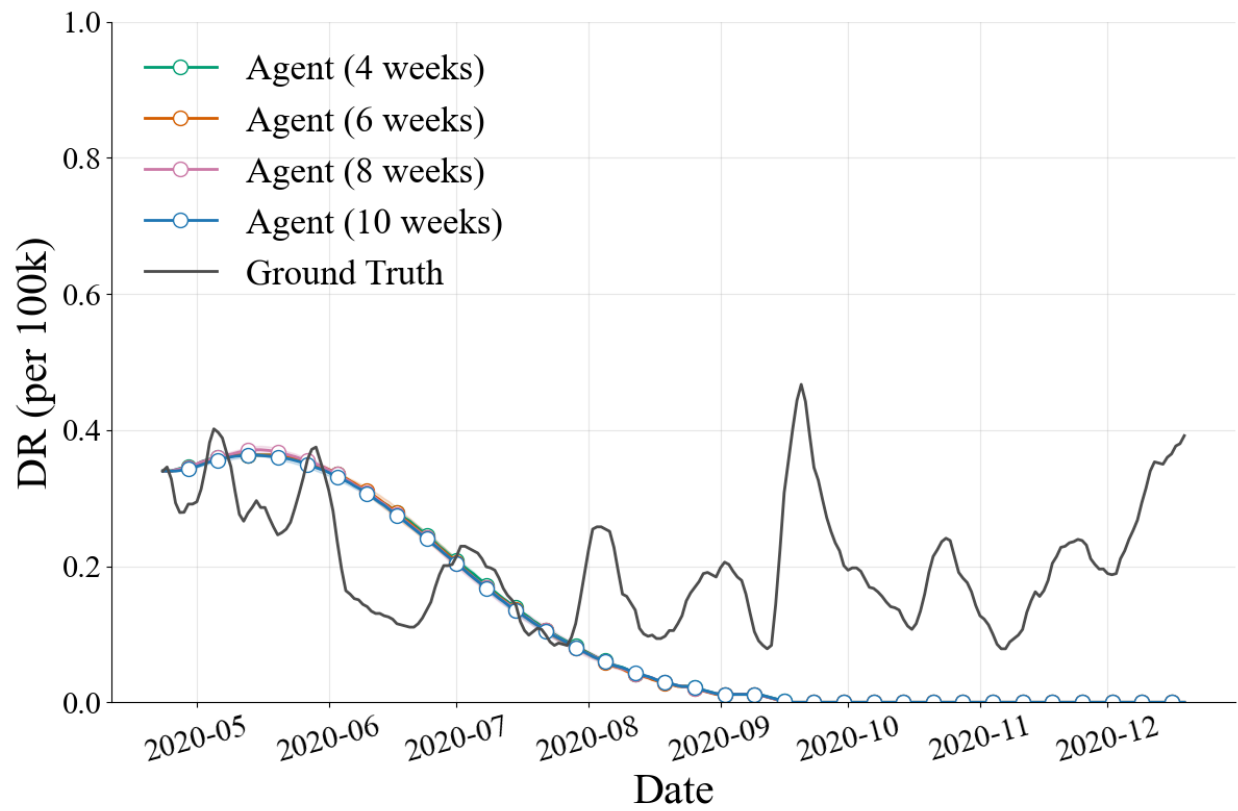
**Supplementary Figure 12.** Daily Death Rate in Texas with different policy frequency. TIR with 4-, 6-, 8-, and 10-week reallocation cycles are evaluated. All interventions reduce DR by the end of 2020; however, during September-October 2020, DR under the 4-, 8- and 10-week TIR exceeds the ground-truth level. Overall, 6-week TIR achieves the best performance.



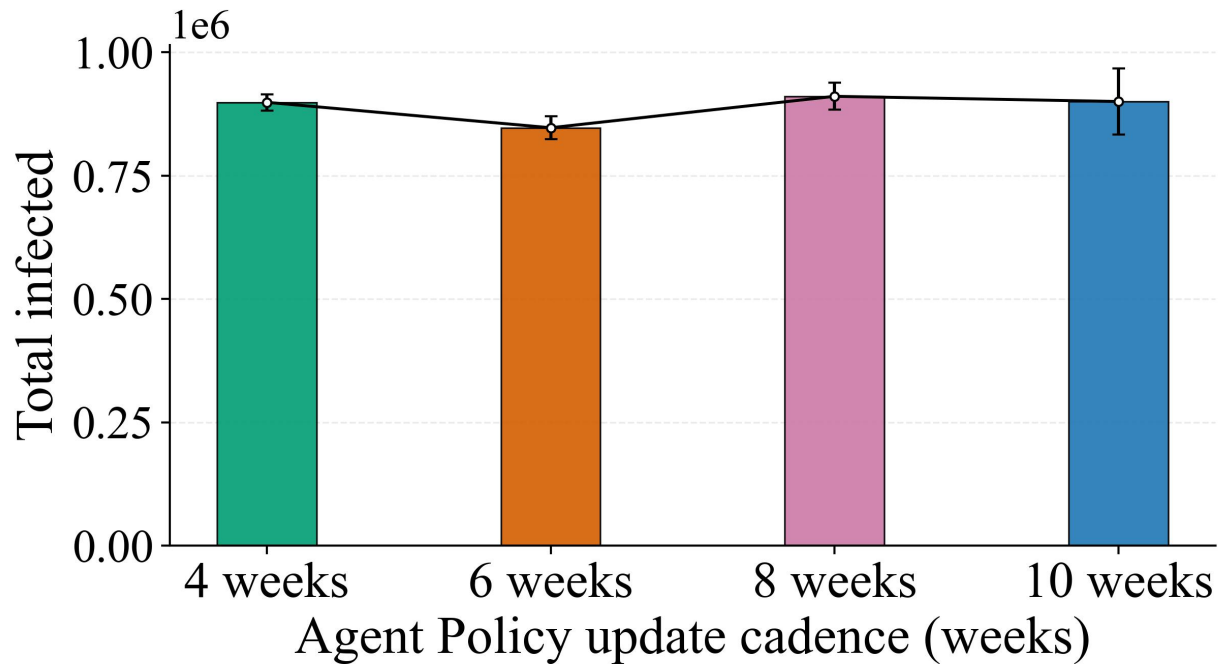
**Supplementary Figure 13.** Daily Active Case Rate in Virginia with different policy frequency. TIR with 4-, 6-, 8-, and 10-week reallocation cycles are evaluated. All of these intervention reduce ACR. 6-week TIR achieves the best performance while 10-week TIR has weak impact in the reduction of ACR.



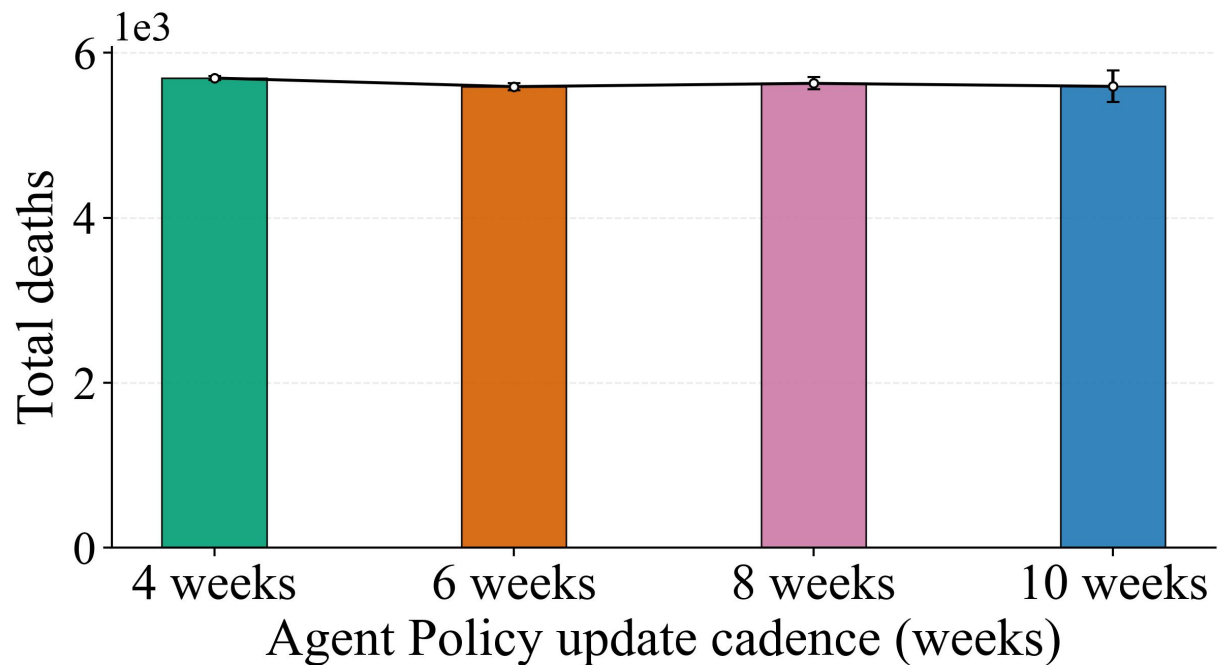
**Supplementary Figure 14.** Daily Incidence Rate in Virginia with different policy frequency. TIR with 4-, 6-, 8-, and 10-week reallocation cycles are evaluated. All of these intervention reduce IR. 6-week TIR achieves the best performance while 10-week TIR has weak impact in the reduction of IR.



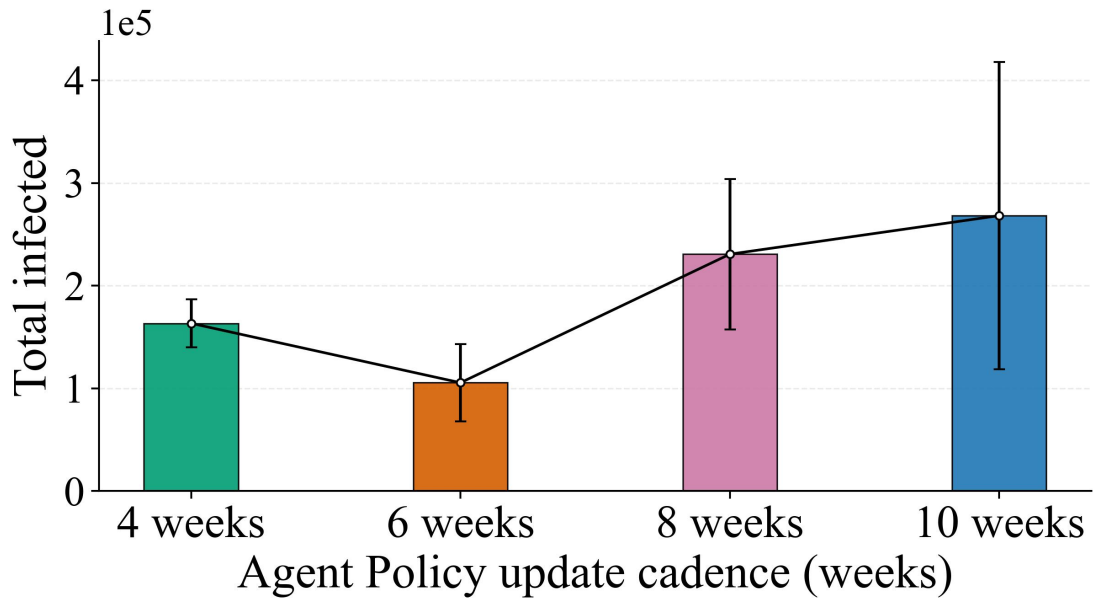
**Supplementary Figure 15.** Daily Death Rate in Virginia with different policy frequency. IR strategies with 4-, 6-, 8-, and 10-week reallocation cycles are evaluated. All interventions reduce DR to nearly zero after August 2020.



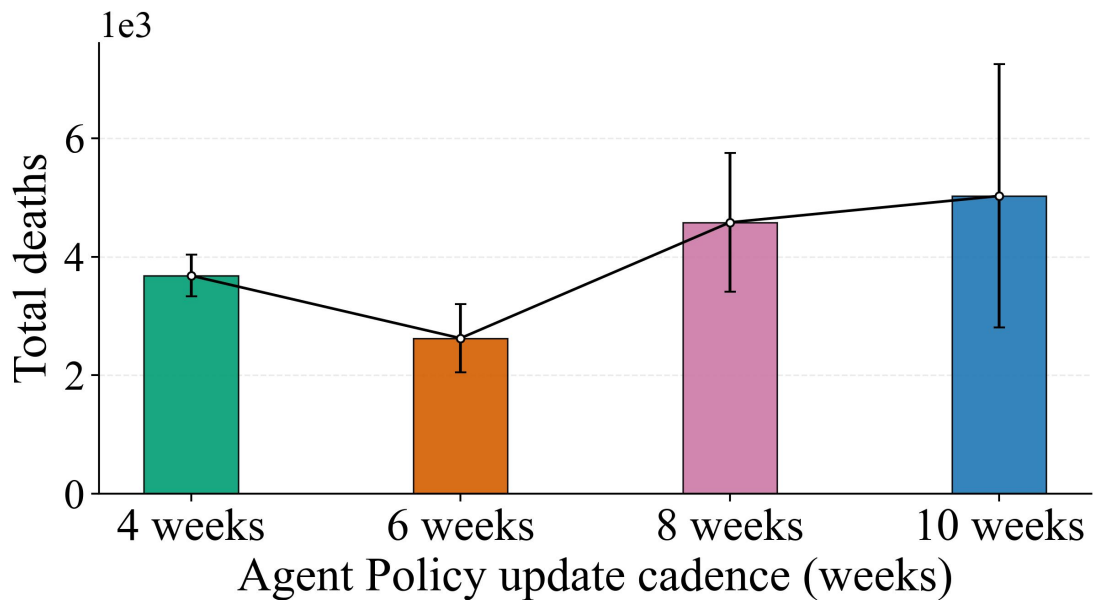
**Supplementary Figure 16.** Total infection in Arizona with different policy frequency. 6-week TIR yields the lowest infections, followed by 10-week TIR.



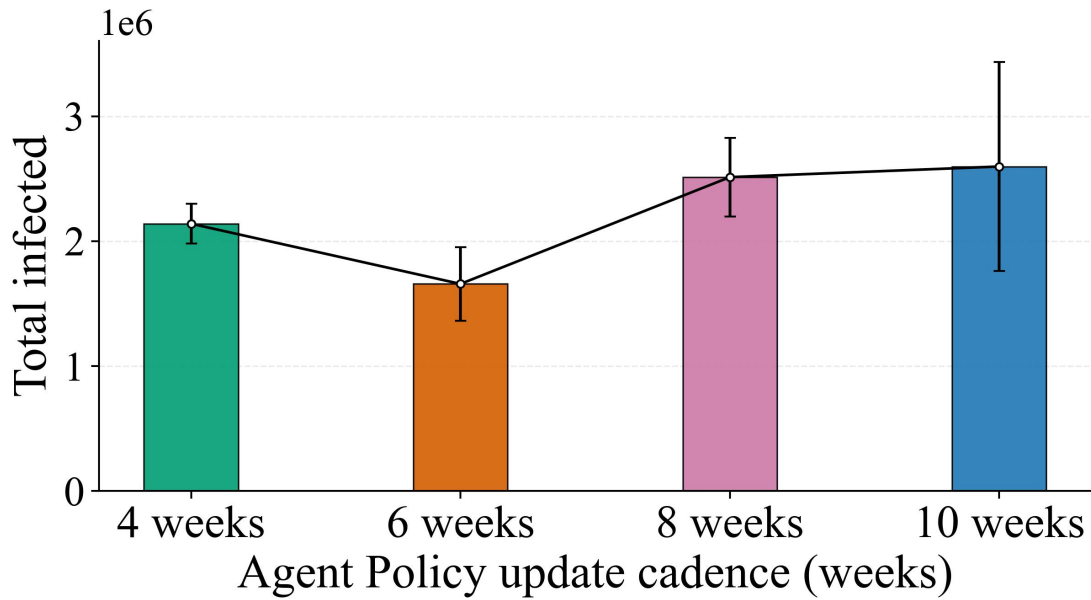
**Supplementary Figure 17.** Total deaths in Arizona with different policy frequency. These four strategies yield comparable level of total deaths.



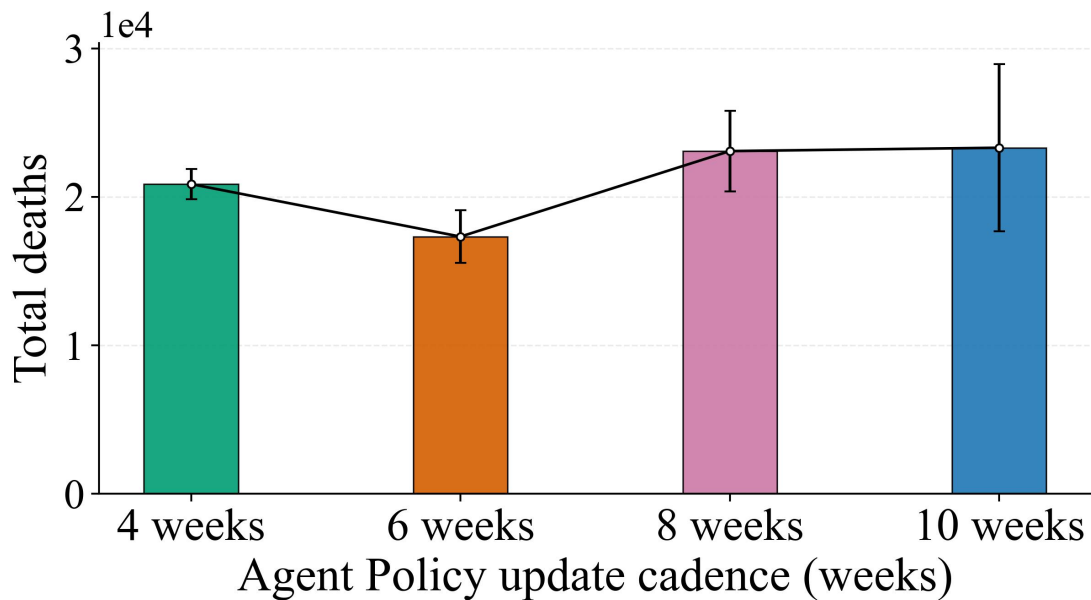
**Supplementary Figure 18.** Total infection in Mississippi with different policy frequency. 6-week TIR yields the lowest infections, followed by 4-week TIR and 8-week TIR.



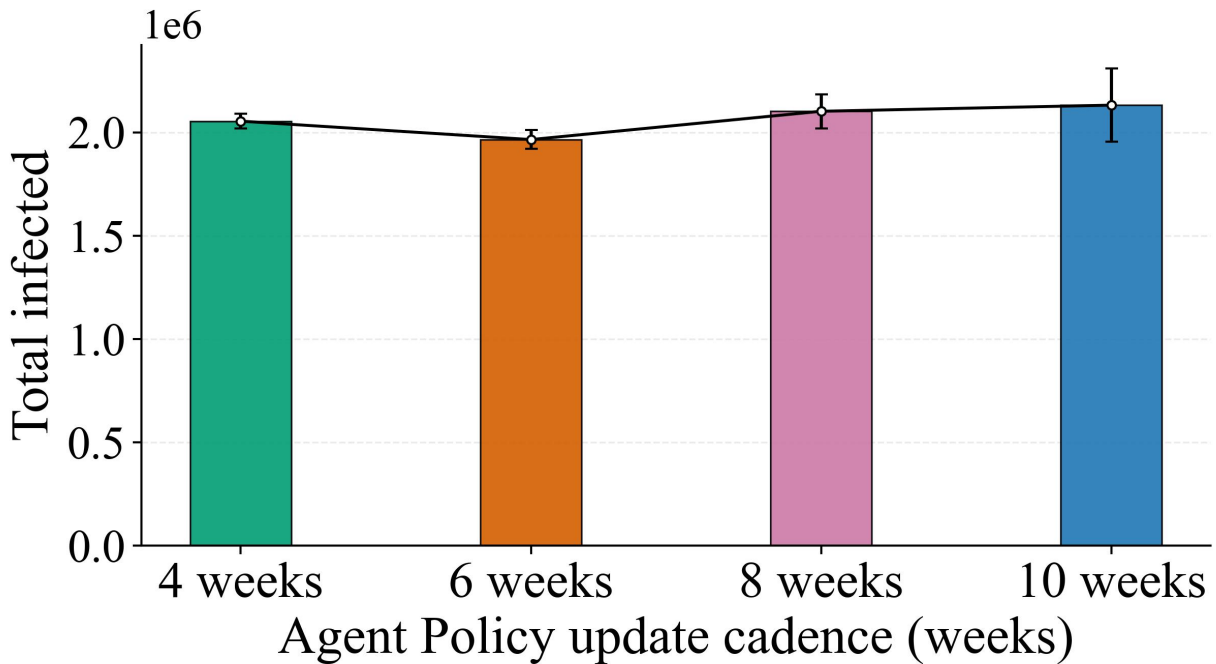
**Supplementary Figure 19.** Total deaths in Mississippi with different policy frequency. 6-week TIR yields the lowest total deaths, followed by 4-week TIR and 8-week TIR.



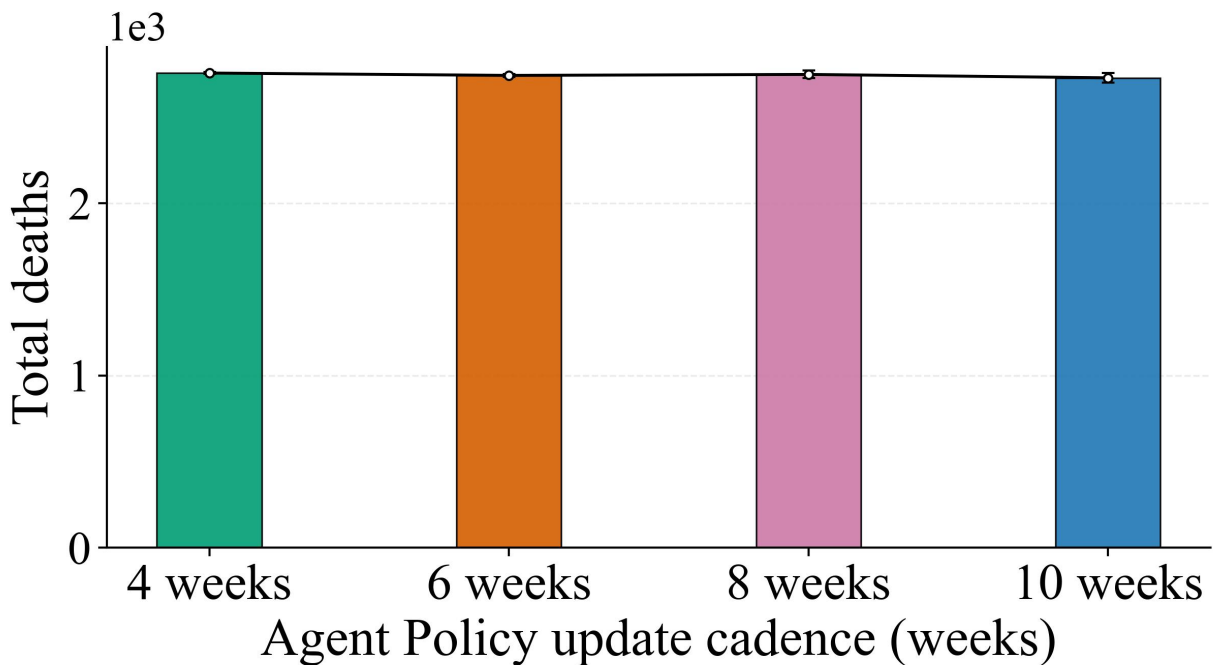
**Supplementary Figure 20.** Total infection in Texas with different policy frequency. 6-week TIR yields the lowest infections, followed by 4-week TIR and 8-week TIR.



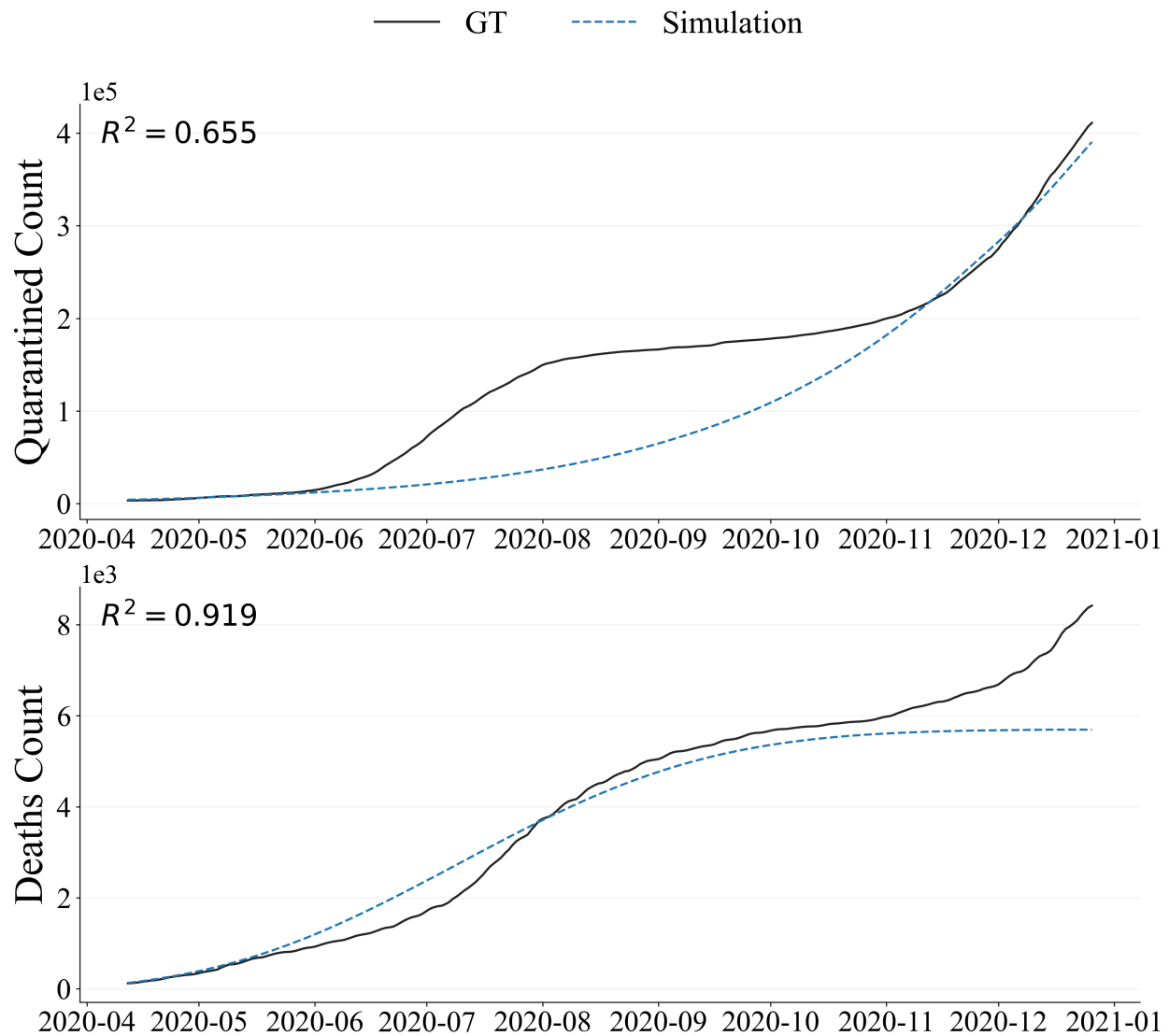
**Supplementary Figure 21.** Total deaths in Texas with different policy frequency. 6-week TIR yields the lowest total deaths, followed by 4-week TIR and 8-week TIR.



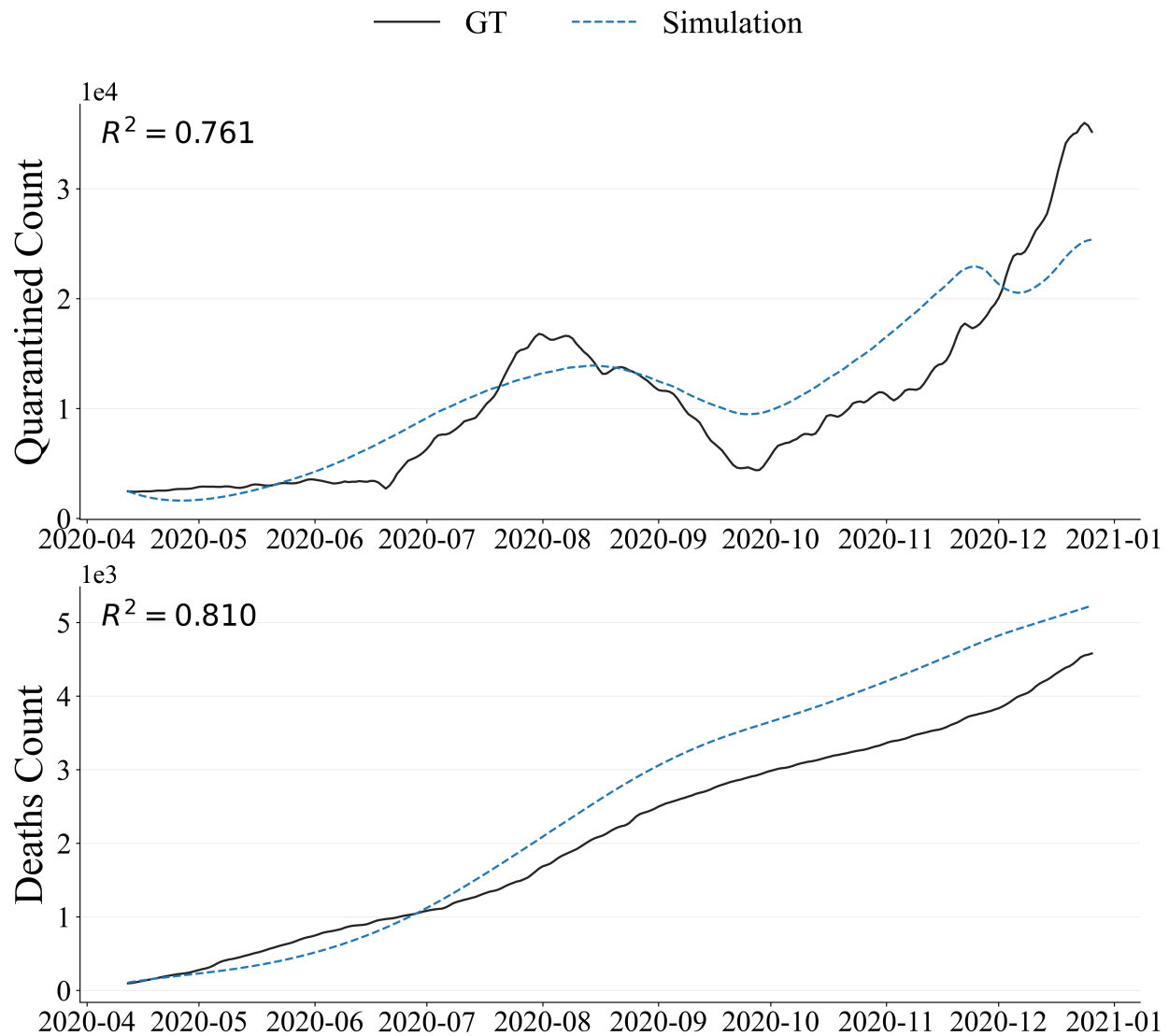
**Supplementary Figure 22.** Total infection in Virginia with different policy frequency. The 6-week TIR yields the lowest infections



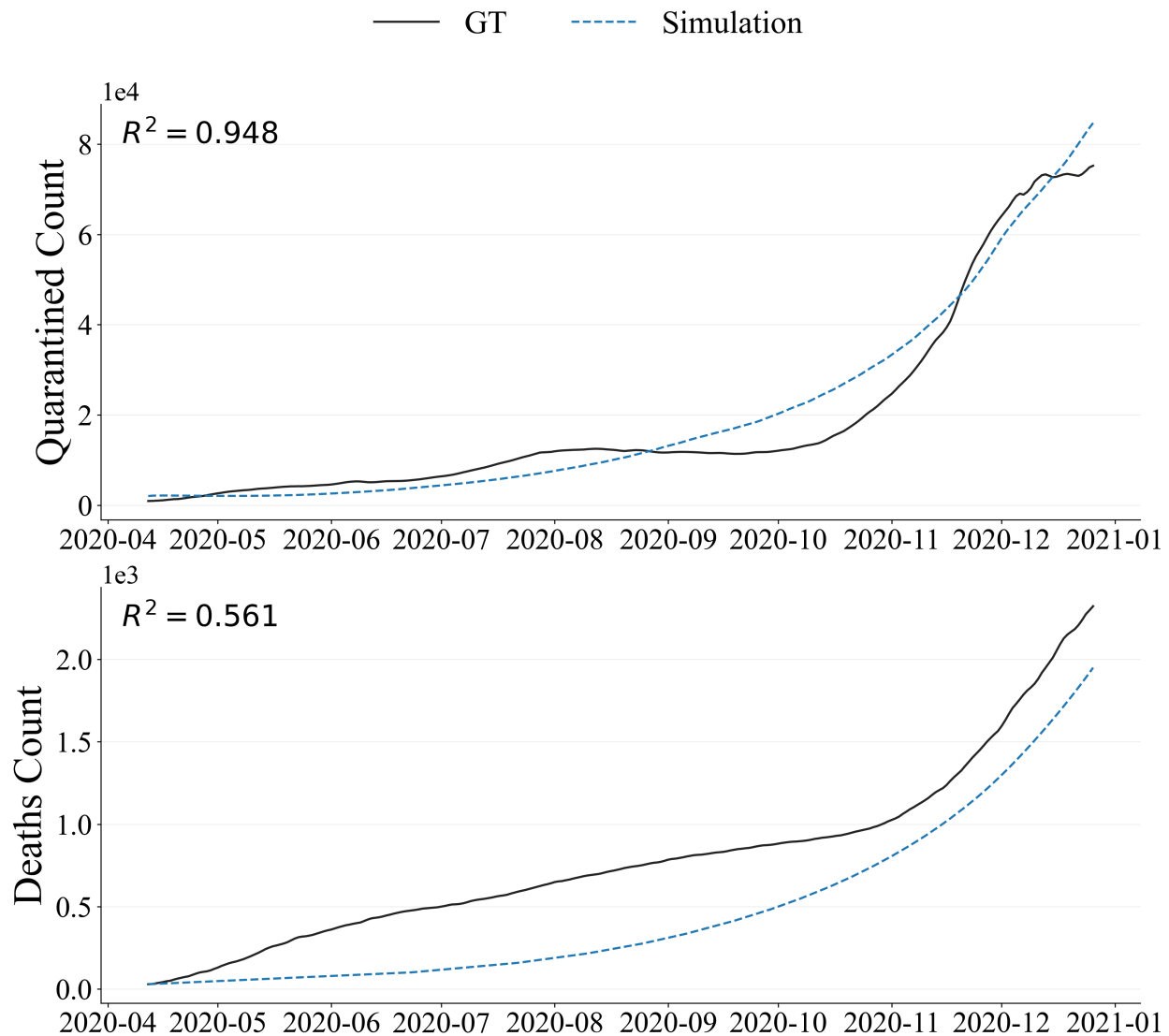
**Supplementary Figure 23.** Total deaths in Virginia with different policy frequency. These four strategies yield comparable level of total deaths.



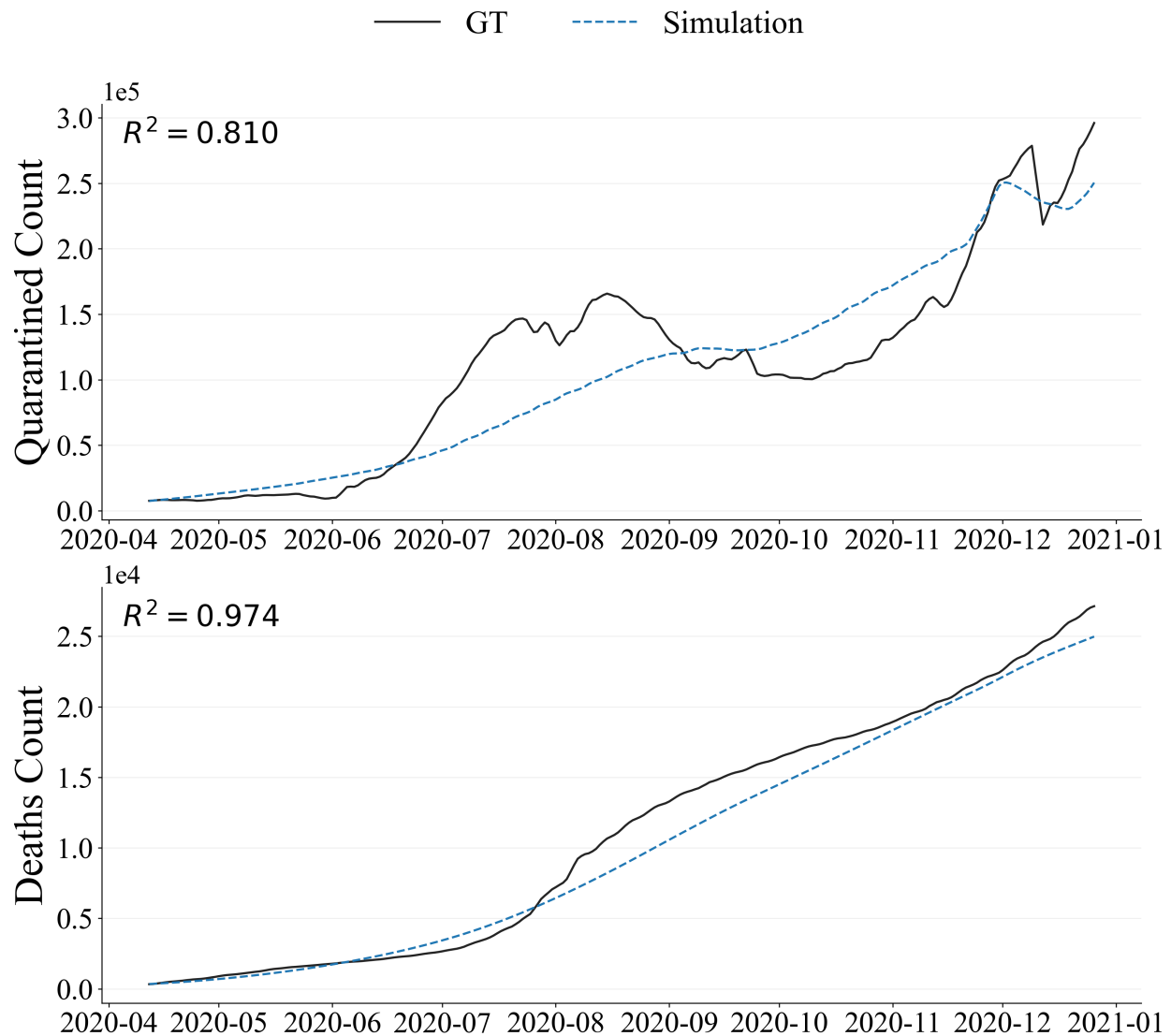
**Supplementary Figure 24.** Simulated results in Arizona. The quarantined and death curves show good fit, with  $R^2 = 0.655$  and  $R^2 = 0.919$ , respectively.



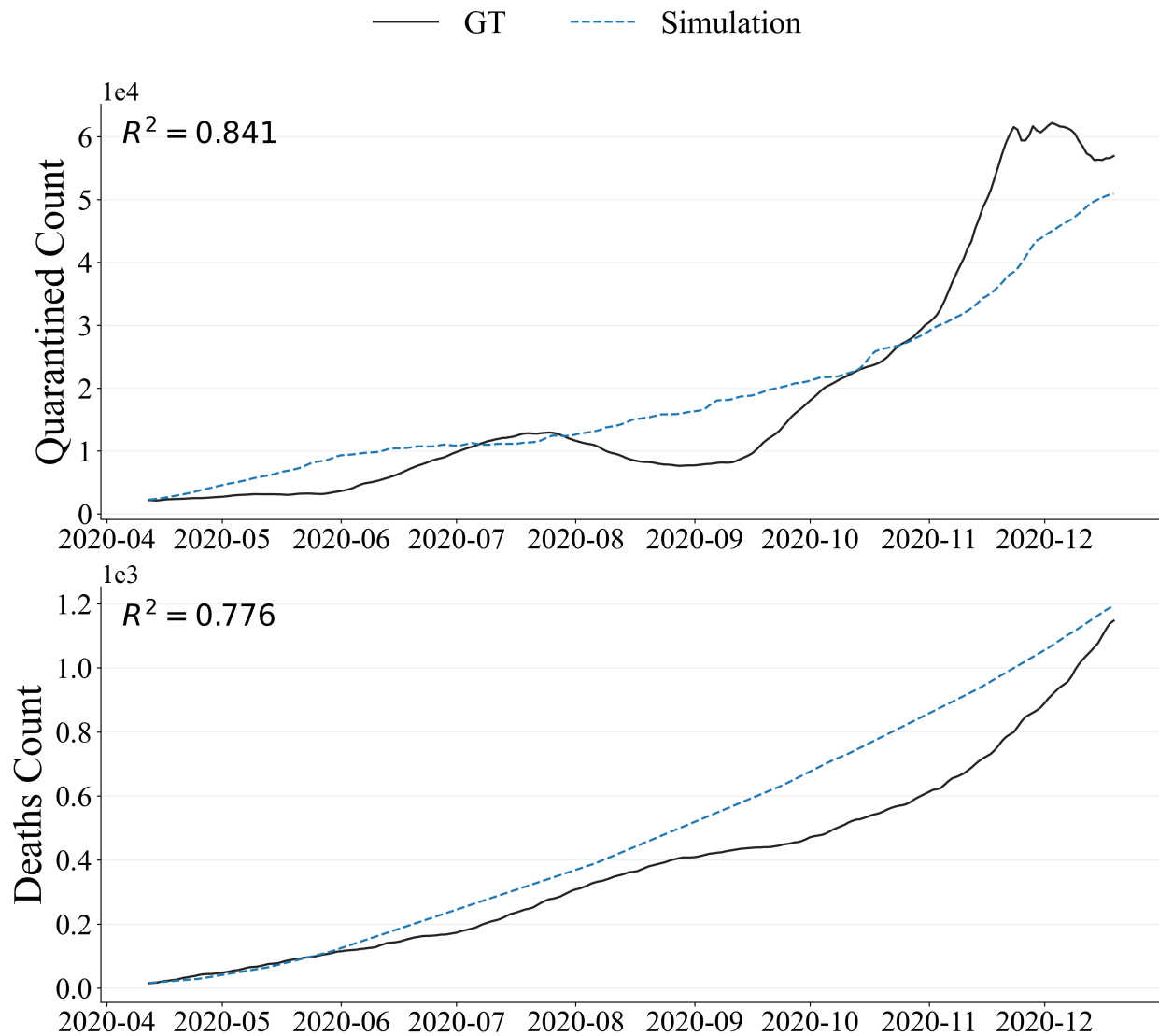
**Supplementary Figure 25.** Simulated results in Mississippi. The quarantined and death curves show good fit, with  $R^2 = 0.761$  and  $R^2 = 0.810$ , respectively.



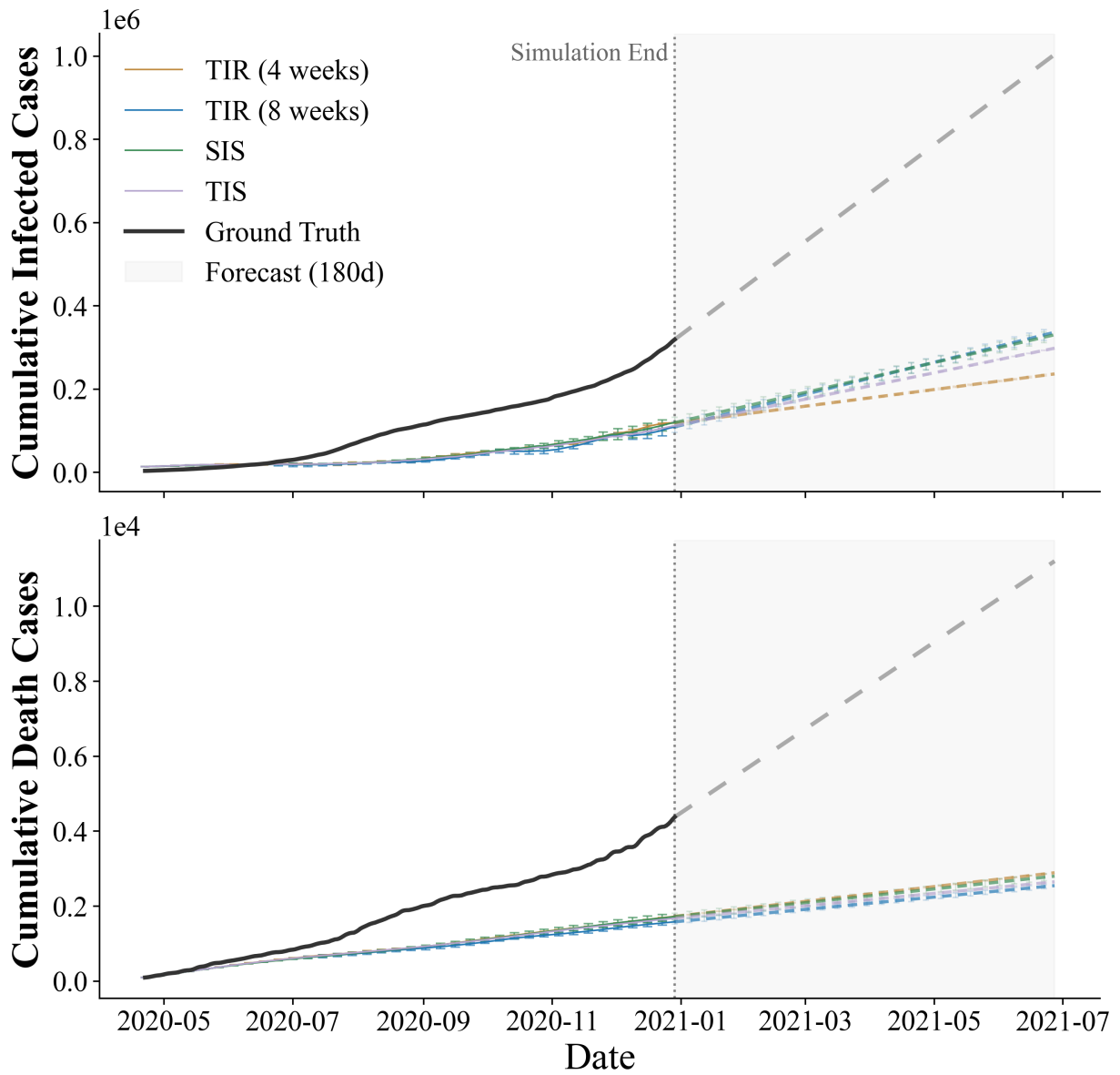
**Supplementary Figure 26.** Simulated results in New Mexico. The quarantined and death curves show good fit, with  $R^2 = 0.948$  and  $R^2 = 0.561$ , respectively.



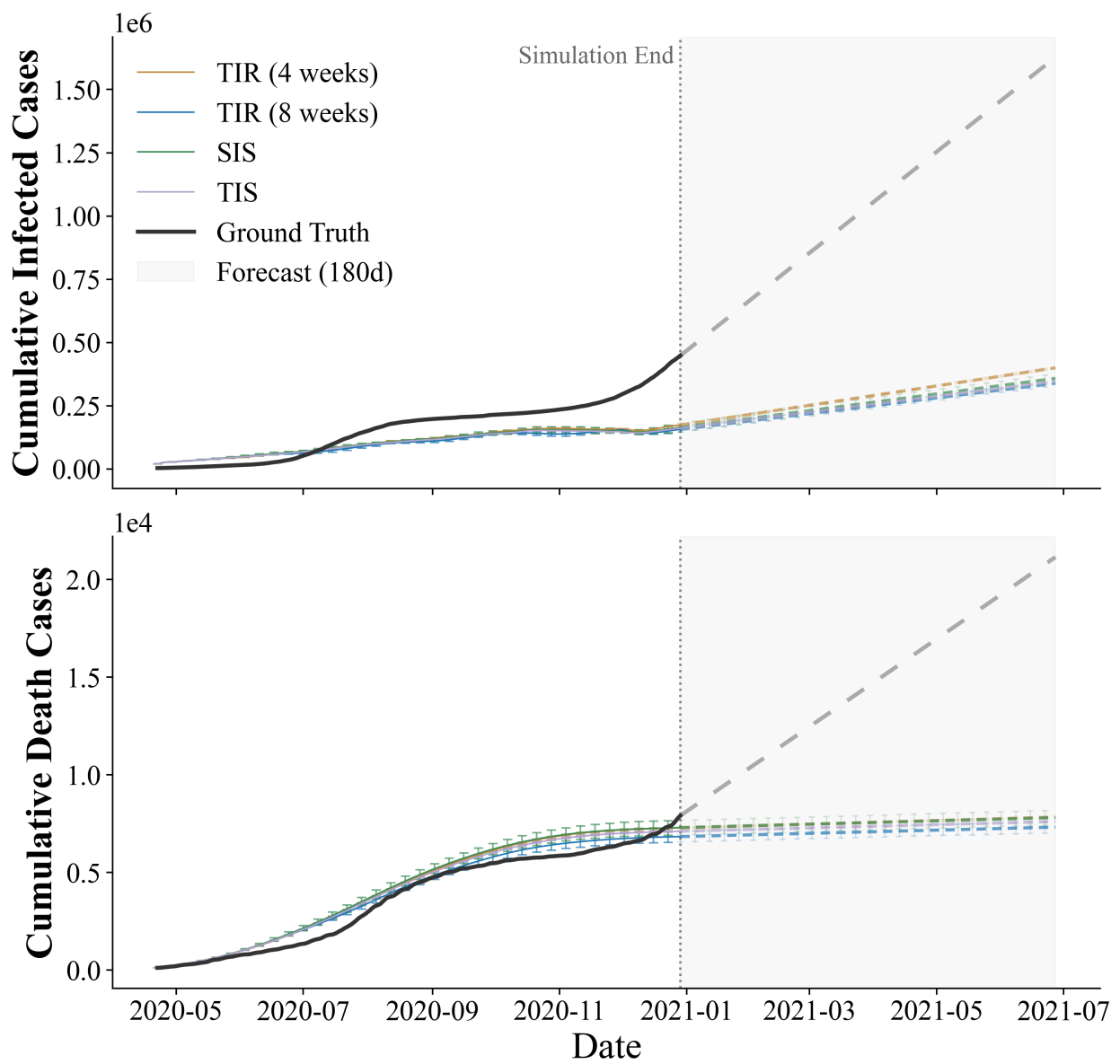
**Supplementary Figure 27.** Simulated results in Texas. The quarantined and death curves show good fit, with  $R^2 = 0.810$  and  $R^2 = 0.974$ , respectively.



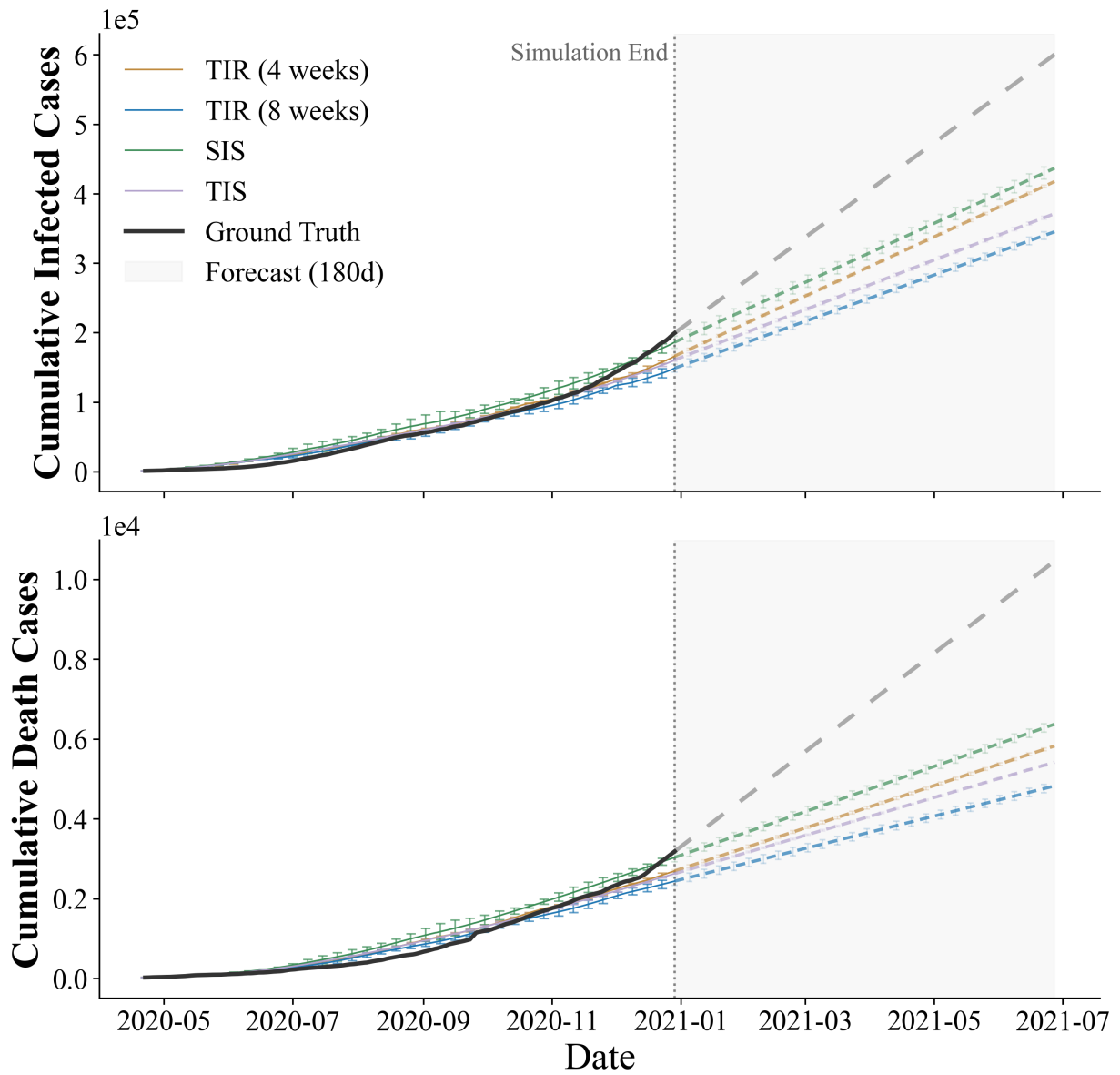
**Supplementary Figure 28.** Simulated results in Virginia. The quarantined and death curves show good fit, with  $R^2 = 0.841$  and  $R^2 = 0.774$ , respectively.



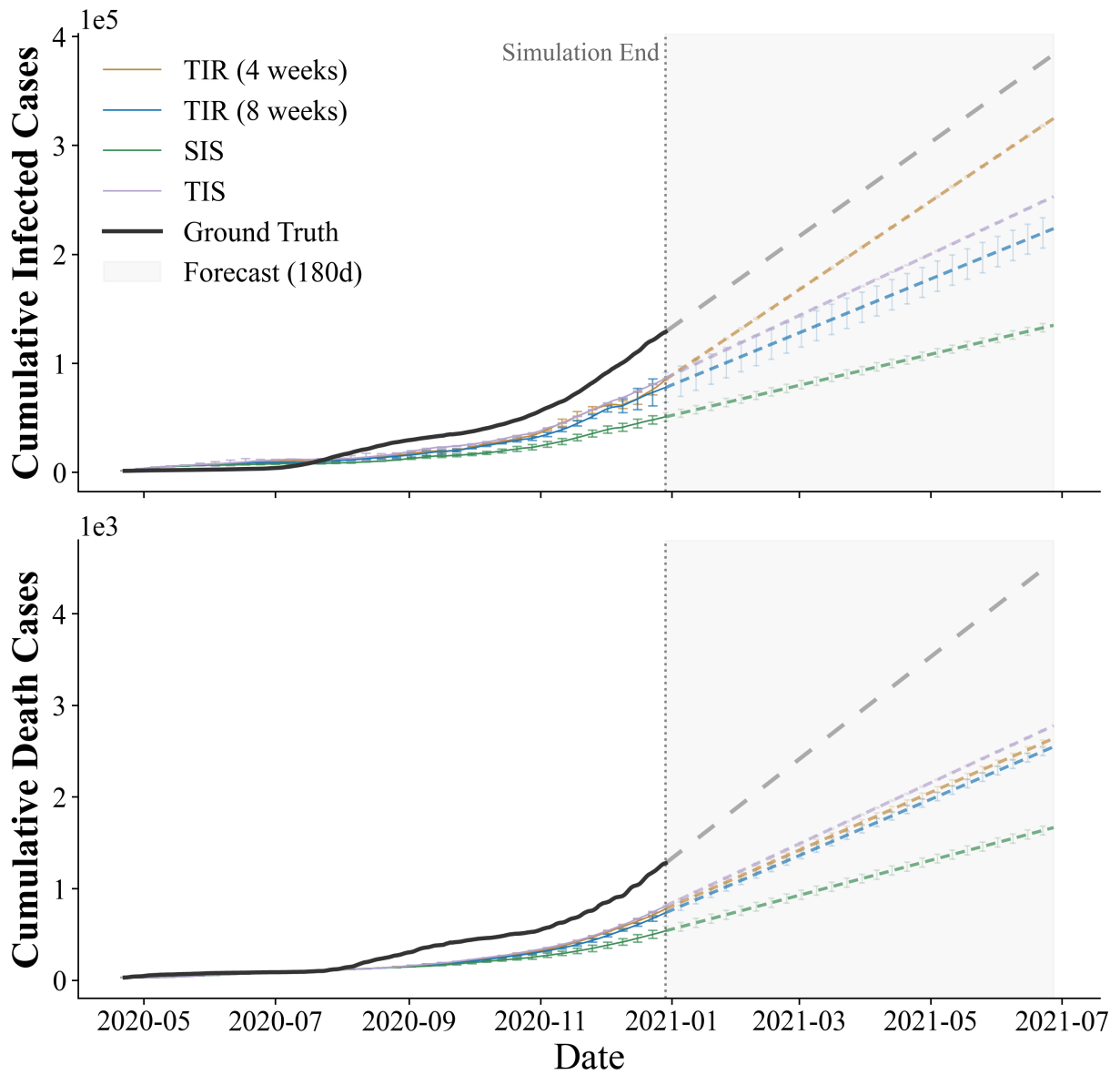
**Supplementary Figure 29.** Pandemic control performance in Alabama of 20-state results. In addition to model-estimated total infections and deaths, 180-day forward trajectories were projected. 4-week TIR achieves the lowest total infection among interventions, while 8-week TIR is most effective in reducing mortality.



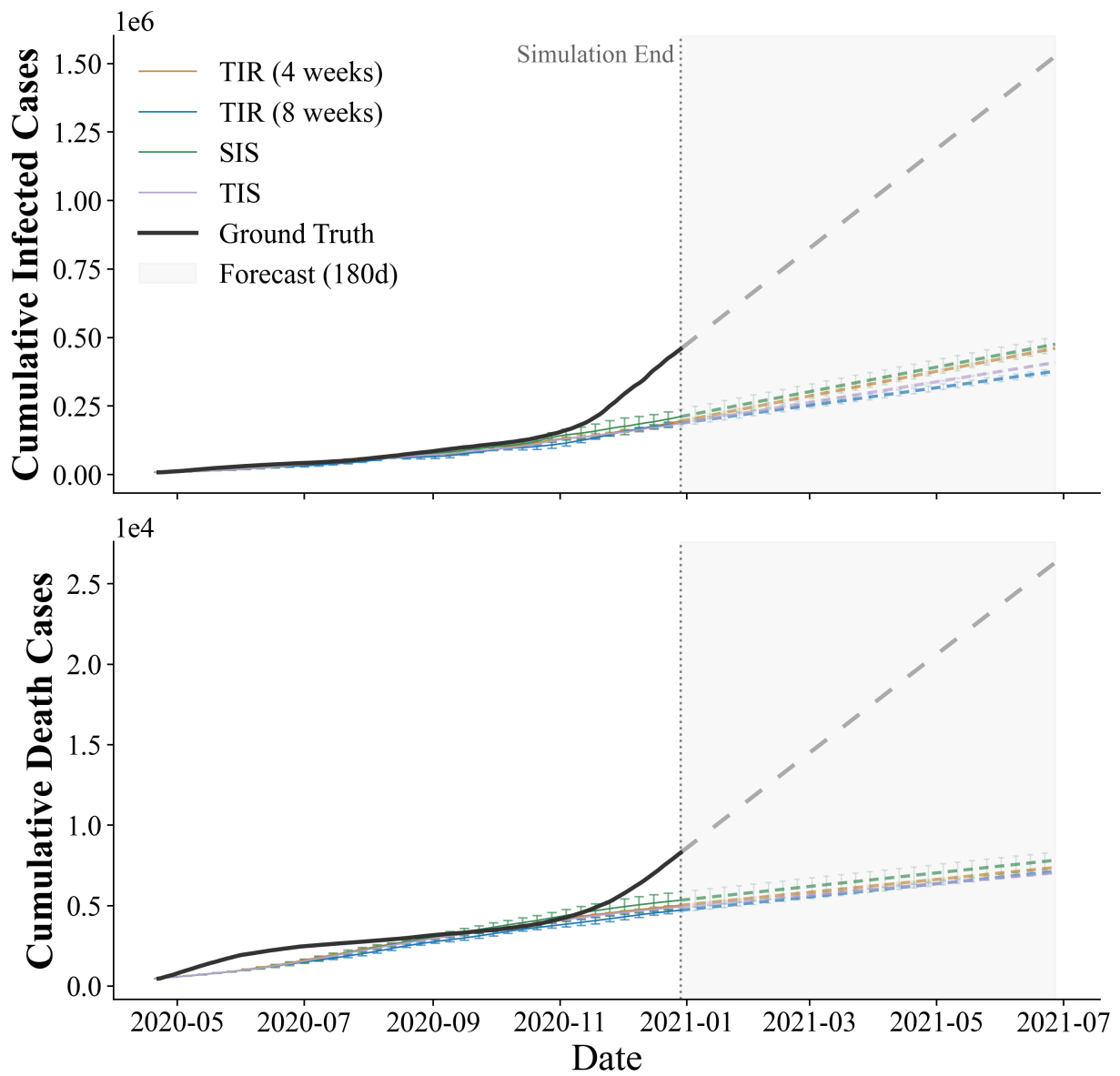
**Supplementary Figure 30.** Pandemic control performance in Arizona of 20-state results. In addition to model-estimated total infections and deaths, 180-day forward trajectories were projected. 8-week TIR is most effective in reducing both infection and mortality.



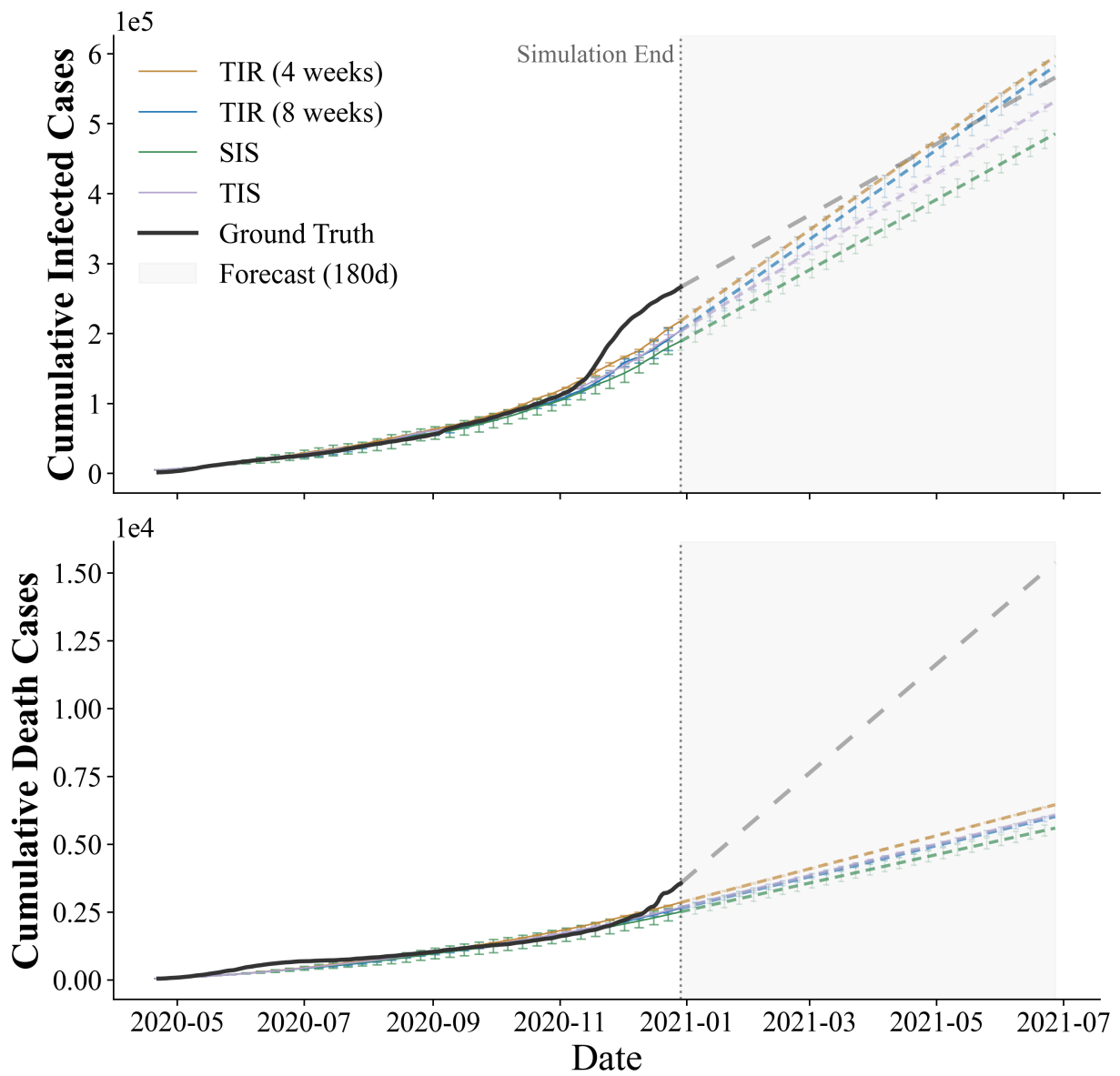
**Supplementary Figure 31.** Pandemic control performance in Arkansas of 20-state results. In addition to model-estimated total infections and deaths, 180-day forward trajectories were projected. 8-week TIR is most effective in reducing both infection and mortality.

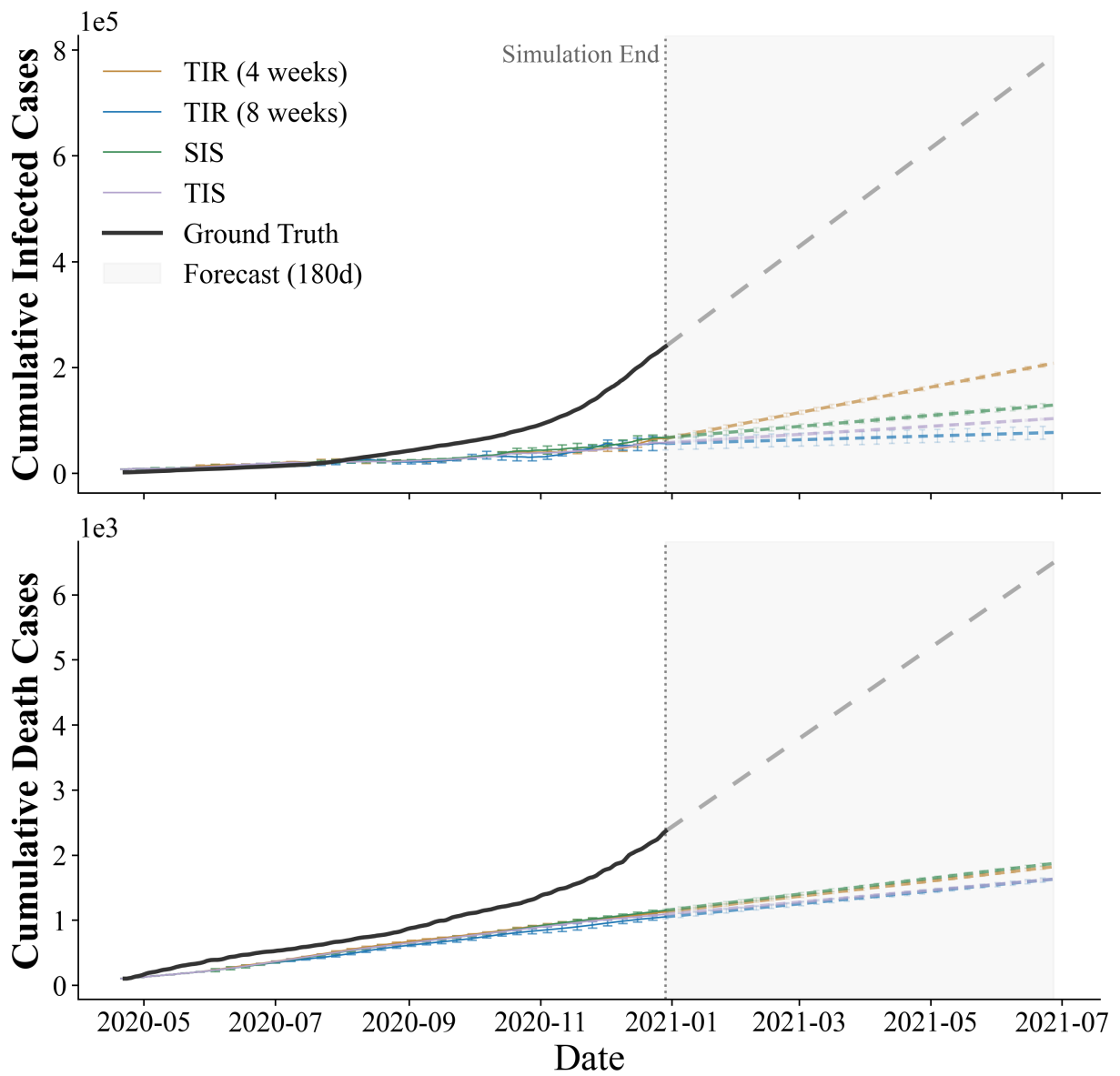


**Supplementary Figure 32.** Pandemic control performance in Idaho of 20-state results. In addition to model-estimated total infections and deaths, 180-day forward trajectories were projected. SIS is most effective in reducing both infection and mortality.

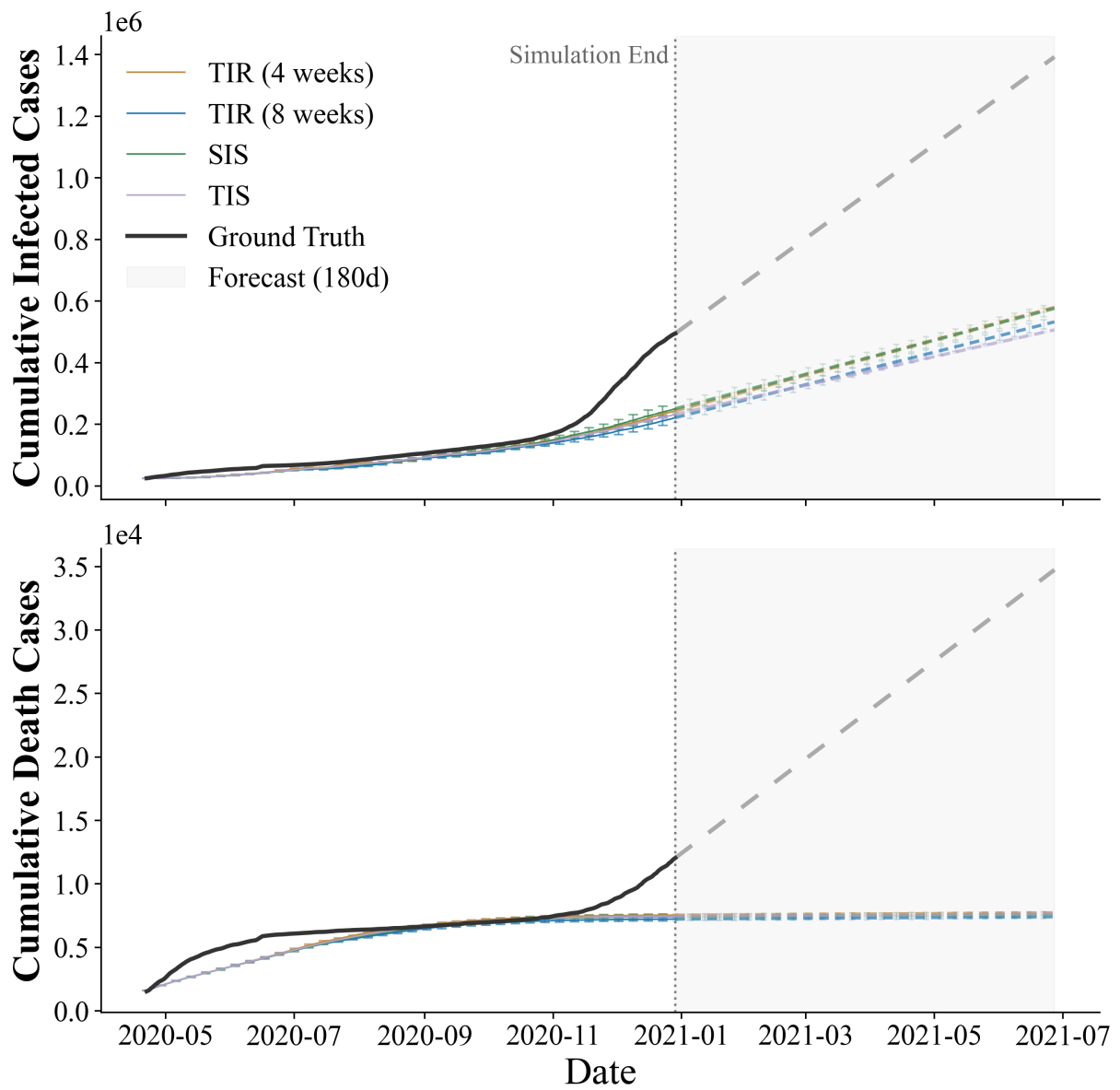


**Supplementary Figure 33.** Pandemic control performance in Indiana of 20-state results. In addition to model-estimated total infections and deaths, 180-day forward trajectories were projected. 8-week TIR achieves the lowest total infection among interventions, while 8-week TIR and TIS are most effective in reducing mortality.

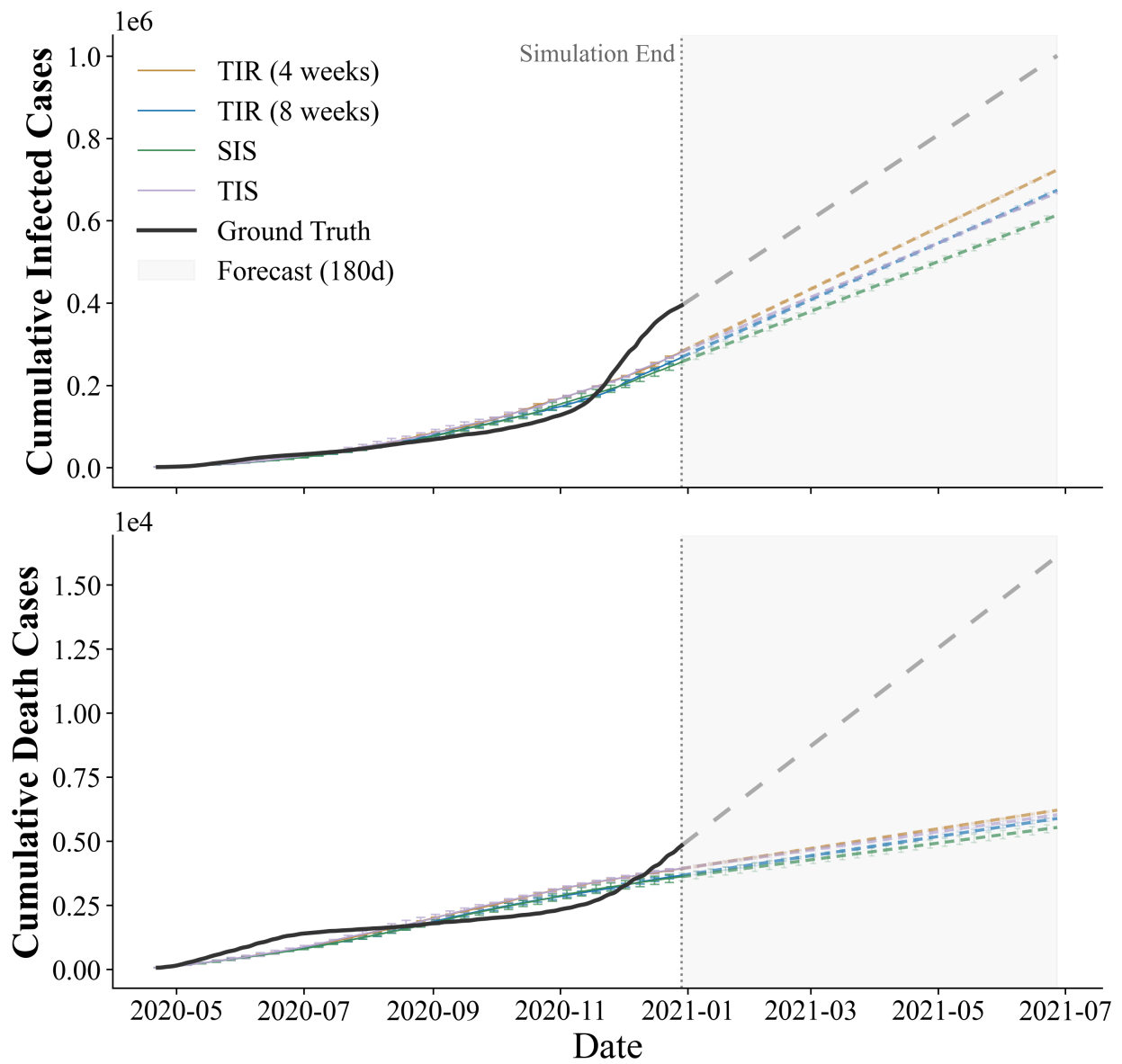




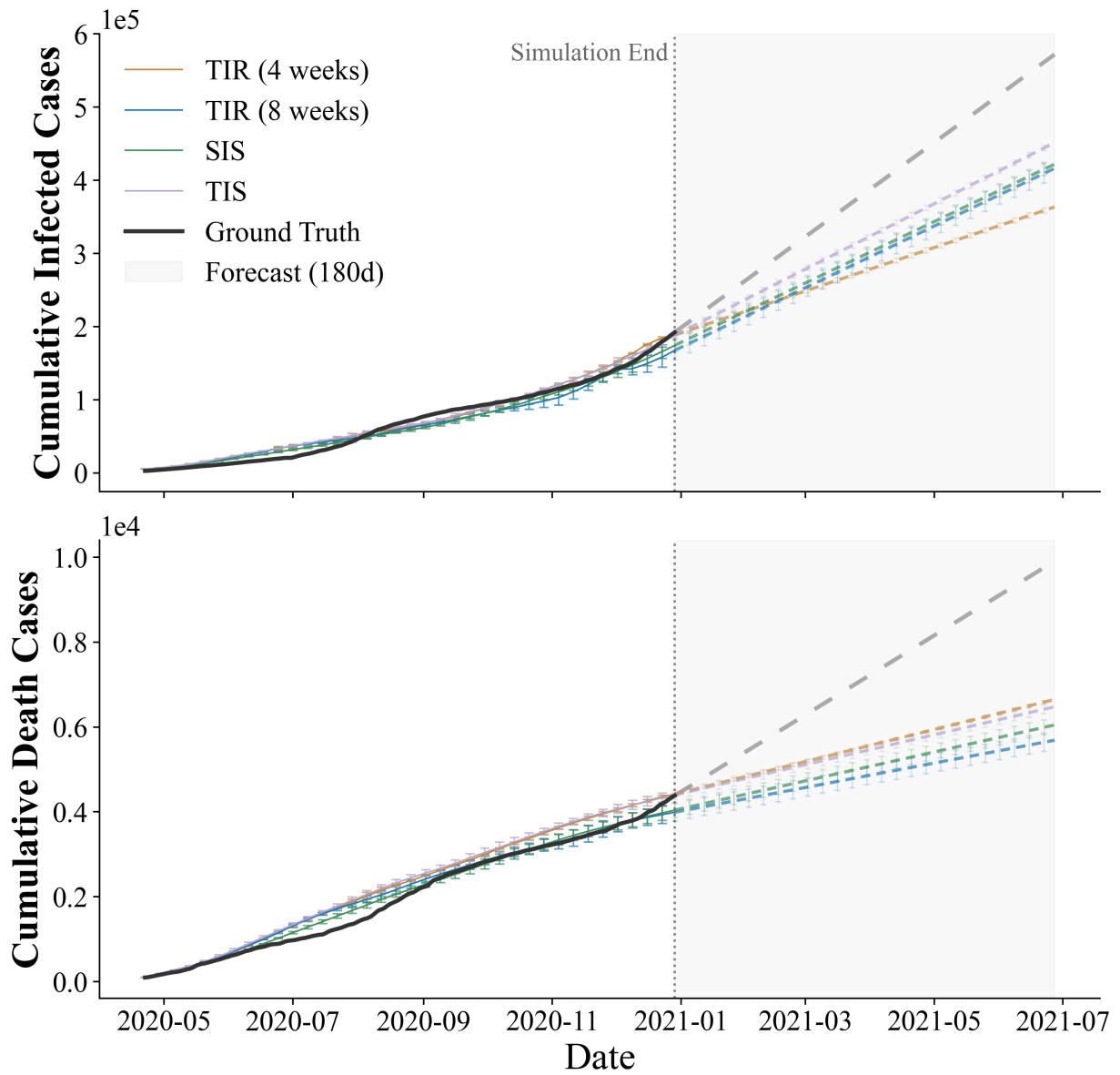
**Supplementary Figure 35.** Pandemic control performance in Kentucky of 20-state results. In addition to model-estimated total infections and deaths, 180-day forward trajectories were projected. 8-week TIR achieves the lowest total infection among interventions, while 8-week TIR and TIS are most effective in reducing mortality.



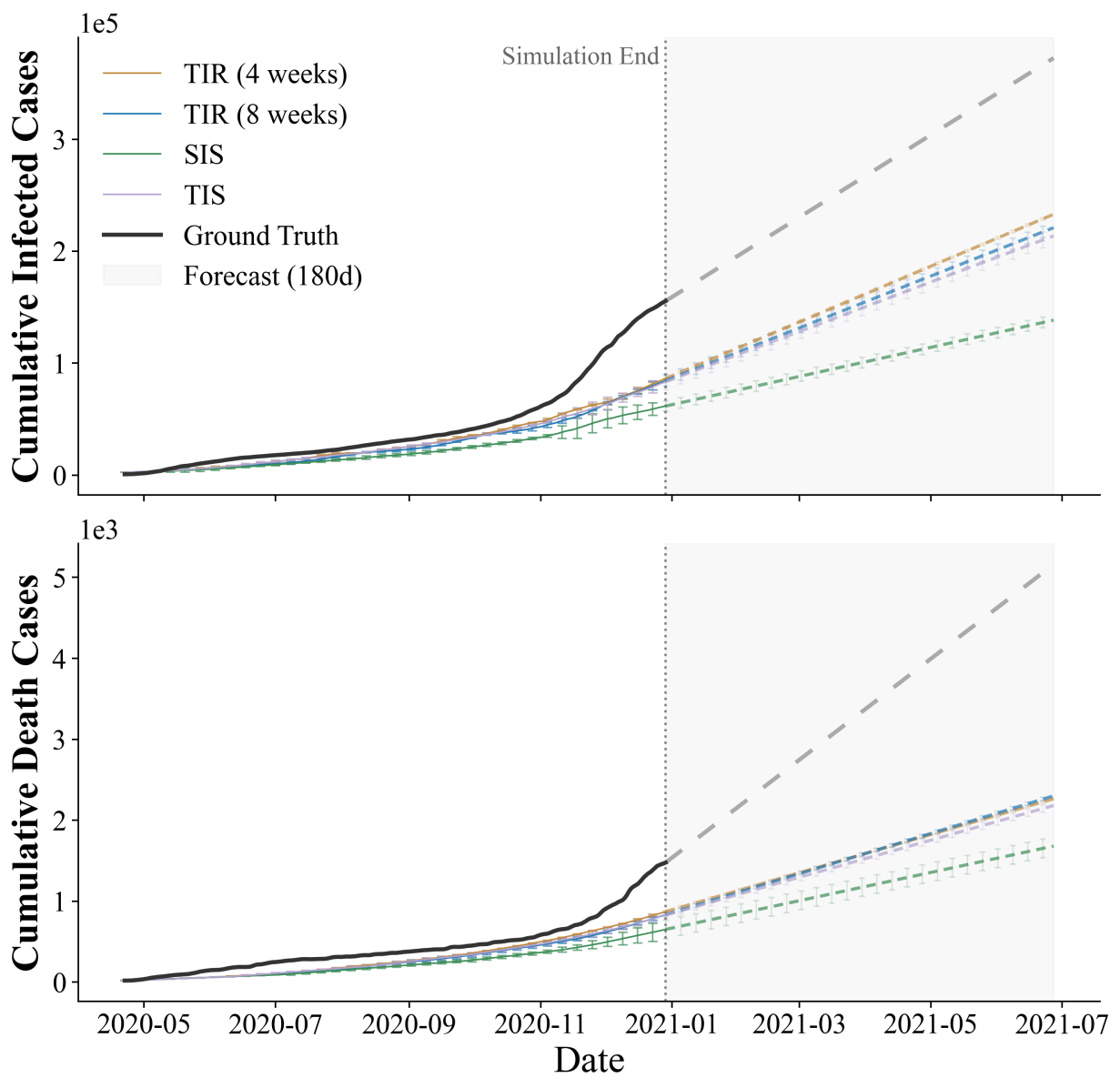
**Supplementary Figure 36.** Pandemic control performance in Michigan of 20-state results. In addition to model-estimated total infections and deaths, 180-day forward trajectories were projected. TIS achieves the lowest total infection among interventions, while all strategies exhibit similar performance in reducing mortality.



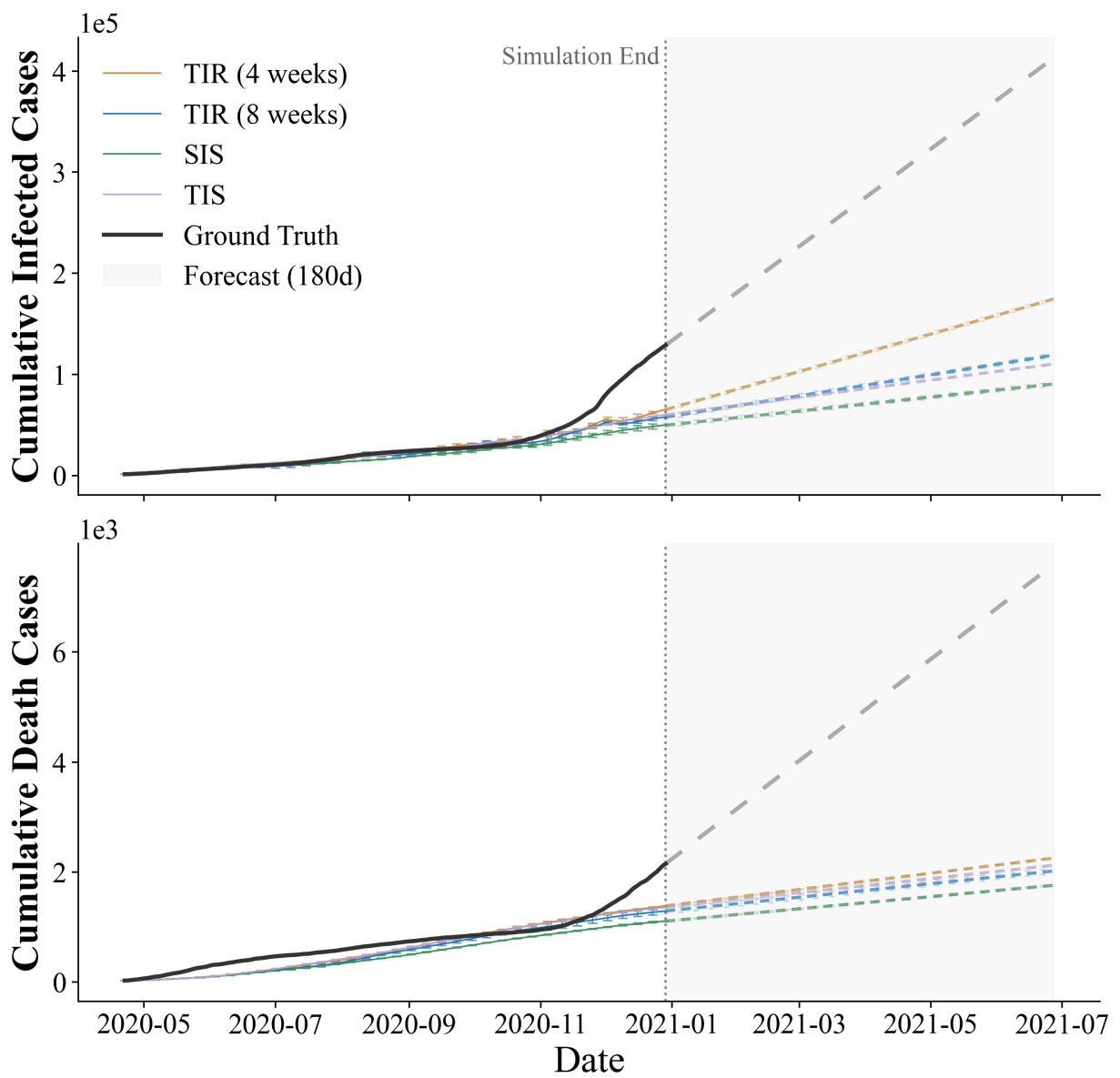
**Supplementary Figure 37.** Pandemic control performance in Minnesota of 20-state results. In addition to model-estimated total infections and deaths, 180-day forward trajectories were projected. SIS is most effective in reducing mortality and infection.



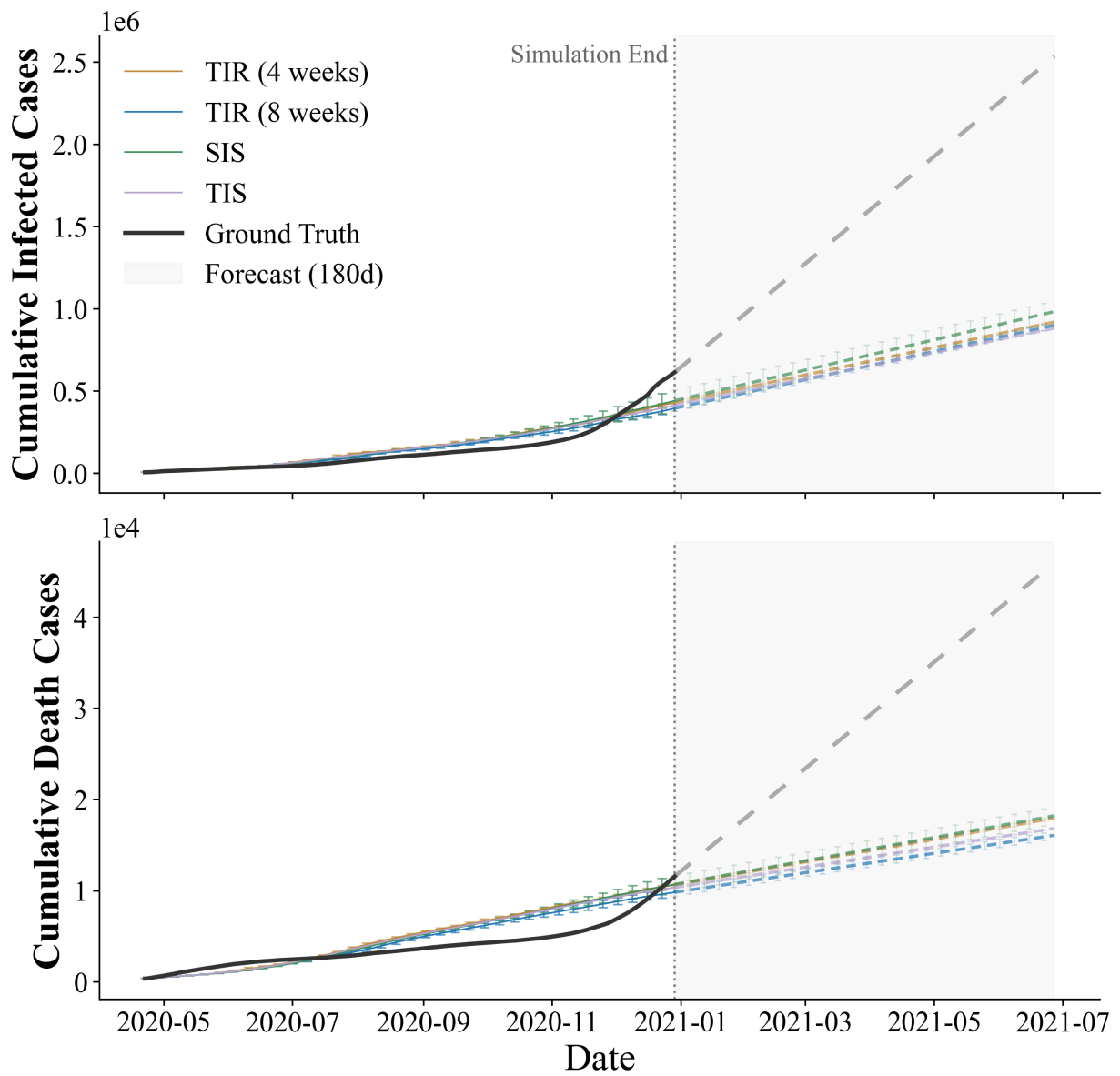
**Supplementary Figure 38.** Pandemic control performance in Mississippi of 20-state results. In addition to model-estimated total infections and deaths, 180-day forward trajectories were projected. 4-week TIR achieves the lowest total infection among interventions, while 8-week TIR is most effective in reducing mortality.



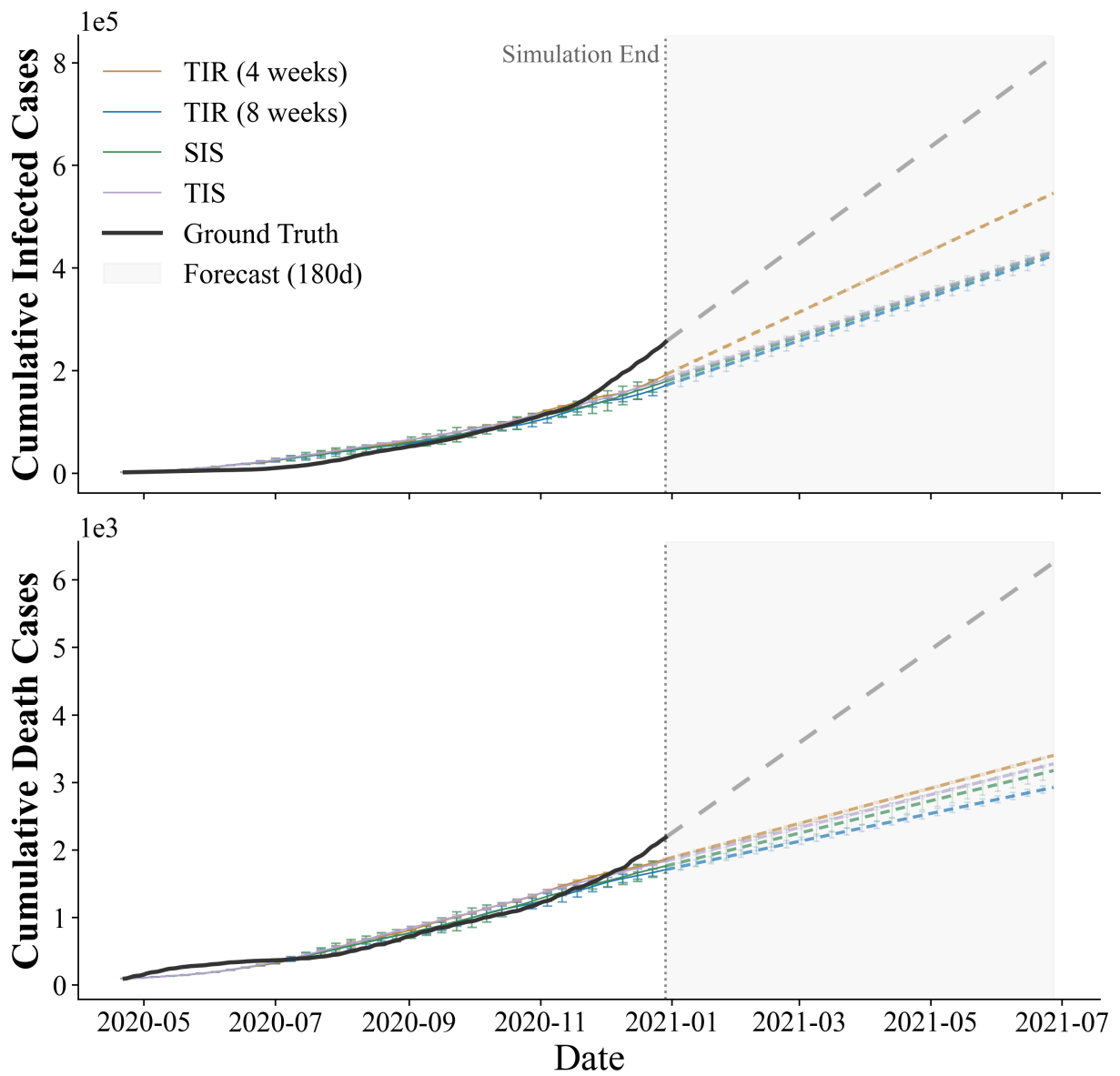
**Supplementary Figure 39.** Pandemic control performance in Nebraska of 20-state results. In addition to model-estimated total infections and deaths, 180-day forward trajectories were projected. SIS is most effective in reducing mortality and infection.

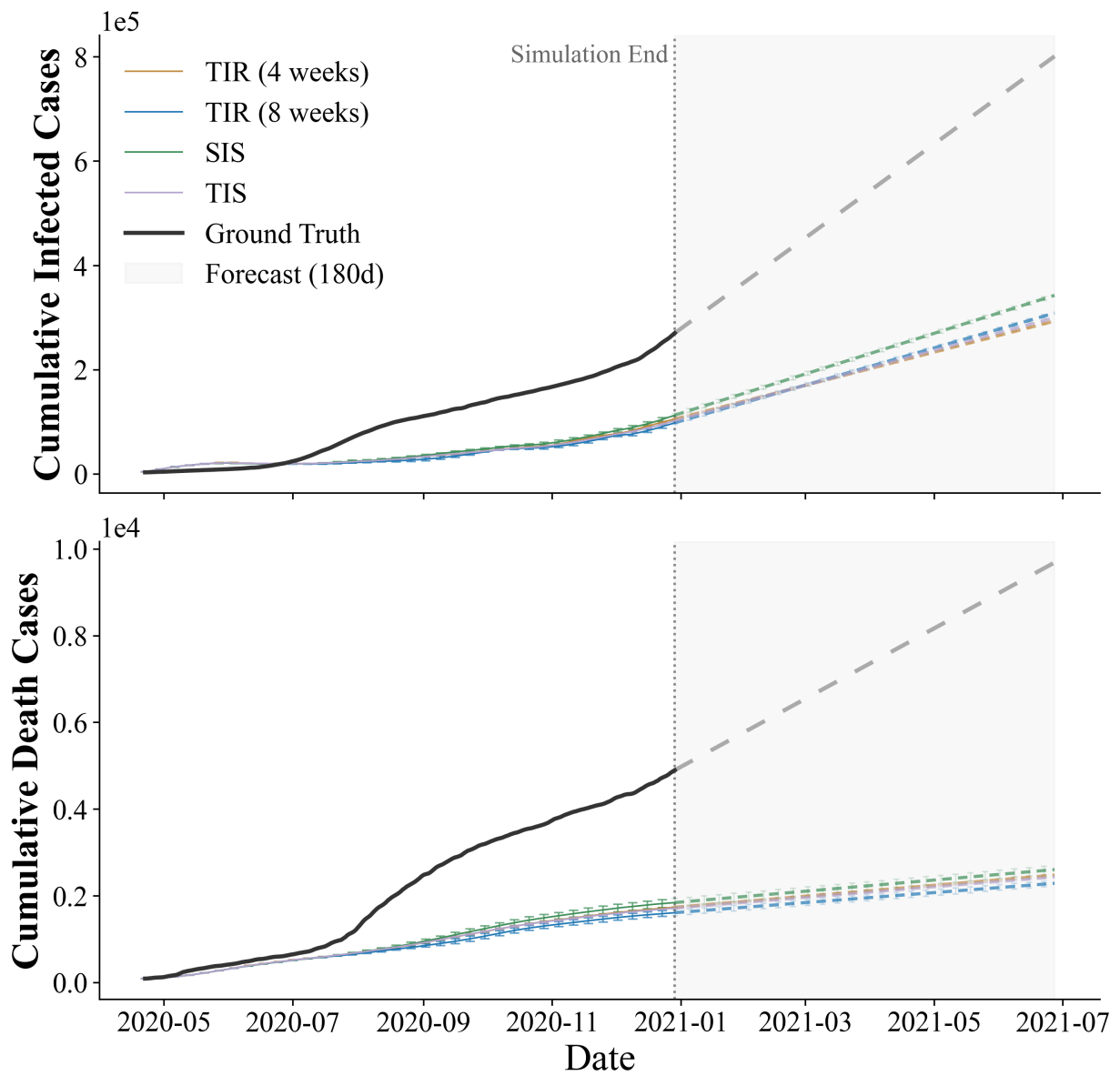


**Supplementary Figure 40.** Pandemic control performance in New Mexico of 20-state results. In addition to model-estimated total infections and deaths, 180-day forward trajectories were projected. SIS is most effective in reducing mortality and infection.

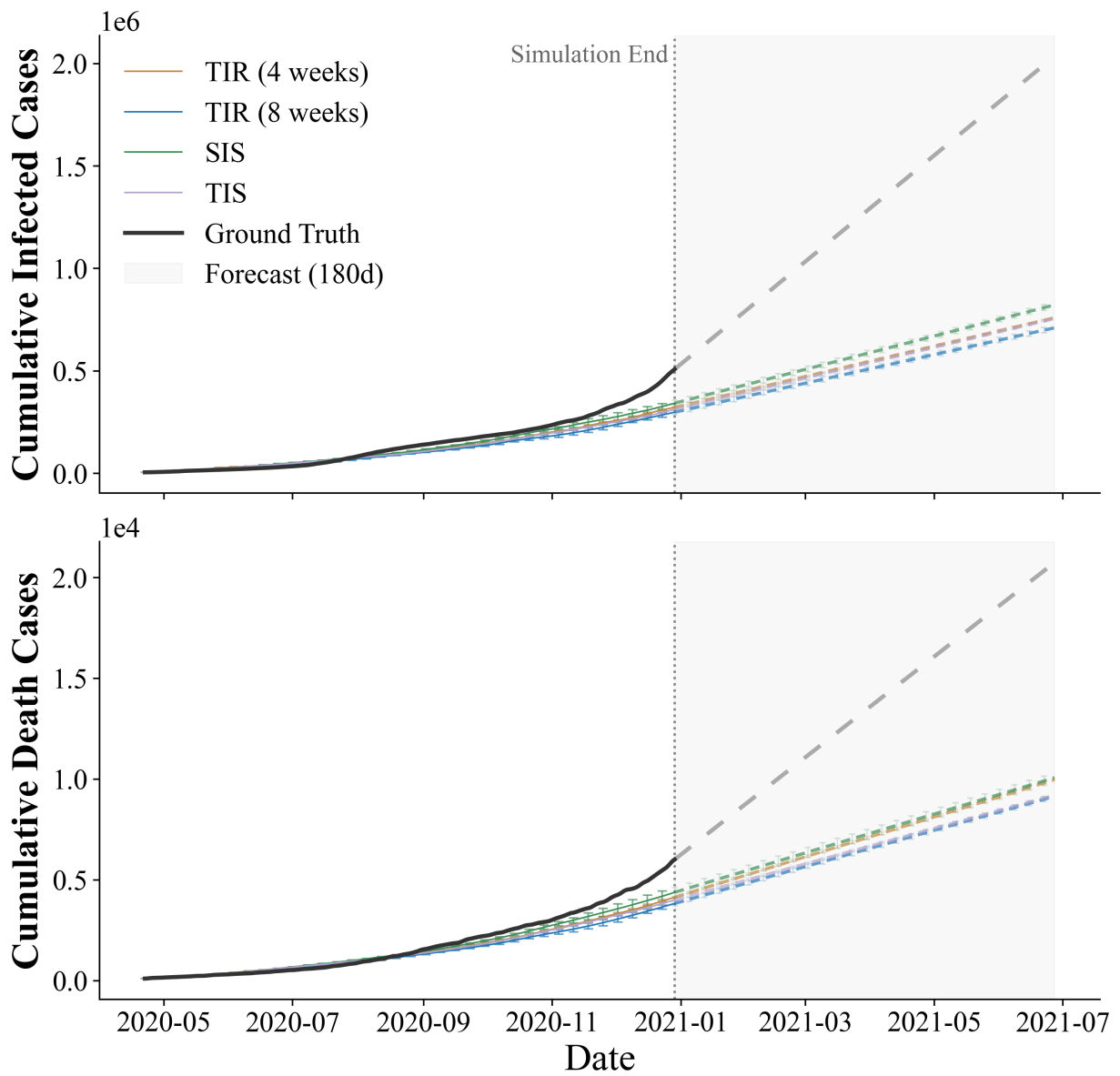


**Supplementary Figure 41.** Pandemic control performance in Ohio of 20-state results. In addition to model-estimated total infections and deaths, 180-day forward trajectories were projected. 8-week TIR and TIS achieve the lowest total infection among interventions, while 8-week TIR is most effective in reducing mortality.

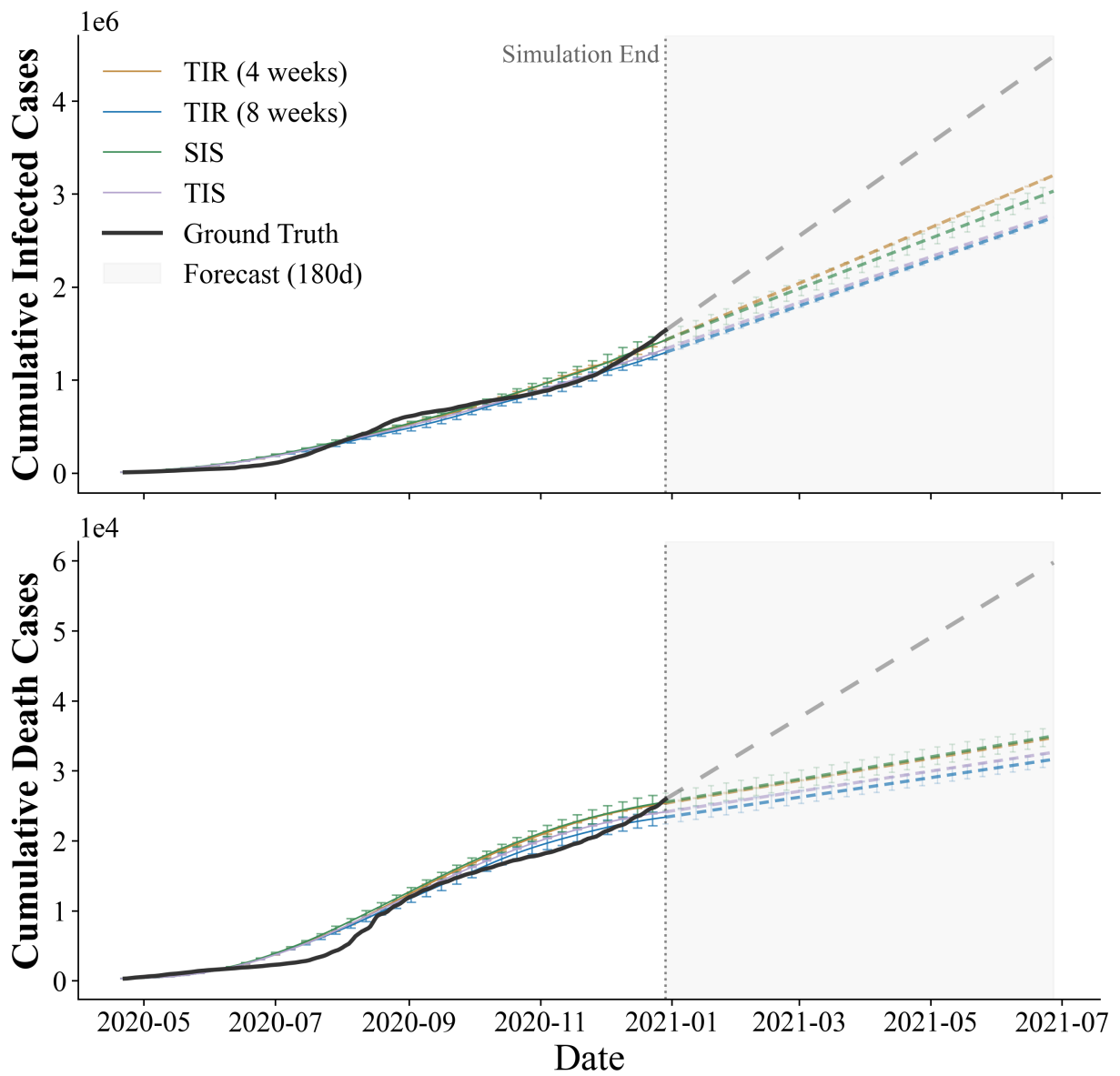




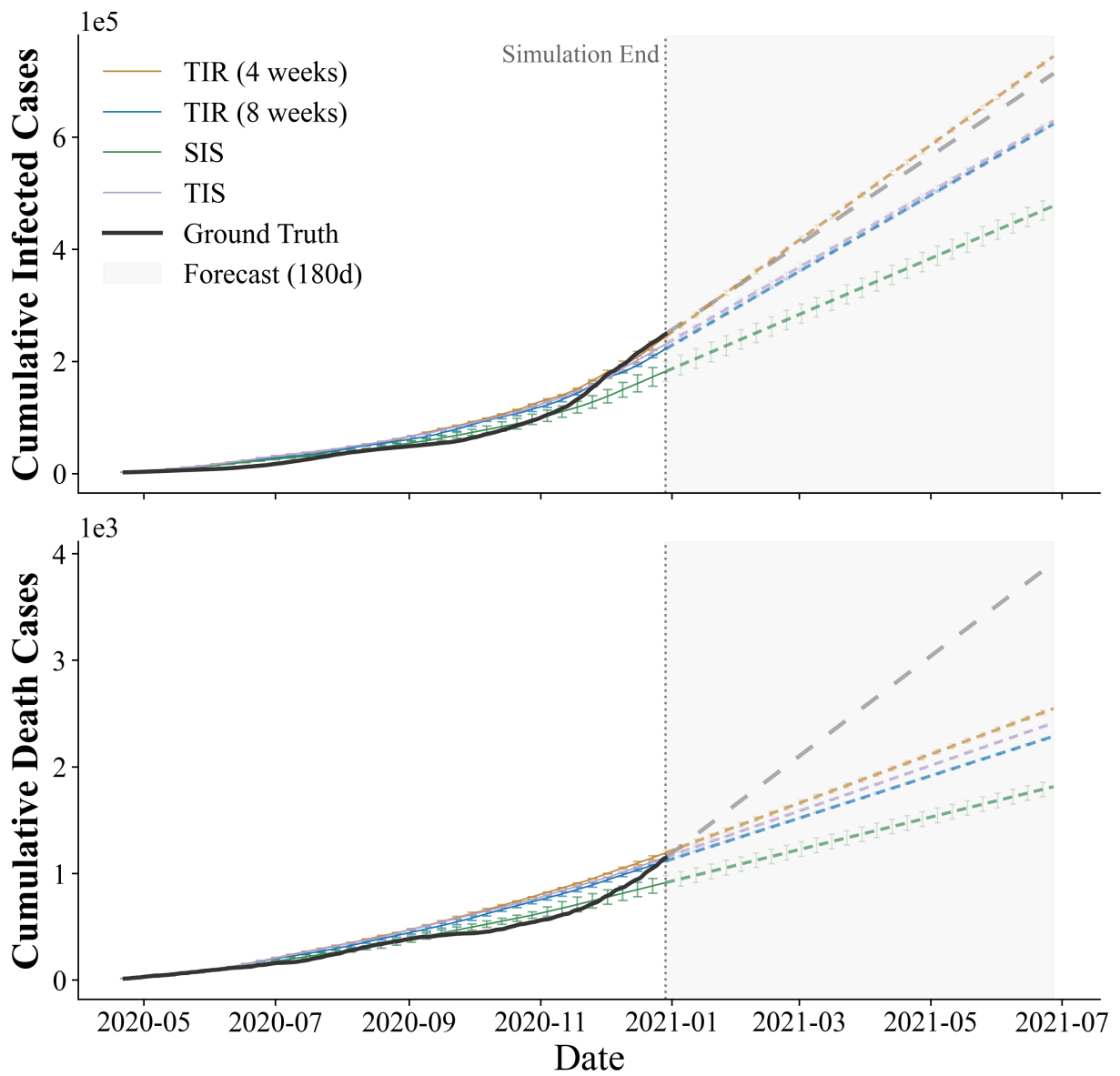
**Supplementary Figure 43.** Pandemic control performance in South Carolina of 20-state results. In addition to model-estimated total infections and deaths, 180-day forward trajectories were projected. 8-week TIR is most effective in reducing mortality and infection.



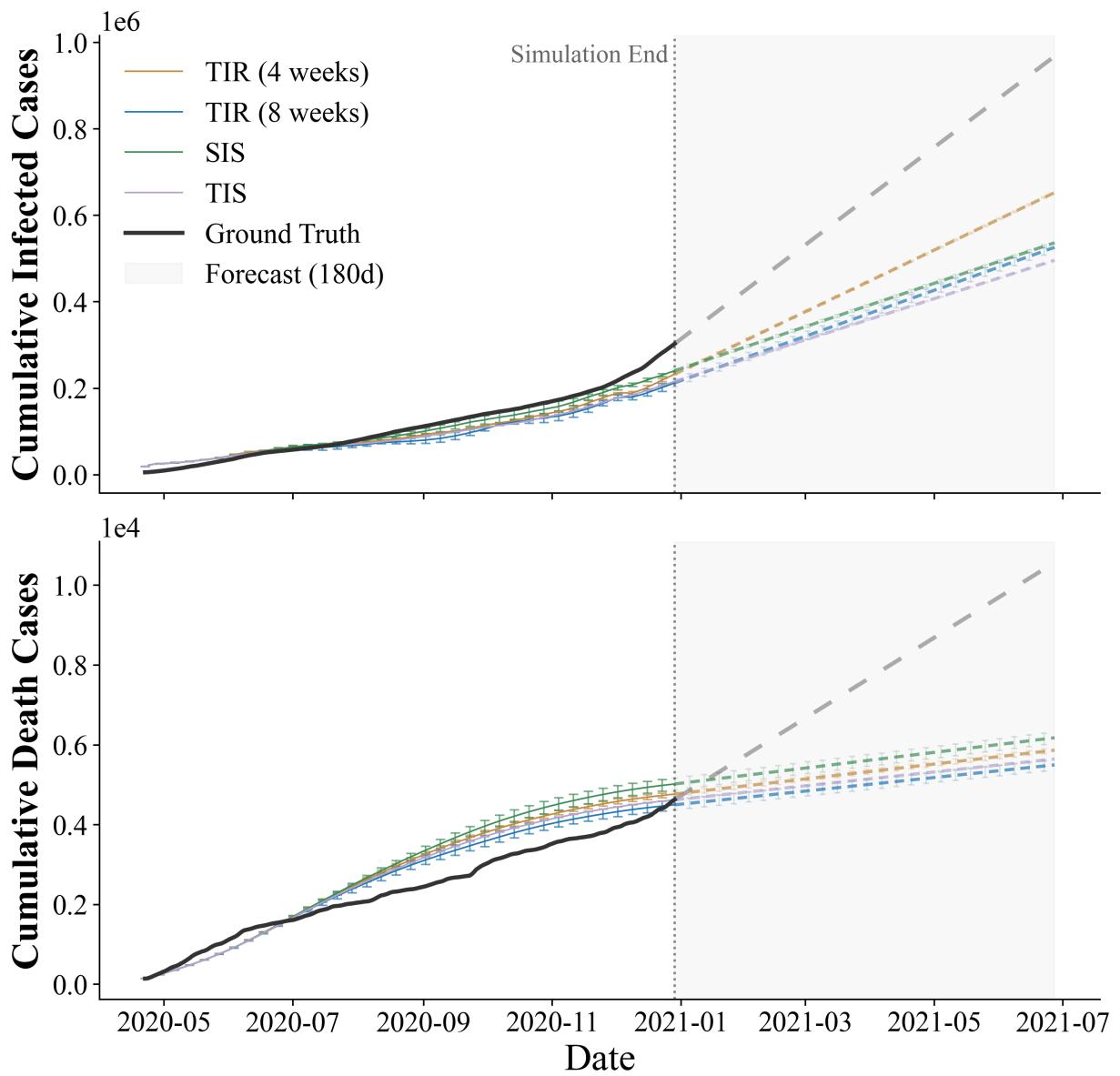
**Supplementary Figure 44.** Pandemic control performance in Tennessee of 20-state results. In addition to model-estimated total infections and deaths, 180-day forward trajectories were projected. 8-week TIR is most effective in reducing morality and infection.

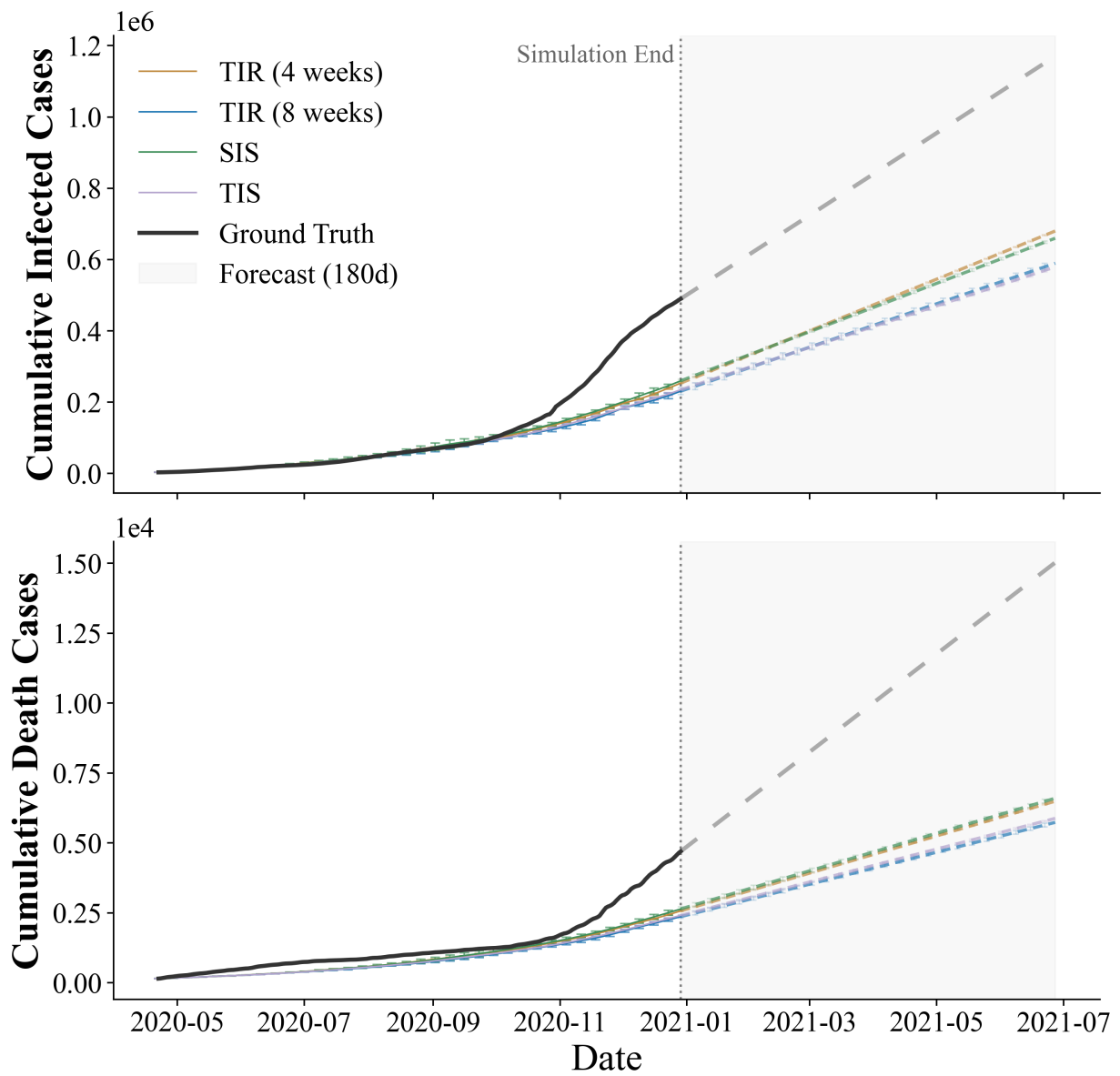


**Supplementary Figure 45.** Pandemic control performance in Texas of 20-state results. In addition to model-estimated total infections and deaths, 180-day forward trajectories were projected. 8-week TIR and TIS are most effective in reducing both infection and mortality.



**Supplementary Figure 46.** Pandemic control performance in Utah of 20-state results. In addition to model-estimated total infections and deaths, 180-day forward trajectories were projected. SIS is most effective in reducing both infection and mortality.





**Supplementary Figure 48.** Pandemic control performance in Wisconsin of 20-state results. In addition to model-estimated total infections and deaths, 180-day forward trajectories were projected. TIS and 8-week TIR are most effective in reducing both infection and mortality.

### 3. Supplementary Tables

**Supplementary Table 1.** ACR (per 100 k) with different intervention strategies across 20 states

State	Abbr	Ground Truth	TIR (4 weeks)	TIR (8 weeks)	SIS	TIS
alabama	AL	1168.97	465.60	417.67	462.87	440.20
arizona	AZ	1921.34	1175.83	1086.54	1151.39	1124.82
arkansas	AR	249.62	211.84	191.04	239.06	206.26
idaho	ID	1075.97	881.32	828.62	580.73	935.57
indiana	IN	567.16	341.89	328.89	374.83	333.34
iowa	IA	781.93	638.71	592.14	556.45	597.04
kentucky	KY	1128.43	496.19	467.71	528.41	481.38
michigan	MI	525.47	380.43	350.00	389.28	369.50
minnesota	MN	168.76	128.12	121.87	117.17	127.86
mississippi	MS	340.12	376.24	327.41	340.40	368.36
nebraska	NE	855.34	541.49	518.16	394.56	523.29
new mexico	NM	867.87	654.60	608.61	522.31	638.13
ohio	OH	323.92	287.66	264.71	294.08	278.09
oklahoma	OK	270.76	219.69	199.11	207.97	214.57
south carolina	SC	849.69	333.66	308.43	354.99	324.97
tennessee	TN	329.84	242.27	224.05	256.43	234.54
texas	TX	382.89	393.16	360.62	395.76	370.84
utah	UT	592.62	594.54	552.31	454.72	571.03
virginia	VA	1203.81	1041.74	971.98	1120.75	996.92
wisconsin	WI	461.38	245.57	225.14	253.14	229.77

**Supplementary Table 2.** DR (per 100 k) with different intervention strategies across 20 states

State	Abbr	Ground Truth	TIR (4 weeks)	TIR (8 weeks)	SIS	TIS
alabama	AL	0.3429	0.1321	0.1200	0.1317	0.1278
arizona	AZ	0.4221	0.4026	0.3772	0.4034	0.3928
arkansas	AR	0.4163	0.3586	0.3250	0.4047	0.3500
idaho	ID	0.2761	0.1661	0.1569	0.1137	0.1736
indiana	IN	0.4485	0.2728	0.2538	0.2923	0.2671
iowa	IA	0.4375	0.3581	0.3306	0.3138	0.3348
kentucky	KY	0.1971	0.0924	0.0855	0.0945	0.0893
michigan	MI	0.3855	0.2297	0.2166	0.2244	0.2259
minnesota	MN	0.3339	0.2788	0.2597	0.2559	0.2796
mississippi	MS	0.5746	0.5856	0.5265	0.5331	0.5825
nebraska	NE	0.3040	0.1761	0.1679	0.1303	0.1672
new mexico	NM	0.3950	0.2647	0.2466	0.2107	0.2602
ohio	OH	0.3682	0.3568	0.3285	0.3586	0.3472
oklahoma	OK	0.2067	0.1815	0.1658	0.1714	0.1789
south carolina	SC	0.3786	0.1306	0.1206	0.1393	0.1290
tennessee	TN	0.3389	0.2379	0.2195	0.2526	0.2300
texas	TX	0.3542	0.3559	0.3277	0.3584	0.3385
utah	UT	0.1387	0.1487	0.1391	0.1135	0.1435
virginia	VA	0.2065	0.2190	0.2060	0.2313	0.2121
wisconsin	WI	0.3042	0.1663	0.1523	0.1713	0.1554

**Supplementary Table 3.** IR (per 100 k) with different intervention strategies across 20 states

State	Abbr	Ground Truth	TIR (4 weeks)	TIR (8 weeks)	SIS	TIS
alabama	AL	25.39	9.55	8.73	8.93	8.21
arizona	AZ	24.10	9.09	8.23	8.17	7.96
arkansas	AR	26.05	21.74	19.46	24.44	21.04
idaho	ID	28.59	18.45	17.04	10.83	18.66
indiana	IN	26.38	11.22	10.87	12.14	10.64
iowa	IA	33.74	26.96	25.10	23.30	25.14
kentucky	KY	21.09	7.70	6.82	5.83	4.86
michigan	MI	18.60	8.93	7.92	9.10	8.38
minnesota	MN	28.15	19.90	18.90	18.12	19.80
mississippi	MS	25.15	24.85	21.83	22.64	24.43
nebraska	NE	32.16	17.32	16.93	12.31	16.70
new mexico	NM	24.12	13.54	11.80	9.12	11.10
ohio	OH	20.30	14.54	13.29	14.90	13.92
oklahoma	OK	25.39	19.04	17.10	17.88	18.38
south carolina	SC	20.56	7.68	6.96	8.04	7.26
tennessee	TN	28.68	18.52	17.08	19.60	17.83
texas	TX	20.94	19.70	17.87	19.72	18.40
utah	UT	30.66	29.85	27.25	22.35	28.38
virginia	VA	13.70	9.81	8.91	10.14	8.94
wisconsin	WI	33.68	17.11	15.56	17.57	15.87

**Supplementary Table 4.** Ground-truth COVID-19 policy timeline for Arizona in 2020.

Date	Policy	Description	Primary mobility impact	Source
2020-04-29	Limited reopening	Extends the stay-at-home framework through May 15 while allowing limited retail reopening under conditions.	Tempered rebound of commuting and discretionary trips; sustained low travel elasticity.	<a href="https://azgovernor.gov/sites/default/files/eo_2020-33_0.pdf">https://azgovernor.gov/sites/default/files/eo_2020-33_0.pdf</a>
2020-06-19	Mask mandates & Pause of high-risk venues	City/county-level face covering requirements for public places and transit riders/operators.	Reduced close-contact transmission risk on transit and in indoor venues.	<a href="https://cronkitenews.azpbs.org/2020/06/19/covid-19-in-arizona...a.gov/DocumentCenter/View/61311/Regulations-on-Face-Coverings">https://cronkitenews.azpbs.org/2020/06/19/covid-19-in-arizona...a.gov/DocumentCenter/View/61311/Regulations-on-Face-Coverings</a>
2020-08-15	Normalization of event approvals	Events exceeding 50 people required local approval with mitigation measures.	Constrained cross-city/cross-county travel surges tied to large events; reduced cluster risks.	<a href="https://azgovernor.gov/executive-orders">https://azgovernor.gov/executive-orders</a>
2020 fall	Local mask mandates	Counties and transportation systems continue to enforce mask requirements and contact reduction measures.	Maintain protective measures in public transportation and indoor activity settings.	<a href="https://www.maricopa.gov/DocumentCenter/View/61311/Regulations-on-Face-Coverings">https://www.maricopa.gov/DocumentCenter/View/61311/Regulations-on-Face-Coverings</a>

**Supplementary Table 5.** Ground-truth COVID-19 policy timeline for Mississippi in 2020.

Date	Policy	Description	Primary mobility impact	Source
2020/4/27	Safer at Home Order	Initiates 'Safer at Home' statewide on 4/27 with limited economic reopening under health safeguards.	Continues stay-at-home posture, dampening rebound in commuting and discretionary travel.	<a href="https://www.sos.ms.gov/content/executiveorders/ExecutiveOrders/1477.pdf">https://www.sos.ms.gov/content/executiveorders/ExecutiveOrders/1477.pdf</a>
2020/6/1	Statewide Safe Return	Moves statewide into 'Safe Return' allowing more sectors to open with capacity and mitigation rules.	Commuting/consumer trips resumed gradually; event-driven mobility still constrained.	<a href="https://www.sos.ms.gov/content/executiveorders/ExecutiveOrders/1492.pdf">https://www.sos.ms.gov/content/executiveorders/ExecutiveOrders/1492.pdf</a>
2020/7/13	County-level mask mandates	First wave of county mask orders with added business limitations, later expanded to more counties.	Raises protection for indoor/commercial travel in hot-spot counties, reducing close-contact risk.	<a href="https://jacksonfreepress.media.clients.ellingtoncms.com/news/documents/2020/07/13/Executive_Order_1507_-_Counties_Require_Masks.pdf">https://jacksonfreepress.media.clients.ellingtoncms.com/news/documents/2020/07/13/Executive_Order_1507_-_Counties_Require_Masks.pdf</a>
2020/8/4	Statewide mask mandate	Statewide face covering requirement starting 8/5; delays in-person start for grades 7–12 in eight counties.	Uniform mitigation in public/transit settings; slows full resumption of school commuting.	<a href="https://www.sos.ms.gov/content/executiveorders/ExecutiveOrders/1516.pdf">https://www.sos.ms.gov/content/executiveorders/ExecutiveOrders/1516.pdf</a>
2020/9/30	Lifts mask mandate	Ends statewide mandate while keeping limits where distancing not possible (e.g., 20 indoor/100 outdoor).	Shifts from statewide to localized control; event/leisure mobility still limited by size caps.	<a href="https://www.sos.ms.gov/content/executiveorders/ExecutiveOrders/1525.pdf">https://www.sos.ms.gov/content/executiveorders/ExecutiveOrders/1525.pdf</a>
2020/10/21	Mask mandate reinstatement	Reimposes mask rules in 9 counties (10/21) and adds 7 more (10/27), adjusted as conditions change.	Tightens indoor activity risk in fall surge hot spots; curbs cross-county event travel.	<a href="https://www.sos.ms.gov/content/executiveorders/ExecutiveOrders/1527.pdf">https://www.sos.ms.gov/content/executiveorders/ExecutiveOrders/1527.pdf</a>
2020/11/10	Gathering limits	Multiple waves broaden coverage; by 12/11, mask mandates cover 61 counties with stricter gathering caps.	Suppresses large gatherings and cross-area movement during winter resurgence.	<a href="https://www.sos.ms.gov/communications-publications/executive-orders">https://www.sos.ms.gov/communications-publications/executive-orders</a>

**Supplementary Table 6.** Ground-truth COVID-19 policy timeline for New Mexico in 2020.

Date	Policy	Description	Primary mobility impact	Source
2020/5/15	Mask mandates	Face coverings required in all public settings while limited retail reopening proceeds.	Reduces close-contact risk in commercial/transit settings; underpins cautious reopening.	
2020/7/1	Self-isolation for incoming travelers	Individuals arriving from out of state must self-isolate for 14 days or for the duration of their stay.	Raises the cost of interstate trips, reducing non-essential travel and visits.	<a href="https://www.nmhealth.org/publication/view/rules/6126/">https://www.nmhealth.org/publication/view/rules/6126/</a>
2020/9/3	Risk-based travel quarantine easing	Quarantine eased for travelers from low-risk states; Safe Certified hotels may increase capacity.	Allows a measured uptick in interstate travel under safeguards.	
2020/10/16	Business restrictions	From 10/16, closing hours imposed for some venues; on 10/23, hotspot retail/food rules strengthened.	Suppresses nightlife/weekend mobility and high-risk contacts.	<a href="https://cv.nmhealth.org/2020/10/16/new-emergency-public-health-order-in-effect/">https://cv.nmhealth.org/2020/10/16/new-emergency-public-health-order-in-effect/</a>
2020/11/16	Statewide stay-at-home	Residents instructed to stay home except for essential trips; mass gatherings capped at five.	Sharp reduction in non-essential trips and cross-area activities during winter surge.	

**Supplementary Table 7.** Ground-truth COVID-19 policy timeline for Texas in 2020.

Date	Policy	Description	Primary mobility impact	Source
2020/4/27	Limited reopening	From 5/1, permitted 25% occupancy for certain retail/dining/movie theaters/malls and set minimum health protocols.	Gradual resumption of discretionary trips under capacity and mitigation rules.	<a href="https://gov.texas.gov/uploads/files/press/EO-GA-18_expanded_reopening_of_services_COVID-19.pdf">https://gov.texas.gov/uploads/files/press/EO-GA-18_expanded_reopening_of_services_COVID-19.pdf</a>
2020/6/26	Restricting gatherings	In response to rising cases/hospitalizations, closed bars to on-premise service, reduced restaurant capacity to 50%, and curtailed large outdoor events.	Nightlife/weekend leisure travel dropped sharply; cross-city recreation suppressed.	<a href="https://www.texastribune.org/2020/06/26/texas-bars-restaurants-coronavirus-greg-abbott/">https://www.texastribune.org/2020/06/26/texas-bars-restaurants-coronavirus-greg-abbott/</a>
2020/7/2	Mandated mask & reopening	Mandated face coverings in most public settings; empowered local officials to restrict outdoor gatherings >10.	Reduced risk in transit/indoor commercial settings; curbed large events.	
2020/9/17	Expanded openings to 75% capacity	Allowed many sectors to operate at 75% occupancy in regions with low COVID-19 hospitalizations.	Further recovery of commuting/consumer mobility, contingent on regional metrics.	<a href="https://gov.texas.gov/uploads/files/press/EO-GA-30_expanded_openings_COVID-19.pdf">https://gov.texas.gov/uploads/files/press/EO-GA-30_expanded_openings_COVID-19.pdf</a>
2020/10/7	County-level business restriction	County judges could allow bars to reopen at 50% capacity with distancing and other protocols.	Nightlife/weekend travel rebounded in opt-in areas but under caps and controls.	<a href="https://www.jw.com/news/insights-texas-reopening-bars-covid19/">https://www.jw.com/news/insights-texas-reopening-bars-covid19/</a>

**Supplementary Table 8.** Ground-truth COVID-19 policy timeline for Virginia in 2020.

Date	Policy	Description	Primary mobility impact	Source
2020/5/15	Limited reopening	Allowed limited operations for retail/dining under capacity and mitigation rules; staggered by region.	Gradual return of discretionary travel under strict caps; regionally differentiated pace.	
2020/5/30	Mandated mask & Gathering cap to 50	Mandated masks in indoor public spaces, aligned with VDH guidance.	Reduced close-contact risk in indoor commercial/transit environments.	
2020/6/30	Gathering cap to 250	Broader reopening with restrictions; gatherings up to 250; continued operational/mitigation standards.	Commuting/consumer and cross-city travel expanded under rules; large events still constrained.	
2020/11/13	Gathering cap to 25	New measures as cases rose: reduce social gathering cap to 25, expand mask requirements, late-evening restrictions.	Suppressed large gatherings and nightlife mobility; reduced indoor transmission risk.	<a href="https://www.governor.virginia.gov/newsroom/all-releases/2020/november/headline-861557-en.html">https://www.governor.virginia.gov/newsroom/all-releases/2020/november/headline-861557-en.html</a>
2020/11/30	Strengthened measures	Instituted a midnight-5 a.m. stay-at-home requirement, 10-person social cap, and broader mask requirements.	Reduced late-night/holiday mobility and gatherings; braking transmission during winter surge.	

## References

Akiba, Takuya, Shotaro Sano, Toshihiko Yanase, Takeru Ohta, and Masanori Koyama. 2019. “Op-tuna: A next-generation hyperparameter optimization framework.” In *Proceedings of the 25th ACM SIGKDD international conference on knowledge discovery & data mining*, 2623–2631.

Alleman, Tijs W, Jenna Vergeynst, Lander De Visscher, Michiel Rollier, Elena Torfs, Ingmar Nopens, Jan M Baetens, et al. 2021. “Assessing the effects of non-pharmaceutical interventions on SARS-CoV-2 transmission in Belgium by means of an extended SEIQRD model and public mobility data.” *Epidemics* 37:100505.

Figueroa, Jonine D, Ewan Gray, Nora Pashayan, Silvia Deandrea, Andre Karch, Diama Bhadra Vale, Kenneth Elder, Pietro Procopio, Nicolien T van Ravesteyn, Miriam Mutabi, et al. 2021. “The impact of the Covid-19 pandemic on breast cancer early detection and screening.” *Pre-ventive medicine* 151:106585.

Guo, Xusen, Xinxi Yang, Mingxing Peng, Hongliang Lu, Meixin Zhu, and Hai Yang. 2025. “Au-tomating traffic model enhancement with AI research agent.” *Transportation Research Part C: Emerging Technologies* 178:105187.

Jiang, Jinhao, Kun Zhou, Wayne Xin Zhao, Yang Song, Chen Zhu, Hengshu Zhu, and Ji-Rong Wen. 2025. “Kg-agent: An efficient autonomous agent framework for complex reasoning over knowledge graph.” In *Proceedings of the 63rd Annual Meeting of the Association for Computational Linguistics (Volume 1: Long Papers)*, 9505–9523.

Oh, Juhwan, Hwa-Young Lee, Quynh Long Khuong, Jeffrey F Markuns, Chris Bullen, Osvaldo Enrique Artaza Barrios, Seung-sik Hwang, Young Sahng Suh, Judith McCool, S Patrick Kachur, et al. 2021. “Mobility restrictions were associated with reductions in COVID-19 incidence early in the pandemic: evidence from a real-time evaluation in 34 countries.” *Scientific reports* 11 (1): 13717.

Ozaki, Yoshihiko, Yuki Tanigaki, Shuhei Watanabe, and Masaki Onishi. 2020. “Multiobjective tree-structured parzen estimator for computationally expensive optimization problems.” In *Proceedings of the 2020 genetic and evolutionary computation conference*, 533–541.

Wang, Jingyuan, Xiaojian Wang, and Junjie Wu. 2018. “Inferring metapopulation propagation network for intra-city epidemic control and prevention.” In *Proceedings of the 24th ACM SIGKDD international conference on knowledge discovery & data mining*, 830–838.